Coherent radiation generation by lasers and particle beams

This book presents a theoretical investigation of coherent radiation generation by particle beams and nonlinear mixing of lasers. The focus is on the broadband generation of microwaves and terahertz waves by power enhancement in sheath helix loaded travelling wave tube, introducing plasmas in the interaction region. In the terahertz band we examine the resonant excitation of terahertz radiation by beating two Gaussian laser beams in a magnetized plasma channel. As an alternative route we study the nonlinear mixing of two infrared lasers of frequencies and propagating in the TM/TE mode in a rippled density semiconductor waveguide to resonantly excite terahertz radiation. Two parallel semiconductor plates, separated by a short distance, are seen to be suitable for the excitation of Terahertz waves by a mildly relativistic electron beam. A relativistic sheet electron beam propagating through the space between the planes resonantly excites a THz surface plasma wave (SPW). The efficacy of n-InSb is examined for linear mode conversion of terahertz radiation into a surface plasma wave. The semiconductor surface is taken to be rippled and magnetized.

Dr Manish Kumar is BE(Electrical Engg), MTech(Energy) and PhD(Plasma Physics). His areas of interest includes Hybrid Energy system, Optical fibers, THz Radiation Gen, Photonics, Surface Plasma Waves and Plasma Physics. He has proved the existence of GOD scientifically and established the theory of everything in the conference held at USA(Nov,2016).

978-3-659-84512-3

Coherent radiation by laser& part. beams

Kumar

Scholars' Press

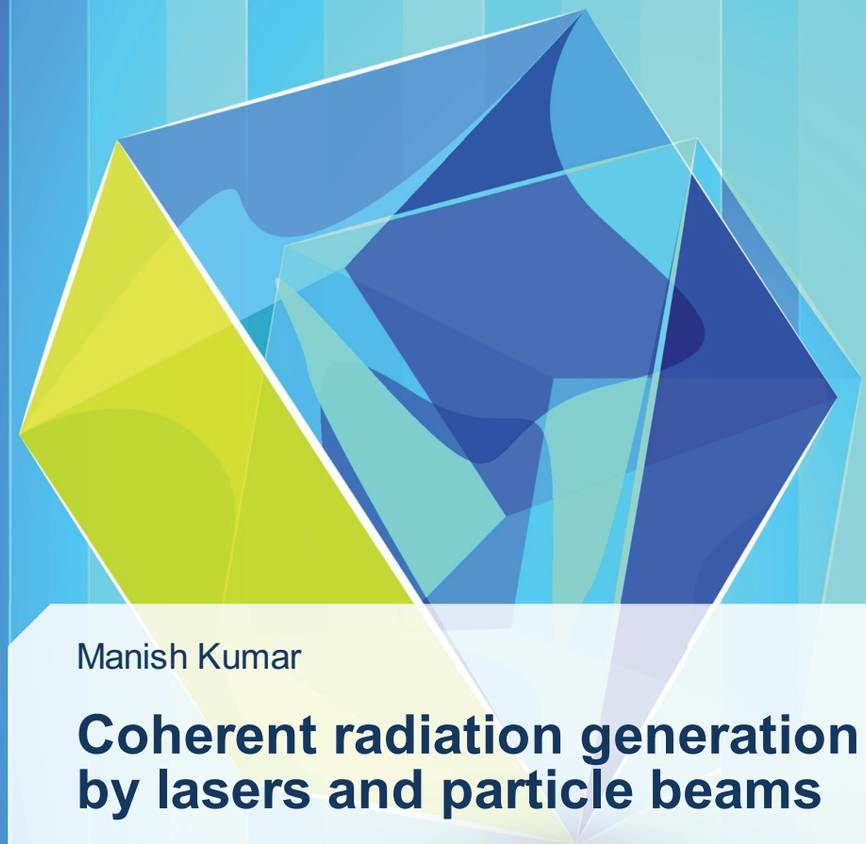

Manish Kumar

Coherent radiation generation by lasers and particle beams

Manish Kumar

Coherent radiation generation by lasers and particle beams

Manish Kumar

Coherent radiation generation by lasers and particle beams

Scholar's Press

Impressum / Imprint
Bibliografische Information der Deutschen Nationalbibliothek: Die Deutsche Nationalbibliothek verzeichnet diese Publikation in der Deutschen Nationalbibliografie; detaillierte bibliografische Daten sind im Internet über http://dnb.d-nb.de abrufbar.

Bibliographic information published by the Deutsche Nationalbibliothek: The Deutsche Nationalbibliothek lists this publication in the Deutsche Nationalbibliografie; detailed bibliographic data are available in the Internet at http://dnb.d-nb.de.

Coverbild / Cover image: www.ingimage.com

Verlag / Publisher:
Scholar's Press
ist ein Imprint der / is a trademark of
OmniScriptum GmbH & Co. KG
Bahnhofstraße 28, 66111 Saarbrücken, Deutschland / Germany
Email: info@omniscriptum.com

Herstellung: siehe letzte Seite /
Printed at: see last page
ISBN: 978-3-659-84512-3

Zugl. / Approved by: New Delhi, IIT Delhi, Dec 2010

Dedicated to

My Parents and Teachers

ACKNOWLEDGEMENT

I take this opportunity to express my deep sense of gratitude and profound indebtness towards Prof. V. K. Tripathi for his invaluable guidance, constant support and encouragement. His deep knowledge in the subject and his humanitarian approach has always been a constant source of inspiration to me.

I would like to thank Dr. Ashok Sharma for his encouragement and support. Dr. Lalita Bhasin and Dr. Pawan Kumar deserve special mention for consistent discussions and support for our collaborative research work. Thanks are due to my friends Dr. Anamika Sharma, Dr. D. B. Singh, Dr. Vivek Sajal, Dr. Ashok Kumar, Dr. Gagan Kumar, Dr. Khaleel, Dr. VishwaBandhu Pathak, Dr. Nafis Ahmed, Dr. Anuraj Panwar, Dr. Sukhdeep Kaur and Dr. Deepak Dahiya for helping me at various stages of this work. I am thankful to all plasma group members Vinod Pandey, Vijay Garg, Updesh, Animesh, Rohtash, Manoj, Ranjeet, Deepak Tripathi and Magesh kumar for their affection and support at campus life.

This acknowledgement would remain incomplete without expressing my sincere feelings towards my sister Asha Kiran, her husband Dhrishtdumnya Bhuyan and to cute Neerav Bhuyan, my brother Animesh, my wife Shwetnisha and my two kids Achintya and Avisha for their love and support. No words can express my feelings and love for my parents, Smt. Manorama Devi and Prof. Jokhan Ram. Their unconditional love and support is unmatchable. They never doubted my choice of pursuing research as a career and always encouraged me to follow my own heart.

I am grateful to the I.T., B.H.U. for providing financial support to carry out my research program. I express my sincere thanks to Physics Department, I. I. T. Delhi for general support and providing congenial working environment.

At last I would like to thank the whole scientific community, who shared their knowledge and experience with me through their research articles and talks, and introduced me to new and fascinating findings and mysteries of Nature.

Manish Kumar

ABSTRACT

The thesis presents a theoretical investigation of coherent radiation generation by particle beams and nonlinear mixing of lasers. The focus is on the broadband generation of microwaves and terahertz waves. We explored the possibility of power enhancement in sheath helix loaded travelling wave tube, by the introduction of plasmas in the interaction region. The plasma allows larger beam current to pass due to charge and current neutralization. The beam excites an azimuthally symmetric slow wave via Cerenkov resonance. In the case of a strongly magnetized plasma when $\omega_p > \omega$ (where ω_p is the plasma frequency), the amplitude of the axial electric field peaks on the axis and phase velocity is suppressed, whereas for $\omega_p < \omega$ the field amplitude peaks at the helix surface and phase velocity is enhanced. As a consequence, when beam is placed close to the helix, the growth rate increases with ω_p as long as $\omega_p < \omega$ and decreases with ω_p when $\omega_p > \omega$. In the case of an unmagnetised plasma, the mode is more strongly localized near the helix and growth rate increases with ω_p.

In the terahertz band we examine the resonant excitation of terahertz radiation by beating two Gaussian laser beams in a magnetized plasma channel. The laser intensities are nonuniform in the transverse (radial) direction, hence the beat frequency ponderomotive force due to them has a finite transverse component. It imparts oscillatory velocity to electrons that couples with the pre-existing density ripple to produce a nonlinear current driving the THz radiation. The density ripple provides phase synchronism while the axial magnetic field enhances the nonlinear coupling through cyclotron resonance. The terahertz power scales as the square of density ripple amplitude and inversely with the square of laser frequencies.

As an alternative route we study the nonlinear mixing of two infrared lasers of frequencies ω_1 and ω_2 propagating in the TM/TE mode in a rippled density semiconductor waveguide to resonantly excite terahertz radiation. The wave vector of the density ripple is along the direction of laser propagation while a static magnetic field is applied transverse to it. The lasers exert a ponderomotive force on electrons at the beat frequency. This force, in the presence of density ripple and transverse magnetic field, produces a nonlinear current at the terahertz frequency. The magnetic field enhances the amplitude of the terahertz wave. The terahertz yield is found to be significantly higher when the lasers propagate in the TM mode than in the TE mode.

Two parallel semiconductor plates, separated by a short distance, are seen to be suitable for the excitation of Terahertz waves by a mildly relativistic electron beam. The structure supports a surface plasmon eigen mode with amplitude maxima at the inner surfaces of the plates and minimum at the middle. A relativistic sheet electron beam propagating through the space between the planes resonantly excites a THz surface plasma wave (SPW). The frequency of the driven SPW decreases with the energy of the beam while the growth rate increases.

The efficacy of n-InSb is examined for linear mode conversion of terahertz radiation into a surface plasma wave. The semiconductor surface is taken to be rippled and magnetized. The radiation, polarized in the direction of ripple wave vector, imparts oscillatory velocity to electrons in the ripple layer. The velocity beats with the ripple density to produce a current that resonantly drives the surface plasma wave. The magnetic field splits the SPW mode into '+' & '-' modes and reduces the cut-off frequency. The amplitude of SPW for '+' mode is higher than as compared to '-'mode.

CONTENTS

Acknowledgement v

Abstract vi

Contents viii

List of Figures xi

Chapter 1: Introduction 1

1.1 Cerencov and Cyclotron Interactions 2

1.2 Terahertz Radiation 3

1.3 Surface Plasma Wave. 5

1.4 Plan of the Thesis 7

Chapter 2: Plasma effects in a travelling wave tube. 19

2.1 Introduction. 19

2.2 Beam and Plasma Response. 20

2.3 Mode Structure 23

2.4 Growth Rate 30

2.5 Results and Discussion 36

Chapter 3: Resonant beat wave excitation of terahertz radiation in a magnetized plasma channel 39

3.1 Introduction. 39

3.2 Beat frequency current density 40

3.3 THz generation 43

3.4 Power of the THz radiation 50

3.5 Discussion. 51

Chapter 4: Beat excitation of terahertz radiation in a semiconductor slab in a magnetic field. 55

4.1 Introduction. 55

4.2 Laser propagation through a semiconductor slab. 58

4.3 Beat excitation of terahertz nonlinear current density in magnetic. . . . . Field 62

4.4 Dispersion relation for the terahertz wave. 63

4.5 Discussion. 70

Chapter 5: Excitation of THz plasmon eigen mode of a parallel plane guiding system by an electron beam. 75

5.1 Introduction. 75

5.2 Surface plasma wave. 76

5.3 Electron beam excitation of surface plasma wave 80

5.4 Discussion. 85

Chapter 6: Mode conversion of terahertz radiation into surface plasma wave on a rippled magnetized n-InSb 89

6.1 Introduction. 89

6.2 Surface plasmon eigenmode. 90

6.3 Mode conversion of THz radiation into surface plasmons 93

6.4 Discussion. 99

Chapter 7: Conclusions and Future Prospects. 103

Appendix A. 107

Bio-data of Author. 109

LIST OF FIGURES

Chapter 1

FIG 1.1 Schematic representation of an electron density wave propagating along a metal - dielectric interface. The exponential dependence of the electromagnetic field intensity on the distance away from the interface is shown on the right. These waves can be excited very efficiently with light in the visible range of the electromagnetic spectrum

Chapter 2

FIG 2.1 System Configuration

FIG 2.2 Retardation c/v_{ph} of a shielded helix (a, helix radius)

FIG 2.3 Retardation c/v_{ph} of a shielded helix (a, helix radius) for $\cot\psi$=13

FIG 2.4 Retardation c/v_{ph} of a shielded helix (a, helix radius) for $\cot\psi$=13

FIG 2.5 Retardation c/v_{ph} of a shielded helix (a, helix radius) for $\cot\psi$=13

FIG 2.6 Growth rate for $\omega_p < \omega$ for $\cot\psi$=13

FIG 2.7 Schematic of beam-wave interaction

FIG 2.8 Growth rate for $\omega_p > \omega$ for $\cot\psi$=13

FIG 2.9 Growth rate for unmagnetized plasma for $\cot\psi$=13

Chapter 3

FIG 3.1 Normalized density ripple wavenumber $|qc/\omega_{po}|$ as a function of normalized frequency ω/ω_{po} for the value of $\omega_c' = 0.2, r_c' = 3, \nu' = 10.$

FIG 3.2 Normalized density ripple wavenumber $|qc/\omega_{po}|$ as a function of normalized frequency ω/ω_{po} for the value of $\omega_c' = 0.2,0.6, r_c' = 3, \nu' = 10.$

FIG 3.3 Normalized amplitude of Terahertz radiation $|F/A_{01}|$ as a function of normalized frequency ω/ω_{po} for the value of $A_{02}' = 10, r_c' = 3, n_q' = 0.3, \nu' = 10.$

FIG 3.4 Normalized amplitude of Terahertz radiation $|F/A_{01}|$ as a function of normalized frequency ω/ω_{po} for the value of $\omega_c' = 0.2,0.6, A_{02}' = 10, r_c' = 3, n_q' = 0.3, \nu' = 10.$

FIG 3.5 Normalized power of Terahertz radiation $|P_{THz}/P_{laser}|$ as a function of normalized frequency ω/ω_{po} for the value of $A_{02}' = 10, r_c' = 3, n_q' = 0.3, \nu' = 10.$

FIG 3.6 Normalized power of Terahertz radiation $|P_{THz}/P_{laser}|$ as a function of normalized frequency ω/ω_{po} for the value of $\omega_c' = 0.2,0.6, A_{02}' = 10, r_c' = 3, n_q' = 0.3, \nu' = 10.$

Chapter 4

FIG 4.1 System configuration.

FIG 4.2 Laser frequency vs axial propagation constant for TM_{10} mode.

FIG 4.3 Laser frequency vs axial propagation constant for TE_{10} mode.

FIG 4.4 Terahertz frequency vs axial propagation constant in TM_{10} mode.

FIG 4.5 Normalized amplitude versus normalized frequency curve for TM_{10} mode laser propagation for $\omega_c a / c = 0.05$.

FIG 4.6 Normalized amplitude versus normalized frequency curve for TE_{10} mode laser propagation for $\omega_c a / c = 0.05$.

FIG 4.7 Normalized density ripple versus terahertz frequency curve for TM_{10} mode propagation.

FIG 4.8 Normalized density ripple versus terahertz frequency curve for TE_{10} mode propagation.

FIG 4.9 Normalized amplitude versus magnetic field for TM_{10} mode.

FIG 4.10 Normalized amplitude versus magnetic field for TE_{10} mode.

Chapter 5

FIG 5.1 Schematic of two semiconducting parallel plane guiding system with free space in between them. A relativistic sheet electron beam, injected in the free space region, excites the surface plasma wave.

FIG 5.2 Plot of mode structure of surface plasma wave for $\omega/\omega_p = 0.15$.

FIG 5.3 Plot of dispersion relation for surface plasma wave in double semiconductor structure for $\varepsilon_L = 17$, $\nu/\omega_p = 0.0472$.

FIG 5.4 Plot of normalized growth rate vs normalized frequency for double semiconductor structure for $a\omega_p/c = 40$, $\nu/\omega_p = 0,0.0472$, $\omega_{pb}/\omega_p = 10^{-3}$, $\varepsilon_L = 17$.

FIG 5.5 Plot of normalized growth rate vs normalized distance between the semiconductor plates for double semiconductor structure for $\omega_{pb}/\omega_p = 10^{-3}$, $\varepsilon_L = 17$, $\omega/\omega_p = 0.15, \nu/\omega_p = 0,0.0472$, $\gamma_o = 5.94$.

Chapter 6

FIG 6.1 Schematic of linear mode conversion of incident THz radiation into surface plasma wave on a rippled semiconductor-air interface in the presence of transverse magnetic field.

FIG 6.2 Dispersion relation of n-InSb for surface plasma wave in the collisionless regime i.e. for parameters $\omega_c/\omega_p = 0,0.2,0.5$, $\varepsilon_L = 17, \nu/\omega_p = 0$.

FIG 6.3 Plot of normalized amplitude vs normalized frequency for '+' mode for the parameters $\varepsilon_L = 17,\ \nu/\omega_p = 0.014, d\omega_p/c = 5.$

FIG 6.4 Plot of normalized amplitude vs normalized electron cyclotron frequency for '+' mode for the parameters $\varepsilon_L = 17,\ \nu/\omega_p = 0.014, d\omega_p/c = 5.$

FIG 6.5 Plot of normalized amplitude vs normalized frequency for '-' mode for the parameters $\varepsilon_L = 17,\ \nu/\omega_p = 0.014, d\omega_p/c = 5.$

FIG 6.6 Plot of normalized amplitude vs normalized electron cyclotron frequency for '-' mode for the parameters $\varepsilon_L = 17,\ \nu/\omega_p = 0.014, d\omega_p/c = 5.$

Chapter 1

Introduction

Coherent radiation generation in all frequency regimes, ranging from radiowaves to X-rays, has been a subject of intensive activity for several decades. It witnessed the rise of lasers, producing coherent radiation at infrared and shorter wavelengths and masers and electron beam devices producing radiation in the microwave range. In last few decades Gyrotron and free electron laser emerged as high power devices at millimeter and shorter wavelengths. Free electron laser infact has the versatility to operate over a wide frequency range, from millimeter to submicron wavelengths. The Gyrotron or electron cyclotron maser (ECM) is based on a stimulated cyclotron emission process involving energetic electrons in gyrational motion. It utilizes the relativistic mass effect for the generation of coherent radiation from free electrons. Chu [1] has given a comprehensive review of the fundamental principles of the ECM and their embodiment in practical devices. Free electron laser employs a magnetic wiggler of finite wavenumber that couples the electromagnetic mode to negative energy beam space charge mode and provides the necessary quantum of momentum required for momentum conservation in the radiation process. Marshall [2], Roberson and Sprangle [3] and Freund and Antonsen [4] have given elegant reviews of free electron laser. However, the field continues to grow at a fast pace [5, 6]. Coherent radiation generation is relevant to space plasmas as well, hence has been widely studied in ionosphere and outer space [7, 8, 9]. In many stances parametric coupling between waves is a source of radiation generation [10-13].

1.1 Cerencov and Cyclotron Interactions

A key element in radiation generation by electron beams is Cerenkov resonance or the cyclotron resonance. In the former the Doppler shifted frequency of the wave, as seen by the beam electron, is nearly zero $(\omega - \vec{k}.\vec{v} = 0)$ whereas in the latter it equals the electron cyclotron frequency $(\omega - \vec{k}.\vec{v} = \omega_c)$. Travelling wave tube (TWT) is a foremost device that relies on Cerenkov resonance for broadband microwave generation. It consists of a Gun assembly which produces an electron beam, a beam focusing system which produces sufficient longitudinal magnetic field to keep the electron beam from spreading, a collector to absorb the spent beam, a cooling system to help dissipate excess heat and a helix through which the electron beam passes before being absorbed by the collector. The helix slows down the microwave that propagates through it. In the presence of a microwave seed signal in the helix region, the electron beam, moving slightly faster than the phase velocity of the wave, bunches in the retarding zones, giving energy to the microwave, thus amplifying the latter. Kompfner [14] has given an elegant review of TWT. Cerenkov free electron laser (CFEL) closely resembles TWT physics where partially dielectric loaded waveguide [15] is used as slow wave structure and a relativistic electron beam is used. Walsh [16] observed the generation of $10\,\mu m$ radiation in a CFEL. In a free electron laser the phase synchronism is achieved via the Cerenkov interaction of the electron beam with the beat space charge mode driven as a beat wave of the radiation mode and the wiggler $(\omega - (\vec{k} + \vec{k}_w).\vec{v} = 0)$.

A common feature of most of theories of slow wave devices is that they consider only a one-dimensional motion of electrons and ignore the effects of any background plasma. As a

matter of fact, the residual gases in the guiding system get ionized by the beam and plasma of appreciable density is formed. Unless the vacuum is kept very high, the plasma density may be comparable or even larger than the density of the electron beam. This should provide some degree of charge and current neutralization and thus e-beam with higher current can propagate. It will also guide the beam without requiring a very strong guide field. Infact, there has been significant interest in filling the waveguide with plasma [17-24] for high-power operation of the device and shortening of the operating wavelength.

1.2 Terahertz Radiation

In recent years terahertz(THz) radiation generation has attracted much attention, as these waves have potential applications in biological imaging [25], remote sensing [26], spectroscopy of solids and liquids, chemical and security identification [27] etc. Conventional sources of radiation do not operate in the THz range. Free electron laser does, however, it is economic only when multi megawatt powers are required. For modest powers alternate concepts have been proposed. A major part of these efforts is based on the employment of intense femtosecond laser. These efforts fall into two general categories. The first involves generating an ultrafast photocurrent in a photoconductive switch or semiconductor using charge carrier acceleration or the photo-Dember effect. In the second category, THz waves are generated by nonlinear optical effects such as optical rectification (limited to sub picosecond laser pulses), difference-frequency generation (DFG) or optical parametric oscillation. The current nonlinear media receiving attention are GaAs, GaSe, GaP, ZnTe, CdTe, DAST (diethyl amino sulphur tetrafluoride) and LiNbO3, although research to find more effective materials continues.

A promising alternative for THz generation involves emission from photoinduced plasma in a gaseous medium, as was first demonstrated by Hamster et al. [27, 28]. By focusing femtosecond pulses with energies greater than a few tens of μJ, one readily reaches the threshold intensities for tunnel ionization of the gas molecules (~10^{14} Wcm^{-2}), leading to significant plasma formation. As the emitter target (gas) is endlessly replenishable for each laser shot, there is no question of a damage threshold for such an emitter. The THz emission mechanism in their experiments was based on the radial acceleration of the ionized electrons due to the ponderomotive force generated by the radial intensity gradient of the optical beam [29], leading to a conical THz emission at an angle to the direction of propagation.

Since then, other plasma-based THz generation (and detection) schemes have been demonstrated, which provide stronger THz emission than the ponderomotive mechanism with the emission in the forward propagation direction. In analogy to biased solidstate emitters, L¨offler et al. [29-31] applied an external DC bias to the plasma region to generate a transverse polarization that resulted in at least an order-of-magnitude increase in the THz field strength (with the maximum attainable THz emission being limited by screening of the applied bias). Cook et al. [32] proposed another method to introduce the required transverse bias, i.e. by using a superposition of both fundamental and second-harmonic (SH) pulse fields to generate the plasma (which is referred to as the ω-2ω, or AC-bias method). Indeed, the use of two-color fields for generating asymmetric electron dynamics in the photoinduced plasma was already well established (e.g. [33]). As the frequency of the optical AC-bias is well above the plasma frequency, this method does not suffer from the strong screening effects of the DC-bias method. Hence this method has emerged as the optimal choice for plasma-THz generation [33-39]. More recently, additional plasma-THz techniques have been reported. In the case of few cycle pulses

(i.e. with <10 fs duration), no additional SH field is required to observe the THz emission [40, 41], the amplitude of which now depends strongly on the carrier-envelope (CE) phase of the pulses, creating a useful application for determining the CE-phase itself, bringing THz methods to the emerging field of attoscience. In another report [43] it was demonstrated that the quasi-inverse process – i.e. sampling detection of an existing THz pulse – is also possible with photoinduced plasma. Given the highly nonlinear nature of the plasma generation mechanism, it is conceivable that the bandwidth for both THz generation and detection are considerably larger than for conventional second-order nonlinear processes. For the case of ponderomotive plasma-THz emission, Xie et al. [44] have shown that the THz pulse can be enhanced by passing through a second photoinduced plasma. Gildenburg et al [45] have proposed a novel scheme of THz generation where THz power scales linearly with the laser power.

1.3 Surface Plasma Wave

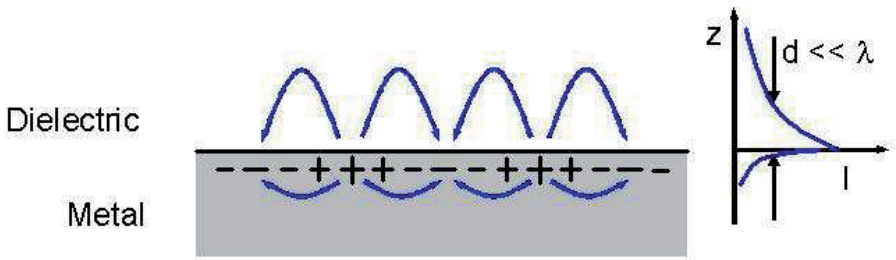

Fig 1.1 Schematic representation of an electron density wave propagating along a metal - dielectric interface. The exponential dependence of the electromagnetic field intensity on the distance away from the interface is shown on the right. These waves can be excited very efficiently with light in the visible range of the electromagnetic spectrum

Surface plasma waves (SPWs) or surface plasmons (SPs), have strong promise for THz generation and detection. SPW is a guided electromagnetic mode that propagates along the interface between a conductor and a dielectric (e.g., a metal and air) or two dissimilar conductors. The amplitude of a SPW falls off rapidly as one moves away from the surface. SPW can be efficiently excited by a laser using attenuated total reflection configuration (in which a metal film is deposited on a glass prism and laser is launched obliquely onto the glass-metal interface at a specific angle when it excites the SPW on the metal-free space interface) or using a surface ripple.

Surface plasmons play a key role in the interpretation of a great variety of experiments and the understanding of various fundamental properties of solids. These include the nature of Van der Waals forces [46–48], the classical image potential acting between a point classical charge and a metal surface [49–52], the energy transfer in gas–surface interactions [53], surface energies [54-56], the damping of surface vibrational modes [57, 58], the energy loss of charged particles moving outside a metal surface [59, 60] and the de-excitation of adsorbed molecules [61]. Surface plasmons have wide ranging applications, in electrochemistry [62], wetting [63] and biosensing [64-66], scanning tunneling microscopy [67], the ejection of ions from surfaces [68], nanoparticle growth [69, 70], surface plasmon microscopy [71, 72] and surface-plasmon resonance technology [73-79]. Renewed interest in surface plasmons has come from recent advances in the investigation of the electromagnetic properties of nanostructured materials [80, 81]. One of the most attractive aspects of these collective excitations is their use to concentrate light in subwavelength structures and to enhance transmission through periodic arrays of subwavelength holes in optically thick metallic films [82, 83]. The emerging field of plasmonics combines the fields of photonics and electronics at the nanoscale [84]. Surface-plasmon

polaritons can serve as a basis for constructing nanoscale photonic circuits that will be able to carry optical signals and electric currents [85, 86]. Surface plasmons can also serve as a basis for the design, fabrication and characterization of subwavelength waveguide components [87-101].

The amplitude of the SPW, produced via the mode conversion of a laser, can far exceed the amplitude of the laser field and it could efficiently excite THz radiation. Lalita and Tripathi [102] have studied the optical rectification of SPW. Kadlec *et al.* [103, 104] have experimentally demonstrated THz radiation generation at gold surfaces. Kupersztch *et al.* [105] reported that the emitted photoelectrons from a gold target due to surface plasma waves were much more energetic than in an ordinary photoelectric effect.

1.4 Plan of the Thesis

The present thesis focuses on coherent radiation generation at microwave and terahertz frequencies employing alternative concepts. We delve into the plasma effects in travelling wave tube which is a versatile broadband device for microwave generation. The plasma is shown to improve the efficiency and power handling capacity of the device. We propose alternate schemes of THz generation using magnetized plasma and a magnetized semiconductor. The cyclotron resonance effect gives rise to significant enhancement in the output THz power. We also study the excitation of a surface plasmon eigen mode over a parallel plane guiding system by an electron beam via Cerenkov resonance. The symmetric SPW mode is seen to be suitable as it helps guiding of the electron beam. We also study the linear mode conversion of laser to SPW on a magnetized semiconductor that may be useful for sensor applications.

A chapter wise summary of the thesis is as follows:

Chapter 1: Introduction

This chapter presents a definition and overview of the work done in above mentioned research areas and their applications.

Chapter 2: Plasma Effects in a Travelling Wave Tube

This chapter deals with the effect of plasma, on a travelling wave tube, comprising a sheath helix. The plasma, taken to be (i) strongly magnetized and (ii) unmagnetised, allows larger beam current to pass due to charge and current neutralization. The beam excites an azimuthally symmetric slow wave via Cerenkov resonance. In the case of a strongly magnetized plasma when $\omega_p > \omega$ (where ω_p is the plasma frequency, and ω is the wave frequency), the amplitude of the axial electric field peaks on the axis and phase velocity is suppressed, whereas for $\omega_p < \omega$ the field amplitude peaks at the helix surface and phase velocity is enhanced. As a consequence, when beam is placed close to the helix, the growth rate increases with ω_p as long as $\omega_p < \omega$ and decreases with ω_p when $\omega_p > \omega$. In the case of an unmagnetised plasma, the mode is more strongly localized near the helix and growth rate increases with ω_p.

Chapter 3: Resonant Beat Wave Excitation of Terahertz Radiation in a Magnetized Plasma Channel

This chapter deals with the nonlinear mixing of two Gaussian laser beams in a magnetized plasma channel, exciting a difference frequency terahertz radiation. The beat frequency ponderomotive force imparts an oscillatory velocity to electrons that couples with the

pre-existing density ripple to produce a nonlinear current driving the THz radiation. The density ripple provides phase matching while the axial magnetic field enhances the nonlinear coupling through cyclotron resonance. The terahertz power scales as the square of density ripple amplitude and inversely with the square of laser frequencies.

Chapter 4: Beat Excitation of Terahertz Radiation in a Semiconductor Slab in a Magnetic Field

This chapter explores the beat excitation of terahertz radiation by nonlinear coupling between two infrared lasers of frequencies ω_1 and ω_2 in a rippled density semiconductor waveguide. The lasers propagate in the TM/TE mode in the direction of density ripple wave vector. A static magnetic field is applied transverse to it. The ripple wave number is suitably chosen to satisfy the phase matching condition. The lasers exert a ponderomotive force on the electrons at the beat frequency $\omega_1 - \omega_2$. This force, in the presence of density ripple and transverse magnetic field, produces a nonlinear current at the terahertz frequency. The magnetic field enhances the amplitude of the terahertz wave. The terahertz yield is significantly higher when the lasers propagate in the TM mode rather than in the TE mode.

Chapter 5: Excitation of THz Plasmon Eigen Mode of a Parallel Plane Guiding System by an Electron Beam

This chapter deals with the two parallel semiconductor plates, separated by a short distance, support surface plasmon eigen mode with amplitude maxima at the inner surfaces of the plates and minimum at the center. A relativistic sheet electron beam propagating through the space between the planes resonantly excites the surface plasma wave (SPW). The frequency of

the driven SPW decreases with the energy of the beam while the growth rate increases. At the beam current $\approx 168 Amp$ the growth rate of $5.93 \times 10^8 rad/s$ is achieved at the frequency $\approx 0.51 THz$ of SPW for the 5mm $\hat{y}$ width and spacing between the two plates of $\approx 2.83 mm$. The growth rate scales as 1/3 root of the electron beam current.

Chapter 6: Mode Conversion of Terahertz Radiation into Surface Plasma Wave on a Rippled Magnetized n-InSb

This chapter develops a formalism of linear mode conversion of terahertz radiation into a surface plasma wave on a rippled surface of magnetized n-InSb. The radiation, polarized in the direction of ripple wave vector, imparts oscillatory velocity to electrons in the ripple layer. The velocity beats with the ripple density to produce a current that resonantly drives the surface plasma wave. The magnetic field splits the SPW mode into '+' & '-'modes and reduces the cut-off frequency. The amplitude of SPW for '+' mode is higher than as compared to '-'mode.

List of Publications

The work presented in the thesis has resulted in following publications:

Published:

1. "Plasma effects in a travelling wave tube ", **Manish Kumar**, Lalita Bhasin and V. K. Tripathi, **Phys. Scr. 81 025502 (2010).**
2. "Resonant beat wave excitation of terahertz radiation in a magnetized plasma channel", **Manish Kumar**, Lalita Bhasin and V. K. Tripathi, **Phys. Scr. 81 045504 (2010).**

3. “Excitation of THz plasmons eigen mode of a parallel plane guiding system by an electron beam”, Pawan Kumar, **Manish Kumar** and V. K. Tripathi, **J. Appl. Phys. 108, 123303(2010)**.

Communicated:

4. “Beat excitation of Terahertz radiation in a semiconductor slab in a magnetic field “, **Manish Kumar**, Lalita Bhasin and V. K. Tripathi.
5. “Mode conversion of terahertz radiation into surface plasma wave on a rippled magnetized n-InSb”, **Manish Kumar**, Pawan Kumar and V. K. Tripathi.

Conferences

1. " Resonant beat wave excitation of terahertz radiation in a magnetized plasma channel ", **Manish Kumar,** Lalita Bhasin and V. K. Tripathi, **International Workshop on the Terahertz Technology 2009,** Osaka, Japan 30 Nov – 03 Dec, 2009.

2. Participated in **International Conference on Multifunctional Material-2010 (ICMM-2010)** held on 6-9 December 2010, at the Department of Physics, Banaras Hindu University, Varanasi, India.

References

[1] K. R. Chu, Rev. of Modern Phys. **76**, 489 (2004).

[2] T.C.Marshall, Free-Electron Lasers (Macmillan, New York, 1985).

[3] C.W.Roberson and P.Sprangle, Phys. Fluids B, **1**, 3(1989).

[4] H.P.Freund and T.M.Antonson, Principles of Free Electron Lasers (Chapman & Hall, New York, 1996).

[5] V. Asgekar and G. Dattolia, J. Appl. Phys. **101**, 063111(2007).

[6] G. Mishra, J. Appl. Phys. **65**, 3264 (1989).

[7] M. Lampe, G. Joyce, W. M. Manheimer and G. Ganguli, Phys. Plasmas, **17**, 022902(2010).

[8] J.E.Maggs and G.J.Morales, Phys. Rev. Lett., **91**, 035004(2003).

[9] R.Pratap, K.Sasidharan and V. Krishan, Phys. Rev. E, **47**(1), 640 (1993).

[10] L. Stenflo and H. Wilhelmsson, Phys. Rev. A, **24**, 1115(1981).

[11] R. A. Ganeev, H. Singhal, P. A. Naik, J. A. Chakera, M. Kumar and P. D. Gupta, Phys. Rev. A **82**, 043812(2010).

[12] O. Jedrkiewicz, M. Clerici, A. Picozzi, D. Faccio, and P. Di Trapani, Phys. Rev. A **76**, 033823 (2007).

[13] T. Baeva, S. Gordienko, and A. Pukhov, Phys. Rev. E **74**, 046404 (2006)

[14] R Kompfner, Rep. Prog. Phys. **15,** 275(1952).

[15] J.Y.Choe, H.S.Uhm, and S.Ahn, J. Appl. Phys. **52**,7067(1981).

[16] J.E. Walsh, Adv. Electron. Electron Phys. **58**, 271(1981).

[17] L. S**.** Bogdankevich, M. V. Kuzelev, and A. A. Rukhadze, Sov. Phys. Usp**. 24,** 1(1981).

[18] M. V. Kuzelev, A. A. Rukhadze, P. **S.** Srelkov, and A. G. Shkavarunets, Sov. J . Plasma Phvs., **13**(11**)**, 793(1987).

[19] K. Murukesapilai, J. Appl. Phys. **62**(9), 3598(1987).

[20] M. V. Kuzelev, F. H. Muhametzyanov, and A. G. Shkavarunets, Sov. J. Plasma Phys. **9**, 1137(1983).

[21] P. H. Bing and C. Y. Shen, Int. J. Electron. **3 ,** 551(1988).

[22] T. D. Pointon and J . S. Groot, Phys. Fluids, **31**, 908(1988).

[23] J. S. Degroot, R. A. Stone, K. Mizuno, J. H. Rogers, and T. D. Pointon, IEEE Trans. Plasma Sci., **16**(2), 206(1988).

[24] J. S. Degroot, R. A. Stone, and J. H. Rogers, SPIE, **873**, Microwave and Particle Beam Sources and Propagation**,** 37(1988).

[25] E. Pickwell and V.P. Wallace, J. Phys. D **39**, R301 (2006).

[26] T. M. J. Antonsen, J. Palastro and H. M. Michberg, Phys. Plasmas **14**, 033107 (2007).

[27] Y.C. Shen, T. Lo, P. F. Taday, B. E. Cole, W.R. Tribe and M.C. Kemp, Appl. Phys. Lett., **86**, 241116(2005).

[28] H. Hamster, A. Sullivan, S. Gordon, W.White and R.W. Falcone, Phys. Rev. Lett. **71**, 2725(1993).

[29] H. Hamster, A. Sullivan, S. Gordon, and R.W. Falcone, Phys. Rev. E **49**, 671 (1994).

[30] T. L¨offler, F. Jacob, and H. G. Roskos, Appl. Phys. Lett. **77**, 453 (2000).

[31] T. L¨offler and H. G. Roskos, J. Appl. Phys. **91**, 2611 (2002).

[32] D. J. Cook and R. M. Hochstrasser, Opt. Lett. **25**, 1210 (2000).

[33] D.W. Schumacher and P. H. Bucksbaum, Phys. Rev. A **54**, 4271 (1996).

[34] M. Kreb, T. L¨offler, S. Eden, M. D. Thomson, and H. G. Roskos, Opt. Lett. **29**, 1120 (2004).

[35] T. L¨offler, M. Kress, M. D. Thomson, and H. G. Roskos, Acta Phys. Pol. A **107**, 99 (2005).

[36] T. Bartel, P. Gaal, K. Reimann, M. Woerner, and T. Elsaesser, Opt. Lett. **30**, 2805(2005).

[37] X. Xie, J. Dai, and X. C. Zhang, Phys. Rev. Lett. **96**, 075005(2006).

[38] H. Zhong, N. Karpowicz, and X. C. Zhang, Appl. Phys. Lett. **88**, 261103(2006).

[39] K.Y. Kim, J. H. Glownia, A. J. Taylor, and G. Rodriguez, Opt. Express **15**, 4577(2007).

[40] K. Reimann, Rep. Prog. Phys. **70**, 1597(2007).

[41] M. Kreb, T. L¨offler, M. D. Thomson, R. D¨orner, H. Gimpel, K. Zrost, T. Ergler, R. Moshammer, U. Morgner, J. Ullrich, and H. G. Roskos, Nat. Phys. **2**, 327(2006).

[42] M. Kreb, T. L¨offler, M. D. Thomson, R. D¨orner, H. Gimpel, K. Zrost, T. Ergler, R. Moshammer, U. Morgner, J. Ullrich, and H. G. Roskos, Acta Phys. Pol. A, in press (2007).

[43] J. Dai, X. Xie, and X. C. Zhang, Phys. Rev. Lett. **97**, 103903(2006).

[44] X. Xie, J. Xu, J. Dai, and X. C. Zhang, Appl. Phys. Lett. **90**, 141104(2007).

[45] V.B.Gildenburg and N.V.Vvedenskii, Phys. Rev. Lett. **98**, 245002(2007).

[46] J. E. Inglesfield and E. Wikborg, J. Phys. F: Metal Phys. **5,** 1475(1975).

[47] E. Zaremba and W. Kohn, Phys. Rev. B **13,** 2270(1976).

[48] B. E. Sernelius, Phys. Rev. B **71,** 235114(2005).

[49] P. J. Feibelman, Surf. Sci. **27,** 438(1971).

[50] R. H. Ritchie, Phys. Lett. A **38,** 189(1972).

[51] R. Ray and G. D. Mahan, Phys. Lett. A **42,** 301(1972).

[52] M. Sunji´c, G. Toulouse and A. A. Lucas, Solid State Commun. **11,** 1629(1972).

[53] J. W. Gadzuk and H. Metiu, Phys. Rev. B **22,** 2603(1980).

[54] J. Schmit and A. Lucas, Solid State Commun. **11,** 415(1972).

[55] E. Wikborg and J. E. Inglesfield, Phys. Scr. **15,** 37(1977).

[56] D. C. Langreth and J. P. Perdew, Phys. Rev. B **15,** 2884(1977).

[57] Y. J. Chabal and A. J. Sievers, Phys. Rev. Lett. **44,** 944(1980).

[58] B. Persson and R. Ryberg, Phys. Rev. Lett. **54,** 2119(1985).

[59] P. M. Echenique and J. B. Pendry, J. Phys. C: Solid State Phys. **8,** 2936(1975).

[60] P. M. Echenique, R. H. Ritchie, N. Barber´an and J. Inkson, Phys. Rev. B **23,** 6486(1981).

[61] H. Ueba, Phys. Rev. B **45,** 3755(1992).

[62] W. Knoll, Annu. Rev. Phys. Chem. **49,** 569(1998).

[63] S. Herminghaus, J. Vorberg, H. Gau, R. Conradt, D. Reinelt, H. Ulmer, P. Leiderer and M. Przyrembel, Ann. Phys. Lpz. **6,** 425(1997).

[64] M. Malmqvist, Nature **261,** 186(1993).

[65] C. M. Braguglia, Chem. Biochem. Eng. Q. **12,** 183(1998).

[66] F. C. Chien and S. J. Chen, Biosensors Bioelectron. **20,** 633(2004).

[67] R. Berndt, J. K. Gimzewski and P. Johansson, Phys. Rev. Lett. **67,** 3796(1991).

[68] M. J. Shea and R. N. Compton, Phys. Rev. B **47,** 9967(1993).

[69] R. C. Jin, Y. W. Cao, C. A. Mirkin, K. L. Kelly, G. C. Schatz and J. G. Zheng, Science **294,** 1901(2001).

[70] R. Jin, C. Cao, E. Hao, G. S. M´etraux, G. C. Schatz and C. Mirkin, Nature **425,** 487(2003).

[71] B. Rothenh¨ausler and W. Knoll, Nature **332,** 615(1988).

[72] G. Fl¨atgen, K. Krischer, B. Pettinger, K. Doblhofer, H. Junkes and G. Ertl, Science **269,** 668(1995).

[73] J. G. Gordon and S. Ernst, Surf. Sci. **101,** 499(1980).

[74] B. Liedberg, C. Nylander and I. Lundstrom, Sensors Actuators **4,** 299(1983).

[75] S. C. Schuster, R. V. Swanson, L. A. Alex, R. B. Bourret and M. I. Simon, Nature **365,** 343(1993).

[76] P. Schuck, Curr. Opin. Biotechnol. **8,** 498(1997).

[77] J. Homola, S. S. Yee and G. Gauglitz, Sensors Actuators B **54,** 3(1999).

[78] A. R. Mendelsohn and R. Brend, Science **284,** 1948(1999).

[79] R. J. Green, R. A. Frazier, K. M. Shakesheff, M. C. Davies, C. J. Roberts and S. J. B. Tendler, Biomaterials **21,** 1823(2000).

[80] J. B. Pendry, Science **285,** 1687(1999).

[81] E. Prodan, C. Radloff, N. J. Halas and P. Nordlander, Science **302,** 419(2003).

[82] T. W. Ebbesen, H. J. Lezec, H. F. Ghaemi, T. Thio and P. A. Wolff, Nature **391,** 667(1998).

[83] H. J. Lezec, A. Degiron, E. Devaux, R. A. Linke, L. Martin-Moreno, F. J. Garcia-Vidal and T. W. Ebbesen, Science **297,** 820(2002).

[84] E. Ozbay, Science **311,** 189(2006).

[85] W. L. Barnes, A. Dereux and T. W. Ebbesen, Nature **424,** 824(2003).

[86] W. Nomura, M. Ohtsu and T. Yatsui, Appl. Phys. Lett. **86,** 181108(2005).

[87] M. Quinten, A. Leitner, J. R. Krenn and F. R. Aussenegg, Opt. Lett. **23,** 1331(1998).

[88] R. Charbonneau, P. Berini, E. Berolo and E. Lisicka-Shrzek, Opt. Lett. **25,** 844(2000).

[89] B. Lamprecht, J. R. Krenn, G. Schider, H. Ditlbacher, M. Salerno, N. Felid j, A. Leitner, F. R. Aussenegg and J. C. Weeber, Appl. Phys. Lett. **79,** 51(2001).

[90] T. Nikolajsen, K. Leosson, I. Salakhutdinov and S. I. Bozhevolnyi, Appl. Phys. Lett. **82,** 668(2003).

[91] J. R. Krenn, B. Lamprecht, H. Ditlbacher, G. Schider, M. Saleno, A. Leitner and F. R. Aussenegg, Europhys. Lett. **60,** 663(2002).

[92] J. R. Krenn and J. C. Weeber, Philos. Trans. R. Soc. Lond. Ser. A **362,** 739(2004).

[93] S. A. Maier, P. G. Kik, H. A. Atwater, S. Meltzer, E. Harel, B. E. Koel and A. A. G. Requicha, Nature Mater. **2,** 229(2003).

[94] W. A. Murray, S. Astilean and W. L. Barens, Phys. Rev. B **69,** 165407(2004).

[95] S. A. Maier, P. E. Barclay, T. J. Johnson, M. D. Friedman and O. Painter, Appl. Phys. Lett. **84,** 3990(2004).

[96] S. A. Maier, M. D. Friedman, P. E. Barclay and O. Painter, Appl. Phys. Lett. **86,** 071103(2005).

[97] P. Berini, R. Charbonneau, N. Lahoud and G. Mattiussi, J. Appl. Phys. **98,** 043109(2005).

[98] I. V. Novikov and A. A. Maradudin, Phys. Rev. B **66,** 035403(2002).

[99] D. F. P. Pile and D. K. Gramotnev, Opt. Lett. **29,** 1069(2004).

[100] S. I. Bozhevilnyi, V. S. Volkov, E. Devaux and T. W. Ebbesen, Phys. Rev. Lett. **95,** 046802(2005).

[101] S. I. Bozhevilnyi, V. S. Volkov, E. Devaux, J.Y. Laluet and T. W. Ebbesen, Nature **440,** 508(2006).

[102] L. Bhasin and V. K. Tripathi, IEEE J. Quan. Elec., **46**(6), 965(2010).

[103] F. Kadlec, P. Kuzel and J. L. Coutaz, Opt. Lett., **29**(22), 2674(2004)

[104] F. Kadlec, P. Kuzel and J. L. Coutaz, Opt. Lett., **30**(11), 1402(2005).

[105] J. Kupersztych, P. Monchicourt, and M. Raynaud, Phys. Rev. Lett., **86**(22), 5180(2001).

Chapter 2

Plasma Effects in a Travelling Wave Tube

2.1 Introduction

Travelling wave tube (TWT) [1] continues to be the most widely used source of broad-band high power microwave generation at centimeter wavelengths. An electron beam passing through a slow wave structure excites a slow electromagnetic wave whose phase velocity closely equals the velocity of the beam. This phenomenon of Cerenkov emission is the basis of all travelling wave tubes. In order to have broad bandwidth microwave amplification, one frequently uses slow wave structures, such as a partially dielectric loaded waveguides [2], disc-loaded waveguide, or a helix [3] which slow down the phase velocity of the electromagnetic wave. In this regard, Chu and Jackson [4] have given a very elegant linear theory of TWT treating the helix as an anisotropic conducting surface. Uhm and Choe [3] examined the properties of the electromagnetic wave propagation through a helix loaded wave guide. Several authors later considered different aspects of travelling wave tube devices. However, a common feature to most of these theories is that they consider only a one-dimensional motion of electrons and ignore the effects of any background plasma.

As a matter of fact, the residual gases in the guiding system get ionized by the beam and a plasma of appreciable density is formed. Unless the vacuum is kept very high, the plasma density may be comparable or even larger than the density of beam. This should provide some degree of charge and current neutralization, allowing for higher beam current and guiding the beam without requiring a very strong guide field. Tripathi [5] has considered the effect of plasma

in a partially dielectric loaded parallel plane guiding system. The plasma modifies the mode structure considerably, leading to reduction in the growth rate, hence in the efficiency of the device. Talukdar and Tripathi [6] have studied the excitation of whistler modes in a cylindrical plasma column by a solid electron beam. The helix slows down the whistler mode and relaxes the requirements on the beam energy for the generation of a given frequency. Pant and Tripathi [7] have reported that plasma loaded sheath helix supports lower hybrid modes that extend outside to the vacuum region. An analysis of lower hybrid mode excitation by a beam propagating in the vacuum region reveals that nonlocal effects significantly reduce the growth rate.

In this chapter, we study the excitation of slow electromagnetic waves in a plasma-loaded sheath helix. We consider two cases of plasma: (i) a strongly magnetized plasma and (ii) unmagnetized plasma. In the first situation, plasma is strongly anisotropic whereas in the second it is isotropic. In section 2.2, we obtain the beam and plasma response to electromagnetic fields of a mode. In section 2.3, we study the mode structure. In section 2.4, we introduce the beam term into the wave equation and evaluate the growth rate of the slow wave mode. The results and discussion are discussed in section 2.5.

2.2 Beam and Plasma Response

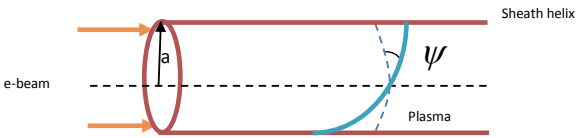

Fig 2.1 System Configuration

Consider a sheath helix, of radius 'a' and pitch angle ψ filled with plasma of density n_p^o. The helix is considered as an anisotropically conducting cylinder with infinite conductivity along the wire of the helix and zero conductivity across it. This is reasonable as long as the phase change over each element of length L of the periodic structure is considerably less than π. The plasma is cold and uniform and is subjected to an axial magnetic field $B_s\hat{z}$. We consider two cases : (i) B_s is very strong so that the plasma dynamics is one dimensional and (ii) when B_s is very small so that the plasma is isotropic. A thin hollow cylindrical electron beam of radius a, and density $n_b^o = N_b\delta(r-a)$ passes through the plasma with velocity $v_{ob}\hat{z}$. We perturb the equilibrium by an azimuthally symmetric microwave eigen mode with electric and magnetic fields,

$$\vec{E} = \vec{A}(r)e^{-i(\omega t-kz)},$$
$$\vec{B} = \vec{A}'(r)e^{-i(\omega t-kz)}.$$

The beam and plasma response to these fields is governed by the equation of motion,

$$m\left[\frac{\partial\vec{v}}{\partial t}+(\vec{v}\cdot\nabla)\vec{v}\right] = -e\vec{E}-\frac{e}{c}\vec{v}\times\vec{B}, \qquad (2.1)$$

where –e and m are the electronic charge and mass. For beam electrons when $\omega - kv_{ob} << \omega_c$, where ω_c is the electron cyclotron frequency, only the $\hat{z}$ component of velocity is important. Writing $v_{bz} = v_{ob} + v_{1bz}$ and Linearizing Eq. (2.1), i.e. , ignoring the products of perturbed quantities we obtain

$$\frac{\partial v_{1bz}}{\partial t} + v_{ob}\frac{\partial v_{1bz}}{\partial z} = -\frac{eE_z}{m}.$$

Replacing $\partial/\partial t$ by $-i\omega$ and $\partial/\partial z$ by ik we obtain,

$$v_{1bz} = \frac{eE_z}{mi(\omega - kv_{ob})}. \tag{2.2}$$

The equation of continuity governing the beam density is

$$\frac{\partial n_b}{\partial t} + \nabla \cdot (n_b \vec{v}_b) = 0. \tag{2.3}$$

Writing $n_b = n_{ob} + n_{1b}$ and linearizing it we get

$$\frac{\partial n_{1b}}{\partial t} + \frac{\partial}{\partial z}(n_{ob} v_{1bz} + n_{1b} v_{ob}) = 0,$$

giving the density perturbation

$$n_{1b} = \frac{n_b^o ekE_z}{mi(\omega - kv_{ob})^2}. \tag{2.4}$$

The perturbed beam current density can be written as

$$\vec{J}_b = -n_b^o e\vec{v}_b - n_b e\vec{v}_{ob}, \tag{2.5}$$

$$= -\frac{n_b^o e^2 \omega E_z}{mi(\omega - kv_{ob})^2}\hat{z}. \tag{2.6}$$

The response of plasma electrons, in the limit $\omega << \omega_c$, can also be taken to be one dimensional and can be recovered from the beam response by taking $v_{ob} = 0$ and replacing beam parameters by plasma parameters,

$$\vec{J}_p = -\frac{n_p^o e^2}{mi\omega} E_z \hat{z}. \tag{2.7}$$

In the opposite limit, $\omega >> \omega_c$, the plasma is unmagnetised and one can write,

$$\vec{J}_p = -\frac{n_p^o e^2}{mi\omega} \vec{E}. \tag{2.8}$$

2.3 Mode Structure

The wave equation for the mode is

$$\nabla^2 \vec{E} - \nabla(\nabla \cdot \vec{E}) + \frac{\omega^2}{c^2} \underline{\underline{\varepsilon}} \cdot \vec{E} = -\frac{4\pi i \omega}{c^2} \vec{J}_b, \tag{2.9}$$

where $\underline{\underline{\varepsilon}}$ is dielectric tensor. For the strong magnetized case($\omega, \omega_p << \omega_c$), $\varepsilon_{xx} = \varepsilon_{yy} = 1, \varepsilon_{zz} = 1 - \omega_p^2 / \omega^2$, $\varepsilon_{xy} = \varepsilon_{yx} = \varepsilon_{zx} = \varepsilon_{xz} = 0$, where $\omega_p = (4\pi n_p^o e^2 / m)^{1/2}$ is the electron plasma frequency. Using Maxwell's equations the radial component of the electric field can be expressed in terms of the axial component, as,

$$E_r = -\frac{ik}{\alpha^2} \frac{\partial E_z}{\partial r}, \tag{2.10}$$

where $\alpha^2 = k^2 - \omega^2 / c^2$. Taking z-component of Eq.(2.9) and using Eqs.(2.6) and (2.10) we obtain

$$\frac{\partial^2 E_z}{\partial r^2} + \frac{1}{r} \frac{\partial E_z}{\partial r} - \beta^2 E_z = -\frac{\omega_{pb}^2 \delta(r-a) \alpha^2 E_z}{(\omega - k v_{ob})^2}, \tag{2.11}$$

where $\omega_{pb} = (4\pi N_b e^2/m)^{1/2}$, is the beam plasma frequency and $\beta^2 = \alpha^2 \varepsilon_{zz}$. Similarly from third and fourth Maxwell's equations, $\nabla \times \vec{E} = -(1/c)\partial \vec{B}/\partial t$, $\nabla \times \vec{H} = 4\pi \vec{J}/c + (1/c)\partial \vec{D}/\partial t$, the wave equation for the z-component of H can be obtained as

$$\frac{\partial^2 H_z}{\partial r^2} + \frac{1}{r}\frac{\partial H_z}{\partial r} - \alpha^2 H_z = 0, \tag{2.12}$$

where we have employed the fact that the z-component of curl of beam current vanishes. In the case of an unmagnetized plasma Eqs.(2.11) and (2.12) are still valid with $\beta = \alpha_1$, $\alpha_1^2 = k^2 + \omega_p^2/c^2 - \omega^2/c^2$ inside the plasma and $\alpha^2 = k^2 - \omega^2/c^2$ outside. We consider three distinct cases,

Case (i) **Strongly magnetized plasma with** $\omega_p < \omega$

In this case, when one ignores the beam contribution, Eqs. (2.11) and (2.12) have the solutions

$$\begin{aligned} E_z &= A_1' I_o(\beta r), && r < a \\ &= A_2' K_o(\alpha r), && r > a \end{aligned}, \tag{2.13}$$

$$\begin{aligned} H_z &= A_3' I_o(\alpha r), && r < a \\ &= A_4' K_o(\alpha r), && r > a \end{aligned}. \tag{2.14}$$

The transverse components of electromagnetic fields can be obtained from Maxwell's equations ,

$$E_r = -\frac{ik}{\alpha^2}\frac{\partial E_z}{\partial r}, \tag{2.15}$$

$$E_\phi = \frac{i\omega}{\alpha^2 c}\frac{\partial H_z}{\partial r}, \tag{2.16}$$

$$H_r = \frac{ic}{\omega}\frac{\partial E_\phi}{\partial z}, \tag{2.17}$$

$$H_\phi = \frac{\omega}{kc}E_r. \tag{2.18}$$

The boundary conditions at the anisotropic helix [7, 8] surface(r=a) are,

1) E_z and H_z are continuous across the helix surface

$$\begin{aligned} E_z^i &= E_z^o, \\ H_z^i &= H_z^o. \end{aligned} \tag{2.19}$$

2) The electric field disappears in the direction of current flow

$$E_z^i \sin\psi + E_\phi^i \cos\psi = 0. \tag{2.20}$$

3) The component of the magnetic field in the direction of conduction is continuous as no current flows perpendicular to it, viz,

$$H_z^i \sin\psi + H_\phi^i \cos\psi = H_z^o \sin\psi + H_\phi^o \cos\psi. \tag{2.21}$$

These lead to the dispersion relation for the slow mode,

$$\frac{c^2\alpha^3 \tan^2\psi}{\beta\omega^2} = \frac{I_1(\alpha a)K_1(\alpha a)}{I_o(\beta a)K_o(\alpha a)}\left[\frac{K_o(\alpha a)I_1(\beta a) + \frac{\alpha}{\beta}I_o(\beta a)K_1(\alpha a)}{K_o(\alpha a)I_1(\alpha a) + I_o(\alpha a)K_1(\alpha a)}\right], \tag{2.22}$$

with $A_2' = \frac{I_o(\beta a)}{K_o(\alpha a)}A_1'$, $A_3' = \frac{i\alpha c I_o(\beta a)\tan\psi}{\omega I_1(\alpha a)}A_1'$, $A_4' = \frac{i\alpha c}{\omega}\frac{I_o(\beta a)I_o(\alpha a)\tan\psi}{K_o(\alpha a)I_1(\alpha a)}A_1'$.

In a sheath helix loaded TWT, the wave even when there is no plasma, is evanescent outside the helix and the phase velocity tends to saturate as the frequency increases. For the other values of ψ the graph is plotted and it is found that by decreasing the pitch angle the phase velocity as well as growth rate increase. As the nature of graph remain same for other values of pitch angle that's why we select cotψ =13.

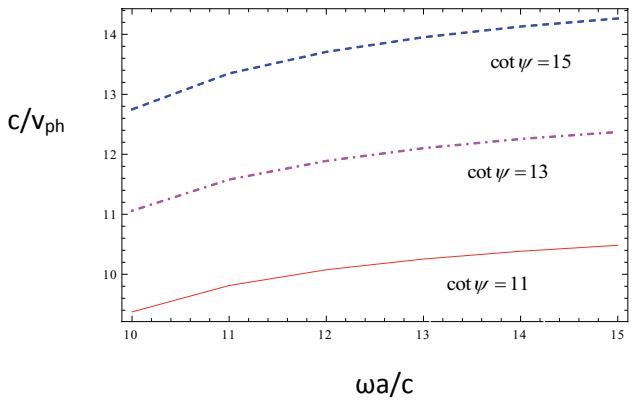

Fig 2.2 Retardation c/v_{ph} of a shielded helix (a, helix radius)

We have solved it numerically for the following parameters: cotψ=13, $\omega_p a/c$=2-5. In fig. 2.3 we plot normalized phase velocity c/v_{ph} of the slow mode vs. frequency ωa/c for different $\omega_p a/c$ values. For $\omega_p a/c$=2,4,5 the normalized phase velocity c/v_{ph} rises slowly with normalized frequency, attaining saturation at higher ωa/c values.

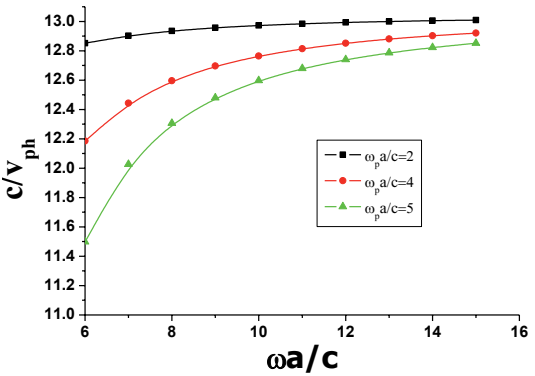

Fig 2.3 Retardation c/v_{ph} of a shielded helix (a, helix radius) for cotψ=13

Case (ii) **Strongly magnetized plasma with** $\omega_p > \omega$

In this case, the solution of Eq. (2.11),on neglecting the contribution of the beam turns out to be

$$\begin{aligned} E_z &= A_1' J_o(\beta_1 r) \qquad r < a \\ &= A_2' K_o(\alpha r) \qquad r > a, \end{aligned} \tag{2.23}$$

where $\beta_1 = \left(k^2 - \frac{\omega^2}{c^2}\right)\left(\frac{\omega_p^2}{\omega^2} - 1\right)$. The solution for H_z is still given by Eq.(2.14). Applying the boundary conditions as above, one obtains the dispersion relation

$$\frac{c^2\alpha^3 \tan^2\psi}{\beta\omega^2} = -\frac{J_1(\alpha a)K_1(\alpha a)}{J_o(\beta_1 a)K_o(\alpha a)}\left[\frac{K_o(\alpha a)J_1(\beta_1 a) - \frac{\alpha}{\beta_1}J_o(\beta_1 a)K_1(\alpha a)}{K_o(\alpha a)J_1(\alpha a) - J_o(\alpha a)K_1(\alpha a)}\right] \tag{2.24}$$

with $A_2' = \frac{J_o(\beta a)}{K_o(\alpha a)} A_1'$, $A_3' = \frac{i\alpha c J_o(\beta a)\tan\psi}{\omega J_1(\alpha a)} A_1'$, $A_4' = \frac{i\alpha c}{\omega} \frac{J_o(\beta a) J_o(\alpha a)\tan\psi}{K_o(\alpha a) J_1(\alpha a)} A_1'$.

We have solved it numerically for cotψ=13, $\omega_p a/c$=20-40. Fig. 2.4 shows the variation of normalized phase velocity c/v_{ph} of the slow mode vs. frequency ωa/c for different $\omega_p a/c$ values. One may note that the phase velocity of the slow mode does not vary appreciably as the normalized frequency goes from 6 to 16. It also does not vary much from $\omega_p a/c$ goes from 20 to 40. However the phase velocity is larger than in the case of no plasma.

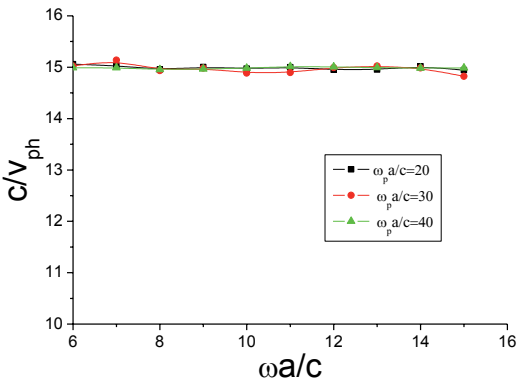

Fig. 2.4 Retardation c/v_{ph} of a shielded helix (a, helix radius) for cotψ=13

Case (iii) **Unmagnetised plasma**

In the case of unmagnetised plasma, the dielectric constant becomes scalar and $\nabla \cdot \vec{E} = 0$, so the wave equation (2.11) takes the form

$$\frac{\partial^2 E_z}{\partial r^2}+\frac{1}{r}\frac{\partial E_z}{\partial r}-\alpha'^2 E_z=-\frac{\omega_{pb}^2\omega^2\delta(r-a)E_z}{(\omega-kv_{ob})^2c^2}, \tag{2.25}$$

where $\alpha'^2=\alpha_1^2$ for $r<a, \alpha_1^2=k^2-(\omega^2-\omega_p^2)/c^2$ and $\alpha'^2=\alpha^2$ for $r>a$. Solving Eq.(2.25) , one obtains

$$\begin{aligned} E_z &= A_5' I_o(\alpha_1 r), && r<a \\ &= A_6' K_o(\alpha r), && r>a \end{aligned}. \tag{2.26}$$

Similarly for H_z

$$\begin{aligned} H_z &= A_7' I_o(\alpha r), && r<a \\ &= A_8' K_o(\alpha r), && r>a \end{aligned}. \tag{2.27}$$

The dispersion relation obtained in this case is

$$\frac{c^2\alpha^3\tan^2\psi}{\alpha_1\omega^2}=\frac{I_1(\alpha a)K_1(\alpha a)}{I_o(\alpha_1 a)K_o(\alpha a)}\left[\frac{K_o(\alpha a)I_1(\alpha_1 a)+\frac{\alpha}{\alpha_1}I_o(\alpha_1 a)K_1(\alpha a)}{K_o(\alpha a)I_1(\alpha a)+I_o(\alpha a)K_1(\alpha a)}\right] \tag{2.28}$$

We have solved it numerically for cotψ=13, $\omega_p a/c$=5, 7, 9. Fig. 2.5 shows the variation of normalized phase velocity c/v_{ph} of the slow mode vs. frequency ωa/c for different $\omega_p a/c$ values. For $\omega_p a/c$=5, 7, 9 the normalized phase velocity c/v_{ph} rises with normalized frequency, attaining saturation at higher ωa/c values.

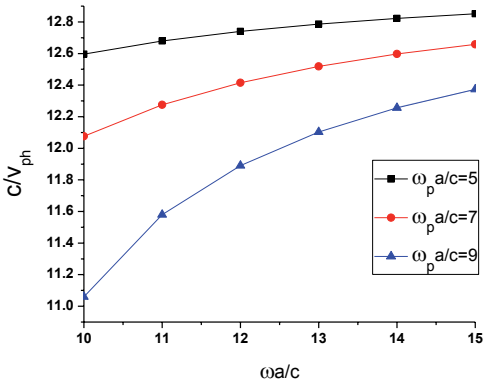

Fig 2.5 Retardation c/v_{ph} of a shielded helix (a, helix radius) for $\cot\psi$=13

2.4 Growth rate

Case (i) **Strongly magnetized plasma with** $\omega_p < \omega$

With finite beam term, we presume that the mode structures remain unmodified, only the eigen frequencies are modified. Thus we write

$$\begin{aligned} \vec{E} &= A_1(t)\vec{E}_s, \\ \vec{H} &= A_2(t)\vec{H}_s, \end{aligned} \tag{2.29}$$

where,

$$\begin{aligned} E_{sz} &= A_1' I_o(\beta r) e^{-i(\omega t - kz)}, && r < a \\ &= \frac{A_2'}{A_1'} K_o(\alpha r) e^{-i(\omega t - kz)}, && r > a \end{aligned} \tag{2.30}$$

$$H_{sz} = \frac{A_3'}{A_1'} I_o(\alpha r) e^{-i(\omega t - kz)}, \qquad r < a$$
$$= \frac{A_4'}{A_1'} K_o(\alpha r) e^{-i(\omega t - kz)}, \qquad r > a \quad , \tag{2.31}$$

where $\vec{E}_s$ and $\vec{H}_s$ represent the mode structures of the electromagnetic fields and satisfy the Maxwell's equations without the beam term,

$$\nabla \times \vec{E}_s = -\frac{i\omega}{c} \vec{H}_s ,$$

$$\nabla \times \vec{H}_s = -\frac{i\omega}{c} \underline{\underline{\varepsilon}} \cdot \vec{E}_s .$$

Using Eq.(2.29) in the Maxwell's equation $\nabla \times \vec{E} = -\frac{1}{c}\frac{\partial \vec{H}}{\partial t}$, one obtains

$$A_1(t) \nabla \times \vec{E}_s = -\frac{1}{c} A_2(t) \frac{\partial \vec{H}_s}{\partial t} - \frac{1}{c} \frac{\partial A_2(t)}{\partial t} \vec{H}_s \tag{2.32}$$

or $$\frac{\partial A_2(t)}{\partial t} = -i\omega \left(A_1(t) - A_2(t) \right) \tag{2.33}$$

since $\partial / \partial t$ variation is slow as compared to $i\omega$, Eq.(2.33) tells that

$$A_1(t) \approx A_2(t) \text{ or } \frac{\partial A_1}{\partial t} \approx \frac{\partial A_2}{\partial t}. \tag{2.34}$$

Similarly, from the fourth Maxwell's equation,

$$\nabla \times \vec{H} = \frac{4\pi \vec{J}_b}{c} + \frac{1}{c} \underline{\underline{\varepsilon}} . \frac{\partial \vec{E}}{\partial t} \quad , \tag{2.35}$$

on using Eqs.(2.31) and (2.34) and taking the z-component one obtains,

$$\frac{\partial A_1(t)}{\partial t}\varepsilon_{zz}E_{sz} = -4\pi J_{bz}, \tag{2.36}$$

where E_{sz} is the z-component of $\vec{E}_s$, multiplying on both sides by $E_{sz}^* r dr$, and integrating over r from r=0 to r=∞, we obtain

$$\frac{\partial A_1(t)}{\partial t} = -\frac{4\pi\int_0^\infty J_{bz}E_{sz}^* r dr}{\varepsilon_{zz}\int_0^\infty E_{sz}E_{sz}^* r dr} = \frac{\omega_{pb}^2\omega a^2\left|E_{sz}^2\right|_{r=a}}{(\omega - kv_{ob})^2 F_1\varepsilon_{zz}}A_1, \tag{2.37}$$

where $F_1 = \int_0^\infty E_{sz}E_{sz}^* r dr = \int_0^a I_o^2(\beta r) r dr + \frac{I_o^2(\beta a)}{K_o^2(\alpha a)}\int_a^\infty K_o^2(\alpha r) r dr$.

One may note that resonant contribution from the beam comes when ω=kv$_{ob}$. The growth of the wave leads to amplitude being a function of time. Thus we write $\omega = \omega_r + \delta$, $\omega_r = kv_{ob}$, $\partial A_1/\partial t = i\delta A_1$. Then Eq. (2.37) gives

$$\delta = \left(\frac{\omega_{pb}^2\omega G}{\varepsilon_{zz}}\right)^{1/3} e^{i(2l+1)\pi/3}, \tag{2.38}$$

where $G = \frac{\left|E_{sz}\right|^2 a^2}{F_1}$, l is integer. For l=0, one obtains a growing mode with growth rate $\gamma = \mathrm{Im}(\delta)$ as

$$\gamma = \frac{\sqrt{3}}{2}\left[\frac{\omega_{pb}^2\omega G}{\varepsilon_{zz}}\right]^{1/3}. \tag{2.39}$$

We have plotted in fig. 2.6 the variation of growth rate as a function of normalized frequency. The growth rate increases with frequency. As one increases the plasma frequency the growth rate is enhanced. This is because the mode has higher field concentration inside the helix than outside. In sheath helix loaded TWT, the theory is valid for the frequency $\omega << c/(2\pi a \cot\psi)$ where a is the radius of sheath helix, that's why the normalized frequency range selected, conforms to that range only. At higher frequencies multiple space harmonics become important. One cannot conjecture the growth rate in that case.

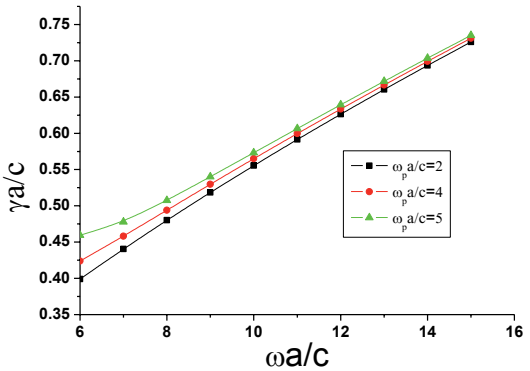

Fig 2.6 Growth rate for $\omega_p < \omega$ for cotψ=13

One may note that δ has a negative real part $\delta = -\gamma/\sqrt{3}$, i.e. , $\omega = kv_{ob} + \delta_r$ or $\omega/k < v_{ob}$. The beam propagates slightly faster than the phase velocity of the wave. This may be understood physically as follows. The beam interacts with only E_z and moves along z axis, hence as far as the beam response is concerned, one may write $E_z = A'\cos(\omega t - kz)$. One may

visualize the beam interaction with E_z in the moving frame, moving with velocity $(\omega/k)\hat{z}$. In this frame the $E_z = A'\cos kz'$ (cf. Fig 2.7). The electric field is –ve in some regions and +ve in others. The regions with negative E_z exert a force along $\hat{z}$ on the electrons and are called accelerating zones. The ones with +ve E_z are called the retarding zones. In the moving frame the beam velocity is $v_{ob} - \omega/k$ which is positive, i.e. , the beam electrons move with a +ve but small velocity. The beam electrons that are in the accelerating zones move faster and quickly go over to the retarding zones. The ones in the retarding zones get slowed down and spend more time over there. Thus there is net bunching of electrons in the retarding zones , and net retardation of electron occurs, giving energy to the wave.

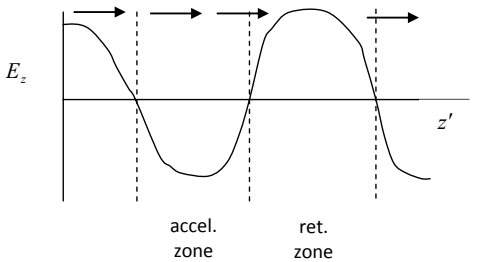

Fig 2.7 Schematic of beam-wave interaction

Case (ii) **Strongly magnetized plasma with** $\omega_p > \omega$

For $\omega_p > \omega$, following the steps as given above, one obtains

$$\gamma = \frac{\sqrt{3}}{2}\left[-\frac{\omega_{pb}^2 \omega G'}{\varepsilon_{zz}}\right]^{1/3}, \tag{2.40}$$

where $G' = \frac{|E_{sz}|^2 a^2}{F_2}$, $F_2 = \int_0^\infty E_{sz} E_{sz}^* r dr = \int_0^a J_o^2(\beta_1 r) r dr + \frac{J_o^2(\beta_1 a)}{K_o^2(\alpha a)} \int_a^\infty K_o^2(\alpha r) r dr$. The variation of growth rate with frequency is shown in fig. 2.8. The growth rate shows oscillatory behavior and decreases with increasing plasma density for $\omega_p > \omega$.

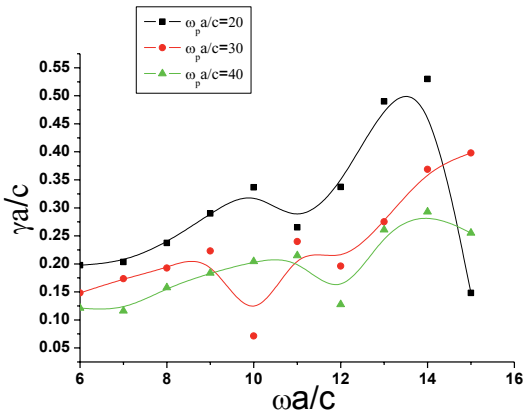

Fig 2.8 Growth rate for $\omega_p > \omega$ for cotψ=13

Case (iii) **Unmagnetized plasma**

In this case one obtains

$$\gamma = \frac{\sqrt{3}}{2} \left[\frac{\omega_{pb}^2 \omega G}{(1 - \frac{\omega_p^2}{\omega^2})} \right]^{1/3}, \qquad (2.41)$$

where $G = \frac{|E_{sz}|^2 a^2}{F_3}$, $F_3 = \int_0^\infty E_{sz} E_{sz}^* r dr = \int_0^a I_o^2(\alpha_1 r) r dr + \frac{I_o^2(\alpha_1 a)}{K_o^2(\alpha a)} \int_a^\infty K_o^2(\alpha r) r dr$. We have plotted in fig. 2.9 the variation of growth rate as a function of normalized frequency. The growth rate increases with frequency. As one increases the plasma frequency the growth rate is enhanced. This is because the mode has higher field concentration inside the helix than outside.

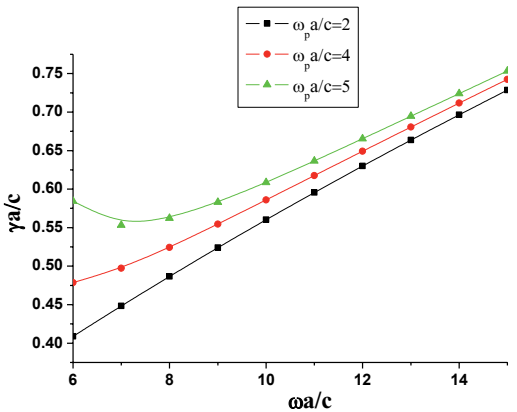

Fig 2.9 Growth rate for unmagnetized plasma for cotψ=13

2.5 Results and discussion

The presence of a strongly magnetized plasma drastically changes the mode structure of the azimuthally symmetric mode at $\omega_p = \omega$. For $\omega_p < \omega$ the mode is evanescent in r inside as well as outside the helix. For $\omega_p > \omega$ the axial electric field has a Bessel function behavior in the interior whereas modified Bessel function behavior outside the helix. The axial magnetic field has modified Bessel function behavior both inside and outside. For $\omega_p < \omega$ as one raises ω_p / ω,

both the phase velocity and the growth rate increases. In a strongly magnetized plasma with $\omega_p > \omega$, mode structure is periodic in r and ω. Since the growth rate is dependent on the mode structure it also varies periodically with frequency. For a broadband TWT this behavior is not desirable. However, for TWT operation at a specific frequency one can choose parameters corresponding to peak in the growth rate. For unmagnetised plasma the mode is more strongly localized close to the helix and the growth rate increases.

The phase velocity of the unstable mode is slightly lower than the beam velocity. As the beam loses energy to the wave and its average velocity falls down to the phase velocity of the mode, the growth of the microwave should stop. From this one may have a rough estimate of efficiency as

$$\eta = (\frac{1}{2}mv_{ob}^2 - \frac{1}{2}m(\omega/k)^2)/(\frac{1}{2}mv_{ob}^2) \approx \delta_r/\omega \approx 2\gamma/\sqrt{3\omega}.$$

By tapering the helix one may have a higher efficiency.

References

[1] C.S.Liu and V.K.Tripathi, *Electromagnetic Theory for Telecommunications* (Cambridge University Press India Pvt. Ltd, 2007), Chap. 3.

[2] J.Y.Choe, H.S.Uhm, and S.Ahn, J. Appl. Phys. **52**, 7067(1981).

[3] H.S.Uhm and J.Y.Choe, J.Appl. Phys. **53**, 8483(1982).

[4] L.J.Chu and J.D.Jackson, Proc. IRE **36**, 853(1948).

[5] V.K.Tripathi, J.Appl. Phys. **56** ,1953(1984).

[6] I.Talukdar and V.K.Tripathi, J.Appl.Phys., **65**, 1479(1989).

[7] K.K.Pant and V.K.Tripathi, IEEE Transactions on Plasma Science, **20**, 973(1992).

[8] R. Chatterjee, *Elements of Microwave Engineering* (Affiliated East-West Press Pvt Ltd, New Delhi 1994), Chap. 9.

Chapter 3

Resonant Beat Wave Excitation of Terahertz Radiation in a Magnetized Plasma Channel

3.1 Introduction

Terahertz(THz) radiation generation has attracted much attention in recent years, as these waves have potential applications in biological imaging [1], remote sensing [2], spectroscopy of solids and liquids, chemical and security identification [3] etc. Conventional sources of THz radiation using short pulse lasers in semiconductors and electro optic crystals are generally limited to energies of the order of μJ/pulse. THz emissions have also been produced from plasmas using energetic electron beams and subpicosecond laser pulses. These include coherent radiation from plasma oscillations driven by ultrashort laser pulses [4], transition radiation of electron beams [5, 6], synchrotron radiation from accelerator electrons [7, 8], Cherenkov wake radiation in magnetised plasmas [9,10] and emission from laser plasma channels in air [11]. Antonsen et al [2] have presented a scheme for THZ radiation generation that involves the creation of miniature corrugated plasma channels of period ~ 40μm. The channel supports laser eigen mode with subluminal phase velocity while radial ponderomotive force due to the mode causes THz radiation generation. Gildenburg et al [18] have proposed a novel scheme of THz generation where THz power scales linearly with the laser power. A femtosecond laser pulse of intensity ~ 10^{14} W/cm^2 is line focussed on a gas through a circular grating-axicon assembly. The pulse tunnel ionises the gas, forming a thin plasma cylinder. The electrons produced during the laser pulse retain transverse momentum after the pulse is gone and set in transverse oscillations

of the plasma cylinder at frequency $\omega \approx \omega_{po}/\sqrt{2}$. Liu and Tripathi [13] have examined the effect of an ambient magnetic field and density ripple on this scheme. The magnetic field provides the frequency tunability while the density ripple controls the angular orientation of the emitted THz radiation. Recent experiments have shown enhanced coherent emission of terahertz radiation from semiconductor surfaces in the presence of magnetic fields. Mclaughlin et al [12] demonstrated continuous increase in terahertz electric field with increasing magnetic field up to B=8 Tesla.

In this chapter we investigate the beat excitation of THz radiation using Gaussian laser beams co-propagating along the direction of ambient magnetic field in a rippled density plasma channel. The density ripple could be produced by laser machining [14, 15] or using axicon-circular grating assembly [16]. The lasers impart oscillatory velocity to plasma electrons and exert a ponderomotive force on them at the beat frequency. The ponderomotive force has transverse component that drives nonlinear current producing THz radiation. In section 3.2 we formulate the problem and solve for beat frequency nonlinear current source. In section 3.3 we solve for THz radiation generation. In section 3.4 we determine the power of the THz radiation. In section 3.5 a brief discussion of results is given.

3.2 Beat Frequency Current Density

Consider a rippled density plasma channel, created by a machining prepulse [14, 15] or by a pulse employing circular grating-axicon assembly [16]. The plasma density can be taken as

$$n_o = n_o' + n_q' \quad , \tag{3.1}$$

$$n_o' = n_o^o(1+\frac{r^2}{r_c^2}), n_q' = n_q(1+\frac{r^2}{r_c^2})e^{iqz} \ ,$$

where q is the ripple wave number, r_c is the plasma channel width and the real part of above equation is implied. The plasma has a static magnetic field $B_s\hat{z}$. Two laser beams with electric fields

$$\vec{E}_j = \vec{A}_j e^{-i(\omega_j t - k_j z)}, j = 1,2, \tag{3.2}$$

propagate through the channel with $\omega_j \rangle \omega_c = eB_s/mc$, where-e and m are the electron charge and mass, ω_c is the electron cyclotron frequency and c is the velocity of light in free space. The amplitude of the lasers, ignoring the effect of the ripple, are governed by

$$\frac{\partial^2 \vec{A}_j}{\partial r^2} + \frac{1}{r}\frac{\partial \vec{A}_j}{\partial r} + \left[\frac{\omega_j^2}{c^2} - k_j^2 - \frac{\omega_{po}^2}{c^2}\left(1 + \frac{r^2}{r_c^2}\right)\right]\vec{A}_j = 0, \tag{3.3}$$

where $\omega_{po} = (4\pi n_o^o e^2 / m)^{1/2}$. Eq. (3.2), for the fundamental modes gives

$$\vec{A}_j = \vec{A}_{oj} e^{-\frac{r^2}{2r_o^2}}, \tag{3.4}$$

$$k_j^2 = \frac{\omega_j^2 - \omega_{po}^2}{c^2} - \frac{2\omega_{po}}{r_c c}, r_o = \left(\frac{r_c c}{\omega_{po}}\right)^{1/2}.$$

The lasers impart oscillatory velocities to electrons

$$\vec{v}_j = \frac{e\vec{E}_j}{mi\omega_j}, j = 1,2, \tag{3.5}$$

and exert a difference frequency ponderomotive force on them

$$\vec{F}_p = e\nabla\phi_p, \tag{3.6}$$

where

$$\phi_p = (\frac{m}{2e})\vec{v}_1.\vec{v}_2^* = \phi_{po} e^{-\frac{r^2}{r_o^2}} e^{-(\omega t - k'z)} \tag{3.7}$$

and $\phi_{po} = \frac{eA_{01}A_{02}}{2m\omega_1\omega_2}, \omega = \omega_1 - \omega_2, k' = k_1 - k_2$. The motion of electrons under the ponderomotive force is governed by the equation of motion

$$m\frac{\partial \vec{v}}{\partial t} = \vec{F}_p - \frac{e}{c}\vec{v} \times \vec{B}_s. \tag{3.8}$$

Linearising and solving for $\vec{v}$, one obtains

$$\begin{aligned} \vec{v}_\perp &= \frac{e\nabla\phi_p \times \vec{\omega}_c}{m(\omega^2 - \omega_c^2)} + \frac{i\omega e\nabla_\perp \phi_p}{m(\omega^2 - \omega_c^2)}, \\ v_z &= -\frac{ek'\phi_p}{m\omega}. \end{aligned} \tag{3.9}$$

This velocity beats with the density ripple to produce a nonlinear current density at $\omega, k' + q$,

$$\vec{J}^{NL} = -\frac{1}{2}n_q' e\vec{v} \quad , \tag{3.10}$$

with,

$$J_x^{NL} = -\frac{n_q' e^2}{2m(\omega^2 - \omega_c^2)}\left[\frac{\partial\phi_p}{\partial y}\omega_c + i\omega\frac{\partial\phi_p}{\partial x}\right] \quad , \tag{3.11}$$

$$J_y^{NL} = \frac{n_q' e^2}{2m(\omega^2 - \omega_c^2)}\left[\frac{\partial\phi_p}{\partial x}\omega_c - i\omega\frac{\partial\phi_p}{\partial y}\right]. \tag{3.12}$$

3.3 THz Generation

The wave equation governing the terahertz wave field is

$$\nabla^2\vec{E}-\nabla(\nabla\cdot\vec{E})+\frac{\omega^2}{c^2}\underline{\underline{\varepsilon}}\cdot\vec{E}=-\frac{4\pi i\omega}{c^2}\vec{J}^{NL} \tag{3.13}$$

where $\varepsilon_{xx}=\varepsilon_{yy}=1-\omega_{po}^2/\left(\omega^2-\omega_c^2\right),\varepsilon_{xy}=-\varepsilon_{yx}=i(\omega_c/\omega)\omega_{po}^2/\left(\omega^2-\omega_c^2\right),\ \varepsilon_{zz}=1-\omega_{po}^2/\omega^2,$

$\varepsilon_{xz}=\varepsilon_{zx}=\varepsilon_{yz}=\varepsilon_{zy}=0.$ In principle the THz could have both the extraordinary ($E_y=iE_x$) and ordinary ($E_y=-iE_x$) modes but the phase matching condition can be satisfied only for one of them. Following Sodha [17] et al we consider the extraordinary mode to be in resonance, i.e., $E_y=iE_x$ .Taking $\nabla\cdot$ of Eq.(3.13), we have

$$\frac{\partial E_z}{\partial z}=-\frac{1}{\varepsilon_{zz}}\left[\frac{\partial}{\partial x}(\varepsilon_{xx}E_x+\varepsilon_{xy}E_y)+\frac{\partial}{\partial y}(\varepsilon_{xx}E_y-\varepsilon_{xy}E_x)\right]-\frac{1}{\varepsilon_{zz}}\frac{4\pi i}{\omega}\nabla\cdot\vec{J}^{NL}\ ,$$

which on using $E_y=iE_x$, gives

$$\nabla\cdot\vec{E}=(1-\frac{\varepsilon_+}{\varepsilon_{zz}})(\frac{\partial E_x}{\partial x}+i\frac{\partial E_x}{\partial y})--\frac{1}{\varepsilon_{zz}}\frac{4\pi i}{\omega}\nabla\cdot\vec{J}^{NL}, \tag{3.14}$$

where $\varepsilon_+=\varepsilon_{xx}+i\varepsilon_{xy}$. Ignoring spatial variation in ε_{xx}, ε_{xy}, ε_{zz}, (valid for paraxial approx.) using Eq.(3.14) in Eq. (3.13) we have

$$\nabla^2E_x-(1-\frac{\varepsilon_+}{\varepsilon_{zz}})\frac{\partial^2E_x}{\partial x^2}-i(1-\frac{\varepsilon_+}{\varepsilon_{zz}})\frac{\partial^2E_x}{\partial x\partial y}+\frac{\omega^2}{c^2}(\varepsilon_{xx}+i\varepsilon_{xy})E_x=R_x+\frac{4\pi}{i\omega\varepsilon_{zz}}\frac{\partial}{\partial x}(\nabla.\vec{J}^{NL})\ , \tag{3.15}$$

$$i\nabla^2 E_x - (1-\frac{\varepsilon_+}{\varepsilon_{zz}})\frac{\partial^2 E_x}{\partial x \partial y} - i(1-\frac{\varepsilon_+}{\varepsilon_{zz}})\frac{\partial^2 E_x}{\partial y^2} + \frac{\omega^2}{c^2}(i\varepsilon_{xx} - \varepsilon_{xy})E_x = R_y + \frac{4\pi}{i\omega\varepsilon_{zz}}\frac{\partial}{\partial y}(\nabla . \vec{J}^{NL}), \tag{3.16}$$

where $\vec{R} = -(4\pi i\omega / c^2)\vec{J}^{NL}$. Multiplying Eq. (3.16) by *i* and subtracting from Eq. (3.15), one obtains

$$\frac{\partial^2 E_x}{\partial z^2} + \frac{1}{2}(1+\frac{\varepsilon_+}{\varepsilon_{zz}})\nabla_\perp^2 E_x + \frac{\omega^2}{c^2}\varepsilon_+ E_x = \frac{1}{2}(R_x - iR_y) + \frac{4\pi}{i\omega\varepsilon_{zz}}(\frac{\partial}{\partial x} - i\frac{\partial}{\partial y})(\nabla . \vec{J}^{NL}), \tag{3.17}$$

where $\nabla_\perp^2 = \frac{\partial^2}{\partial x^2} + \frac{\partial^2}{\partial y^2}, \varepsilon_+ = 1 - \frac{\omega_p^2}{\omega(\omega - \omega_c)}, \varepsilon_{zz} = 1 - \frac{\omega_{po}^2}{\omega^2}$. In the limit $\partial/\partial x, \partial/\partial y << k' + q$ the last term in Eq(3.17) can be neglected. In the r-dependent density profile of Eq.(3.1), ε_+ can be written as $\varepsilon_{o+} + \varepsilon_{2+} r^2/r_c^2$, where $\varepsilon_{o+} = 1 - \omega_{po}^2/(\omega(\omega - \omega_c))$, $\varepsilon_{2+} = -(\omega_{po}^2/(\omega(\omega - \omega_c)))$. The $\varepsilon_{2+} r^2/r_c^2$ term is more pronounced in Eq.(3.17) than elsewhere, hence we write Eq.(3.17) as

$$\begin{aligned} &\frac{\partial^2 E_x}{\partial z^2} + \frac{1}{2}(1+\frac{\varepsilon_{o+}}{\varepsilon_{zz}})\nabla_\perp^2 E_x + \frac{\omega^2}{c^2}(\varepsilon_{o+} + \varepsilon_{2+}\frac{r^2}{r_c^2})E_x \\ &= \frac{1}{2}(\frac{\omega_{po}^2}{c^2})(\frac{\phi_{po} r}{r_o^2})(\frac{\omega}{\omega - \omega_c})(\frac{n_q}{n_o^o})(1+\frac{r^2}{r_c^2})e^{-\frac{r^2}{r_o^2}} e^{-i(\omega t - kz + \phi)}, \end{aligned} \tag{3.18}$$

where $k \equiv k' + q$.

Writing

$$E_x = A(r,z)e^{-i(\omega t - kz + \phi)} \tag{3.19}$$

Eq. (3.18) takes the form

$$2ik\frac{\partial A}{\partial z}+\frac{1}{2}(1+\frac{\varepsilon_{o+}}{\varepsilon_{zz}})(\frac{\partial^2 A}{\partial r^2}+\frac{1}{r}\frac{\partial A}{\partial r}-\frac{A}{r^2})+(\frac{\omega^2}{c^2}\varepsilon_{o+}-k^2-\frac{\omega^2}{c^2}\varepsilon_{2+}\frac{r^2}{r_c^2})A=G(r)$$
$$G(r)=\frac{1}{2}(\frac{\omega_{po}^2}{c^2})(\frac{\phi_{po}r}{r_o^2})(\frac{\omega}{\omega-\omega_c})(\frac{n_q}{n_o^o})(1+\frac{r^2}{r_c^2})e^{-\frac{r^2}{r_o^2}}. \tag{3.20}$$

If one ignores the first term on LHS and take G=0, then Eq.(3.20) becomes

$$\frac{\partial^2 A}{\partial r^2}+\frac{1}{r}\frac{\partial A}{\partial r}+(\alpha_1^2-\frac{1}{r^2}-\frac{r^2}{r_1^4})A=0 \tag{3.21}$$

where $\alpha_1^2=2(\frac{\omega^2}{c^2}\varepsilon_{o+}-k^2)/(1+\frac{\varepsilon_{o+}}{\varepsilon_{zz}}), r_1=(-r_c^2\frac{c^2}{\omega^2}(1+\frac{\varepsilon_{o+}}{\varepsilon_{zz}})/2\varepsilon_{2+})^{1/4}$.

Writing $\xi=r/r_1$, this equation takes the form

$$\frac{\partial^2 A}{\partial \xi^2}+\frac{1}{\xi}\frac{\partial A}{\partial \xi}+(\lambda-\frac{1}{\xi^2}-\xi^2)A=0, \tag{3.22}$$

where $\lambda=\alpha_1^2 r_1^2$. For the fundamental mode this equation gives

$$A=\psi(r)=\frac{r}{r_1}e^{-\frac{r^2}{2r_1^2}}, \tag{3.23}$$

with eigenvalue $\lambda = 4$. The phase matching condition requires

$$q=\left[\frac{\omega^2}{c^2}\varepsilon_{o+}-\left(-\frac{8\omega^2\varepsilon_{2+}(1+\frac{\varepsilon_{o+}}{\varepsilon_{zz}})}{c^2r_c^2}\right)^{1/2}\right]^{1/2}-k_1+k_2, \tag{3.24}$$

When the RHS of Eq.(3.20) is finite we write A as

$$A = F(z)\psi(r), \tag{3.25}$$

presuming that the eigen function remains the same only amplitude becomes function of z. Employing Eq. (3.25) in Eq.(3.20), multiplying the resulting equation by $\psi^* r dr$ and integrating over *r* from *0* to ∞ one obtains

$$\frac{\partial F}{\partial z} = -i\beta, \tag{3.26}$$

where $\beta = \frac{1}{8}\frac{\omega_{po}^2}{c^2}\frac{\phi_{po}}{r_o^2}\frac{\omega}{\omega-\omega_c}\left(\frac{r_2^4}{2}+\frac{r_2^6}{r_c^2}\right)\frac{1}{kr_1^3}$ $\quad , r_2 = \frac{1}{\left(\frac{1}{2r_1^2}+\frac{1}{r_o^2}\right)^{1/2}}$.

Had one included the collisional damping of the terahertz wave, Eq. (3.26) would take the form

$$\frac{\partial F}{\partial z} + k_i F = -i\beta, \tag{3.27}$$

At large values of z this gives

$$F = -i\beta / k_i, \tag{3.28}$$

where, $k_i = \frac{\omega_{po}^2 \nu}{2c((\omega-\omega_c)^2+\nu^2)\left(1-\frac{\omega_{po}^2(\omega-\omega_c)}{\omega((\omega-\omega_c)^2+\nu^2)}\right)^{1/2}}$.

So the normalized amplitude of terahertz wave is

$$\left|\frac{F}{A_{01}}\right| = \left|\frac{1}{8}\left(\frac{1}{k'k_i'r_1'}\left(\frac{r_2'^4}{2r_1'^2r_o'^2}+\frac{r_2'^6}{r_1'^2r_o'^2r_c'^2}\right)\right)\frac{\omega'}{\omega'-\omega_c'}\left(\frac{A_{02}'}{\omega_1'\omega_2'}\right)n_q'\right| \tag{3.29}$$

where $A'_{02} = eA_{02}/mc\omega_{po}, n'_q = n_q/n_o^o$ and all the primed quantities are normalized w.r.t. ω_{po}. The plot of normalized ripple factor $|qc/\omega_{po}|$ as a function of normalized frequency $|\omega/\omega_{po}|$ is plotted in fig.3.1. The relevant parameters are $\omega'_c = 0.2, r'_c = 3, \nu' = 10$. It is observed that for $\omega_c/\omega_{po} \approx 0.2$, the normalized ripple factor decreases steadily from 0.77 to 0.15 as ω/ω_{po} is varied from 2 to 10.

.

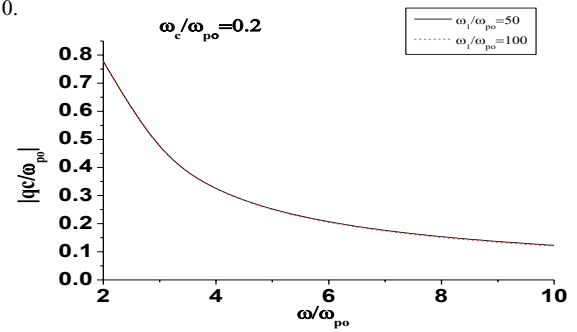

FIG. 3.1 Normalized density ripple wavenumber|qc/ω_{po}| as a function of normalized frequency ω/ω_{po} for the value of $\omega'_c = 0.2, r'_c = 3, \nu' = 10$.

Also in fig. (3.2) we have plotted requisite normalized ripple wave number for $\omega'_c = 0.2, 0.6$. The requisite plasma density for the THz generation is $1.2\times10^{16} cm^{-3}$. As the magnetic field increases, the required ripple wave number for phase matched terahertz generation rises. In fig. (3.3) we plot normalized terahertz amplitude as a function of normalized frequency ω/ω_{po} for $\omega_1/\omega_{po} = 50, 100$. It is observed that for $\omega_c/\omega_{po} \approx 0.2$, the normalized THz amplitude decreases monotonically from 5.56x10^{-4} to 1.5x10^{-4} as ω/ω_{po} is varied from 2 to 10 for $\omega_1/\omega_{po} = 50$.

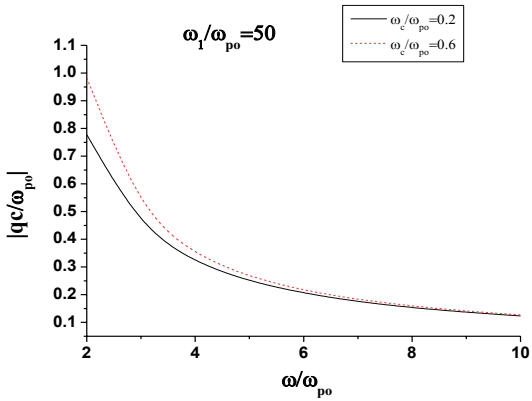

FIG. 3.2 Normalized density ripple wavenumber$|qc/\omega_{po}|$ as a function of normalized frequency ω/ω_{po} for the value of $\omega_c' = 0.2,0.6, r_c' = 3, \nu' = 10.$

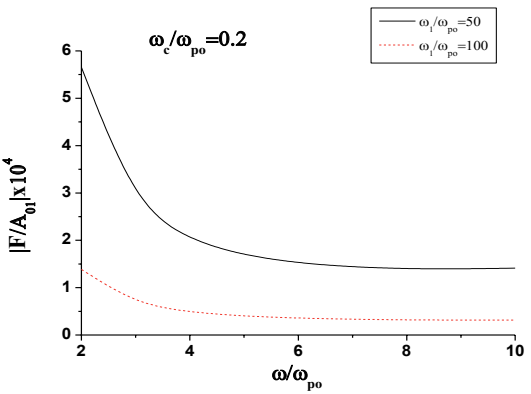

FIG. 3.3 Normalized amplitude of Terahertz radiation $|F/A_{01}|$ as a function of normalized frequency ω/ω_{po} for the value of $A_{02}' = 10, r_c' = 3, n_q' = 0.3, \nu' = 10.$

In fig. (3.4) for $\omega_c / \omega_{po} = 0.2 - 0.6$ i.e. by increasing the magnetic field the normalized terahertz amplitude rises approx. two fold at $\omega / \omega_{po} = 2$. These parameters for $\omega_{po} / 2\pi = 1\,\text{THz}$, $\omega_1 = 3.14 \times 10^{14}\,\text{rad/s}$ (CO_2 laser) correspond to $B_s = 72 \,\&\, 215\,\text{kG}$.

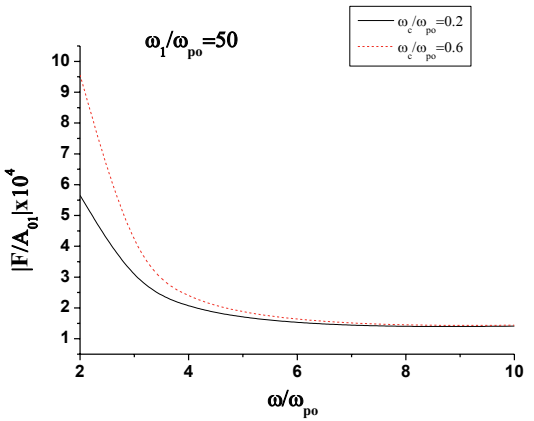

FIG. 3.4 Normalized amplitude of Terahertz radiation $|F/A_{01}|$ as a function of normalized frequency ω/ω_{po} for the value of $\omega_c' = 0.2, 0.6, A_{02}' = 10, r_c' = 3, n_q' = 0.3, \nu' = 10$.

The magnetic field could be internally generated or applied externally. A typical magnetic circuit may comprise of a current carrying coil of N turns and magnetic core of mean length l_c and cross-sectional area A_g. For iron core with magnetic permeability μ_c=1000, l_c=40cm, A_c=10^{-2} m^2, $l_g \approx 1\,\text{cm}$, $A_g \approx 10^{-4}$ m^2, and μ_g=μ_o, a current of 200 A along N=1000 turns produces a magnetic field of 240kG appropriate to our calculations in this chapter.

3.4 Power of the THz Radiation

Power of the THz radiation can be obtained as

$$P_{THz} = \int_0^\infty \frac{c}{4\pi} |F|^2 \eta 2\pi r dr \tag{3.30}$$

where $\eta = \left(1 - \frac{\omega_{po}^2}{\omega(\omega - \omega_c)}\right)^{\frac{1}{2}}$ is the refractive index of the magnetized plasma. Normalised power of the THz radiation can be written as

$$\left|\frac{P_{THz}}{P_{Laser}}\right| = \left|\frac{F}{A_{01}}\right|^2 \eta \tag{3.31}$$

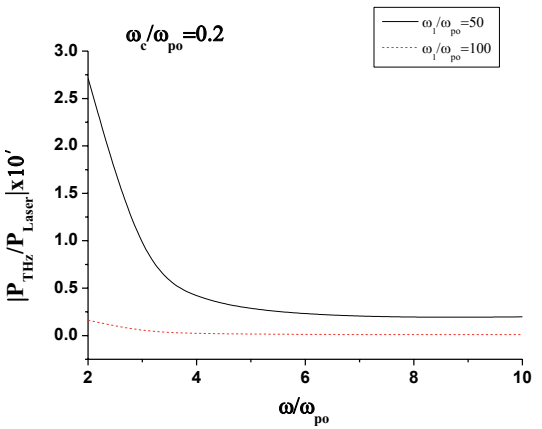

FIG. 3.5 Normalized power of Terahertz radiation $|P_{THz}/P_{laser}|$ as a function of normalized frequency ω/ω_{po} for the value of $A'_{02} = 10, r'_c = 3, n'_q = 0.3, \nu' = 10.$

Plot of the normalised power of THz radiation as a function of normalised frequency is shown in fig (3.5). It is observed that normalized power also decreases as ω/ω_{po} increases. For $\omega_1/\omega_{po}=50, |P_{THz}/P_{laser}|$ decreases from 2.6x10^{-7} to 0.25x10^{-7} as ω/ω_{po} is varied from 2 to 10, whereas from fig. (3.6) we observed that for $\omega_c/\omega_{po}=0.2-0.6$ i.e. by increasing the magnetic field the normalized terahertz power rises approx. three fold at $\omega/\omega_{po}=2$.

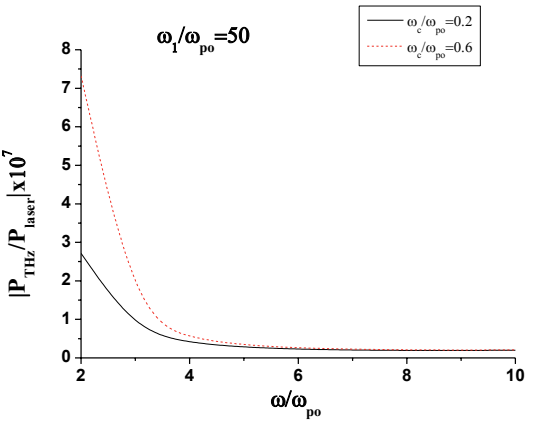

FIG. 3.6 Normalized power of Terahertz radiation $|P_{THz}/P_{laser}|$ as a function of normalized frequency ω/ω_{po} for the value of $\omega_c'=0.2,0.6, A_{02}'=10, r_c'=3, n_q'=0.3, \nu'=10.$

3.5 Discussion

In the present chapter, the lasers were assumed to be self guided such that self focussing was balanced by the diffraction losses. In actual cases, the effect of self focussing/diffraction could be quite important. One would like to solve the equation governing beam width parameter and incorporate its effect. The pre-existing plasma channel employed here can be created by

sending a prepulse of ps durations and allowing substantial time $t' \approx r_c / c_s$ where c_s is the sound speed, before launching the main laser pulses, for plasma to expand under self pressure gradient via ambipolar diffusion. This requires prepulse intensity $\geq 10^{14}$ W/cm^2. Alternatively, one may skip the prepulse and employ the nonlinearities induced by the two main laser beams to create a plasma channel and propagate without self convergence or divergence. Following Sodha et al., the condition for self guiding of the two laser beams by offsetting diffraction turns to be [17]

$$\frac{\omega_{po}^2}{\omega_1^2}\left(\frac{e^2(A_{01}^2+A_{02}^2)}{4m^2\omega_1^2 v_{th}^2}\right)\frac{1}{r_o^2} > \frac{1}{k_1^2 r_o^4}.$$

References

[1] E. Pickwell and V.P. Wallace, J. Phys. D **39**, R301 (2006).

[2] T. M. J. Antonsen, J. Palastro and H. M. Michberg, Phys. Plasmas **14**,033107 (2007).

[3] Y.C. Shen, T. Lo, P. F. Taday, B. E. Cole, W. R. Tribe and M. C. Kemp, Appl.Phys. Lett. **86**, 241116(2005).

[4] H. Hamster, A. Sullivan, S. Gordon, W. White and R.W. Falcone, Phys. Rev. Lett. **71**,2725(1993).

[5] W. P. Leemans, C. G. R. Geddes, J. Faure, Cs. Tóth, J. van Tilborg, C. B. Schroeder, E. Esarey, G. Fubiani, D. Auerbach, B. Marcelis, M. A. Carnahan, R. A. Kaindl, J. Byrd, and M. C. Martin, Phys. Rev. Lett. **91**, 074802(2003).

[6] C.B.Schroeder, E. Esarey, J. van Tilborg and W.P.Leemans, Phys. Rev. E **69**, 016501(2004).

[7] G.L.Carr, M.C. Martin, W.R.McKinney, K.Jordan, G.R. Neil and G.P.Williams, Nature(London) **420**, 153(2002).

[8] M. Abo-Bakr, J. Feikes, K.Holldack, P. Kuske, W.B. Peatman, U. Schade, G. Wüstefeld and H.-W. Hübers, Phys. Rev.Lett. **90**, 094801(2003).

[9] J. Yoshii, C. H. Lai, T. Katsouleas, C. Joshi and W. B. Mori, Phys. Rev. Lett. **79**, 4194(1997).

[10] N. Yugami, T. Higashiguchi, H. Gao, S. Sakai, K. Takahashi, H. Ito, Y. Nishida and T. Katsouleas, *ibid*. **89**, 065003(2002).

[11] H. Schillinger and R. Sauerbrey, Appl. Phys. B:Lasers Opt. **68**, 753(1999); S. Tzortzakis, G. Mechain, G. Patalano, Y.-B. Andre, B. Parde, M. Franco, A Mysyrowicz, J.-M. Munier, M. Gheudin, G. Beaudin and P. Encrenaz, Opt. Lett. **27**, 1944(2002).

[12] R. Mclaughlin, A. Corchia, M. B. Johnston, Q. Chen, C. M. Ciesla, D.D.Arnone, G. A. C. Jones, E. H. Linfield, A. G. Davies, and M. Pepper, Appl. Phys. Lett. **76**, 2038 (2000).

[13] C. S. Liu and V. K. Tripathi, J. Appl. Phys. **105**, 013313(2009).

[14] C.-H Pai, S.-Y. Huang, C.-C. Kuo, M.-W. Lin, J. Wang. S.-Y. Chen, C.-H. Lee and J.-Ylin, Phys. Plasmas **12**, 070707(2005).

[15] T.-Y. Chien, C.-L. Chang, C.-H. Lee, J.-Y. Lin, J.Wang and S.-Y. Chen, Phys. Rev. Lett. **94**, 115003(2005).

[16] B. D. Layer, A. York, T. M. J. Antonsen, S. Verma, Y. H. Chen, Y. Leng and H. M. Milchberg, Phys. Rev. Lett. **99**, 035001(2007).

[17] M. S. Sodha, A. K. Ghatak and V. K. Tripathi, *Self-Focussing of Laser Beams in Dielectrics, Plasmas and Semiconductors,* Tata McGraw-Hill Publishing Co. Ltd.,New Delhi, 1974.

[18] V. B. Gildenburg and N. V. Vvedenskii, Phys. Rev. Lett. **98**, 245002(2007).

Chapter 4

Beat Excitation of Terahertz Radiation in a Semiconductor Slab in a Magnetic Field

4.1 Introduction

The generation of terahertz (THz) radiation has attracted attention of many researchers worldwide in recent years. These waves, ranging from 0.1 to 50 THz, have found widespread applications in the field of biological imaging [1], remote sensing [2], spectroscopy of solids and liquids [3], chemical and security identification [4], etc. One may generate THz radiation by the following optical methods: i) optical rectification, ii) difference frequency generation(DFG), iii) parametric generation. These are basically second order nonlinear processes and occur in non-centrosymmetric materials. In the optical rectification process, one requires a fs laser pulse. The electric field of the THz pulses may be calculated from the wave equation by including a nonlinear current source. The basic limitation of this process is difficult phase matching and limited output power. Only in specific spectral range of pump pulse and generated THz wave, the phase matching can be achieved. Another obvious disadvantage is broad linewidth which is proportional to τ_L^{-1} where τ_L is the pulse duration [5]. THz generation by DFG and parametric oscillation is possible with ns laser pulses or cw lasers. Continuously tunable and coherent radiation in the wide spectral range has been achieved [6-8]. In the DFG , two collinear phase matched laser beams are required. The process has high conversion efficiency which leads to high output power. CW THz waves thus obtained have narrow linewidths [9]. THz wave parametric oscillators are based on stimulated scattering in crystals such as LiNbO3. The

advantages of this method include continuous tunability, design simplicity and room temperature operation. However one obtains limited output power due to phase mismatch [10].

THz emissions have also been produced from plasmas using energetic electron beams and subpicosecond laser pulses. These include coherent radiation from plasma oscillations driven by ultrashort laser pulses [11], transition radiation of electron beams [12], synchrotron radiation from accelerator electrons [13], Cherenkov wake radiation in magnetized plasmas [14]. Earlier Hamster et al [11] observed high power terahertz radiation from short pulse laser produced plasma, employing 1TW, 100 fs laser focused onto gas and solid targets. Recently, Antonsen et al [15] proposed a scheme of ponderomotive force induced resonant terahertz generation in a rippled density plasma. The terahertz power scales as the square of laser intensity. Bhasin et al [16] introduced a scheme of resonant terahertz radiation generation by the optical rectification of a picosecond laser pulse in a rippled density magnetized plasma .The terahertz power scales as the square of density ripple amplitude and rises with the magnetic field strength. Kumar et al [17] have investigated the beat excitation of THz radiation using Gaussian laser beams co-propagating along the direction of ambient magnetic field in a rippled density plasma channel. The density ripple provides phase synchronism while the axial magnetic field enhances the nonlinear coupling through cyclotron resonance.

Tunable terahertz radiation generated in semiconductors by an ultrashort light pulse is known to be due to coherent effects in the photogenerated plasma during optical excitation in the surface depletion region or in the electric field region of a biased semiconductor . Hashimshony et al [18] reported tunable radiation in the range of 0.1 to a few THz by the interaction of a superluminous photoconducting front with an electrostatic frozen wave configuration. Glinka et

al [19] have reported the generation of THz oscillation by a femtosecond optical pulse in the μm-sized LT-GaAs slab grown on the GaAs substrate. McLaughlin et al [20] have reported substantial enhancement in TE mode in the presence of magnetic field in InAs. The conversion efficiency continues to rise with an increasing magnetic field up to B=8 T. Such enhancement of the visible to THz conversion efficiency is extremely beneficial for potential applications of THz radiation such as imaging [21]. Furthermore, recent studies [22-24] have demonstrated that increased THz powers may be achieved at low magnetic fields, B=1.7 T. Heyman et al [25] studied terahertz emission from InAs and GaAs in a magnetic field and observed ultrashort THz pulses. They observed 12 μW average terahertz power from n-InAs at B= 3.2T.

In this chapter we study beat excitation of THz radiation by TM/TE mode lasers propagating through a rippled semiconductor slab while there exists a static magnetic field is transverse to the direction of laser propagation. The process of laser machining [26, 27] is capable of producing density ripple in the semiconductor slab. Alternately a surface ripple on the semiconductor can also do the job. Our calculations are based on two semiconductors viz., Ge ($\varepsilon_L = 14$) and InSb ($\varepsilon_L = 17$). The wave vector of the density ripple is along the direction of laser propagation. Two laser pulses, co-propagating in the semiconductor, exert a ponderomotive force on the electrons at the beat frequency. This force, in the presence of density ripple and transverse magnetic field, produces a nonlinear current at the terahertz frequency. The density ripple wave number provides the requisite phase matching. In section 4.2 we study laser propagation in the semiconductor slab and obtain the dispersion relation. In section 4.3 we examine the nonlinear process of beat excitation of terahertz wave. In section 4.4 we derive the dispersion relation for the THz radiation. In section 4.5, a brief discussion of results is given.

4.2 Laser propagation through a semiconductor slab.

Consider a semiconductor slab of thickness 2a, where origin passes through the center of the slab as shown in fig. 4.1. Two TM mode lasers propagate through it in the $\hat{z}$ direction. A static magnetic field $\vec{B}_s$ is also applied in the $\hat{y}$ direction. The variation along *y*-direction is assumed to be zero i.e. $\partial/\partial y = 0$.

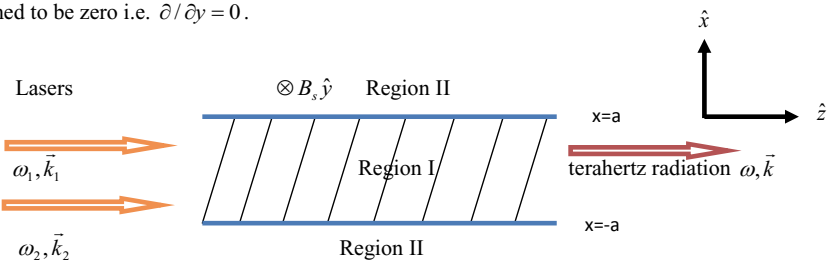

FIG 4.1 System configuration.

The electric fields of the two lasers are

$$\vec{E}_j = \vec{A}_{j0}(x)e^{-i(\omega_j t - k_z z)}, j = 1,2 \tag{4.1}$$

From third and fourth Maxwell's equations viz., $\nabla \times \vec{E} = -\frac{1}{c}\frac{\partial \vec{B}}{\partial t}, \nabla \times \vec{B} = \frac{4\pi}{c}\vec{J} + \frac{1}{c}\frac{\partial}{\partial t}(\underline{\underline{\varepsilon}} \cdot \vec{E})$, in the limit $\nabla \cdot \vec{E} = 0$ and $\vec{J} = 0$ the wave equation turns out to be,

$$\nabla^2 \vec{E}_j - \nabla(\nabla \cdot \vec{E}_j) + \frac{\omega_j^2}{c^2}(\underline{\underline{\varepsilon}}_j \cdot \vec{E}_j) = 0 \tag{4.2}$$

where $\underline{\underline{\varepsilon_j}}$ is the permittivity tensor with components (cf. Appendix A),

$$\varepsilon_{jxx} = \varepsilon_{jzz} = \varepsilon_L - \frac{\omega_p^2}{\omega_j^2 - \omega_c^2}, \qquad ,\varepsilon_{jxz} = -\varepsilon_{jzx} = -i\frac{\omega_c}{\omega_j}\frac{\omega_p^2}{\omega_j^2 - \omega_c^2}, \qquad \varepsilon_{xy} = \varepsilon_{yx} = \varepsilon_{yz} = \varepsilon_{zy} = 0,$$

$\varepsilon_{jyy} = \varepsilon_L - \frac{\omega_p^2}{\omega_j^2}$, $\omega_c = \frac{eB_s}{mc}$ is the electron cyclotron frequency, $\omega_{po} = \sqrt{(4\pi n_0 e^2/m)}$ is the electron plasma frequency. -e and m are the electron charge and mass respectively, n_0 is the equilibrium electron density in the slab and ε_L is the lattice permittivity of the semiconductor. For ω_1, $\omega_2 >> \omega_c$, the permittivity tensor turns out to be $\underline{\underline{\varepsilon_j}} = \varepsilon_j \underline{\underline{I}}$, where $\varepsilon_j = \varepsilon_L - \omega_p^2/\omega_j^2$ In region I , the z-component of wave equation can be written as

$$\frac{\partial^2 E_{jz}}{\partial x^2} + k_{jx}^2 E_{jz} = 0, \quad (-a < x < a) \tag{4.3}$$

where $k_{jx}^2 = \frac{\omega_j^2}{c^2}(\varepsilon_j) - k_{jz}^2$. The solution of Eq.(4.3) is given by

$$E_{jz} = A_I \cos k_{jx} x \quad \text{(For symmetric mode)} \tag{4.4}$$

In region II, the z-component of the wave equation can be written as

$$\frac{\partial^2 E_{jz}}{\partial x^2} - \alpha_{jII}^2 E_{jz} = 0, \qquad (|x| > a) \tag{4.5}$$

where $\alpha_{jII}^2 = k_{jz}^2 - \omega_j^2/c^2$. The solution of Eq.(4.5) is given by

$$\begin{aligned} E_{jz} &= A_{II} e^{-\alpha_{jII} x} && x > a \\ &= A_{II} e^{\alpha_{jII} x} && x < -a \end{aligned} . \tag{4.6}$$

The x-component of electric fields in regions I and II can be obtained by assuming $\nabla \cdot \vec{E} = 0$. It gives

$$E_{jx} = -\frac{ik_{jz}}{k_{jx}} A_I \sin k_{jx} x \qquad \text{-a < x < a,} \tag{4.7}$$

$$E_{jx} = \frac{ik_{jz}}{\alpha_{jII}} A_I \cos k_{xj} a e^{-\alpha_{jI}(x-a)} \qquad \text{x > a.} \tag{4.8}$$

Applying the boundary condition viz.,

$$D_{jx}^{I} = D_{jx}^{II} \text{ at x = a} \tag{4.9}$$

as $\omega_j >> \omega_c$, the dispersion relation for TM mode laser is

$$\tan k_{jx} a = -\frac{k_{jx}}{\alpha_{jII} \varepsilon_{xx}}. \tag{4.10}$$

By the similar analysis, the dispersion relation for TE mode laser is

$$\tan k_{jx} a = \frac{\alpha_{jII}}{k_{jx}}, \tag{4.11}$$

where for TE mode $k_{jx} = \left((\omega_j^2 / c^2)\varepsilon_{jyy} - k_{jz}^2\right)^{1/2}$. In fig. 4.2, we plot normalized laser frequency $\omega_1 a / c$ as a function of axial propagation for TM_{10} mode. It shows that lower laser frequencies in the TM_{10} mode are more guided in the semiconductor than higher frequencies. For $\varepsilon_L = 14$(Ge), 17(InSb), $\omega_p a / c = 1.5$, $k_z a$ increases continuously as $\omega a / c$ varies in the range 5- 40. In fig. 4.3, we plot normalized laser frequency as a function of axial propagation respectively for TE mode.

The laser wave vectors axial component increases continuously as the normalized laser frequency varies in the range 5-40. Also it shows that lower laser frequencies in the TE_{10} mode are more guided in the semiconductor than higher frequencies.

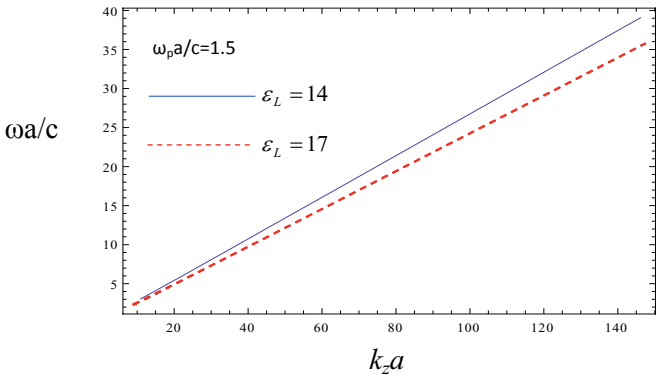

FIG. 4.2 Laser frequency vs axial propagation constant for TM_{10} mode.

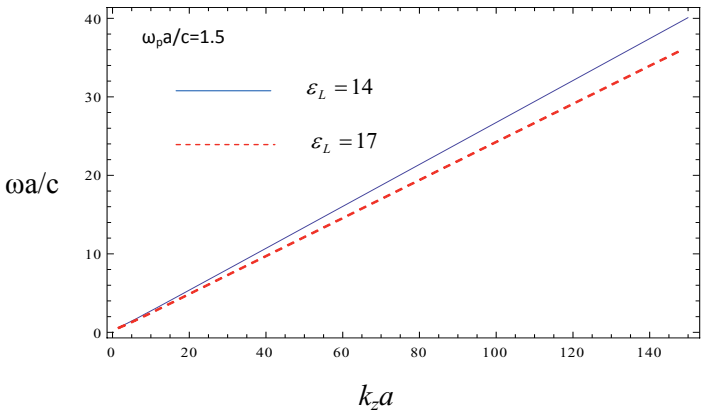

FIG. 4.3 Laser frequency vs axial propagation constant for TE_{10} mode.

4.3 Beat excitation of terahertz nonlinear current density in magnetic field

Consider the propagation of two TM_{10} mode laser beams of frequencies ω_1, ω_2 and wave vector $\vec{k}_{1z}$, $\vec{k}_{2z}$ respectively inside the rippled semiconductor slab ($n = n_{qo} e^{iqz}$, where q is the ripple wave vector), whose x and z components of electric fields are given by,

$$E_{jz} = A_j \cos k_{jx} x e^{-i(\omega_j t - k_{jz} z)}$$

$$E_{jx} = A_j i \frac{k_{jz}}{k_{jx}} \sin k_{jx} x e^{-i(\omega_j t - k_{jz} z)} \tag{4.12}$$

where, $k_{jx} = \left((\omega_j^2 / c^2)((\varepsilon_{jxx}^2 + \varepsilon_{jxy}^2)/\varepsilon_{jxx}) - k_{jz}^2\right)^{1/2}$ and j=1,2.

Similarly, for two TE_{10} mode laser beams the transverse electric field inside the semiconductor slab can be written as

$$E_{jy} = A_j \cos k_{jx} x e^{-i(\omega t - k_{jz} z)} \tag{4.13}$$

where, $k_{jx} = \left((\omega_j^2 / c^2)\varepsilon_{jyy} - k_{jz}^2\right)^{1/2}$

These exert a ponderomotive force on the electrons given by

$$\vec{F}_p = -\frac{e^2}{2m\omega_1\omega_2} \nabla(\vec{E}_1 \cdot \vec{E}_2^*) \tag{4.14}$$

The nonlinear velocity response due to ponderomotive force is governed by the equation of motion

$$\frac{\partial \vec{v}_{\omega}^{NL}}{\partial t} = \frac{\vec{F}_p}{m} - \vec{v}_{\omega}^{NL} \times \vec{\omega}_c \tag{4.15}$$

where $\omega = \omega_1 - \omega_2$, $k_z = k_{1z} - k_{2z}$. The *x* and *z* components of Eq. (4.15) can be written as

$$v_{\omega x}^{NL} = \frac{1}{m(\omega^2 - \omega_c^2)} \left[i\omega F_{px} - \omega_c F_{pz} \right] \quad , \tag{4.16}$$

$$v_{\omega z}^{NL} = \frac{1}{m(\omega^2 - \omega_c^2)} \left[\omega_c F_{px} + i\omega F_{pz} \right] \quad , \tag{4.17}$$

where F_{px} and F_{pz} are the *x* and *z* component of ponderomotive force respectively. The nonlinear current at $\omega, \vec{k} + \vec{q}$ in the presence of density ripple $n_{qo} e^{iqz}$ can be written as

$$\vec{J}^{NL} = -\frac{1}{2} n_{qo} e \vec{v}_{\omega}^{NL} e^{iqz} \tag{4.18}$$

4.4 Dispersion relation for the terahertz wave

The wave equation for the THz wave can be written as

$$-\nabla^2 \vec{E} + \nabla(\nabla \cdot \vec{E}) = \frac{4\pi i\omega}{c^2} \vec{J}^{NL} + \frac{\omega^2}{c^2} (\underline{\underline{\varepsilon}} \cdot \vec{E}) \tag{4.19}$$

From the *x*-component of wave equation, neglecting the current source term, one obtains

$$E_x = -\frac{\left(\frac{\omega^2}{c^2} \varepsilon_{xz} - ik_z \frac{\partial}{\partial x} \right)}{\left(\frac{\omega^2}{c^2} \varepsilon_{xx} - k_z^2 \right)} E_z \tag{4.20}$$

Substituting this into the *z*-component of wave equation, replacing $k_z -> k_z - i\partial / \partial z$, one obtains

$$\frac{\partial^2}{\partial x^2}E_z + k_x^2 E_z + 2ik_z \frac{\partial}{\partial z}E_z = \frac{4\pi i}{\omega \varepsilon_{xx}}\left(\frac{\omega^2}{c^2}\varepsilon_{xx} - k_z^2\right)J_z^{NL} \tag{4.21}$$

where $k_x = \left((\omega^2/c^2)(\varepsilon_{xx}^2 + \varepsilon_{xz}^2)/\varepsilon_{xx} - k_z^2\right)^{1/2}$. In order to deduce the mode structure of the THz wave in the semiconductor, we neglect the current source and the last term on LHS, so Eq. (4.21) reduces to

$$\frac{\partial^2}{\partial x^2}E_z + k_x^2 E_z = 0, \tag{4.22}$$

whose solution is given by

$$\begin{aligned} E_z &= A_3 \cos k_x x && -a < x < a \\ &= A_3' e^{-\beta x} && x > a \\ &= A_3' e^{\beta x} && x < -a \end{aligned} \tag{4.23}$$

where, $\beta = \left(k_z^2 - \omega^2/c^2\right)^{1/2}$, $A_3' = A_3 \cos k_x a e^{\beta a}$. Applying the boundary conditions viz.,

1. $E_z^I = E_z^{II}$, $\quad x = \pm a$

2. $D_x^I = D_x^{II}$, $\quad x = \pm a$

one obtains a dispersion relation

$$\tan k_x a - i\frac{\varepsilon_{xz} k_z}{\varepsilon_{xx} k_x} = \frac{1}{\beta k_x \varepsilon_{xx}}\left(\frac{\omega^2}{c^2}\frac{\varepsilon_{xz}^2}{\varepsilon_{xx}} - k_x^2\right). \tag{4.24}$$

In fig. 4.4 we plot the dispersion relation for terahertz wave in TM_{10} mode. As the normalized terahertz frequency $\omega a/c$ is increased from 0.4 to 1.2, its transverse propagation constant

increases linearly showing that lower terahertz frequencies are more guided than higher frequencies. The axial propagation constant increases almost linearly with normalized frequency.

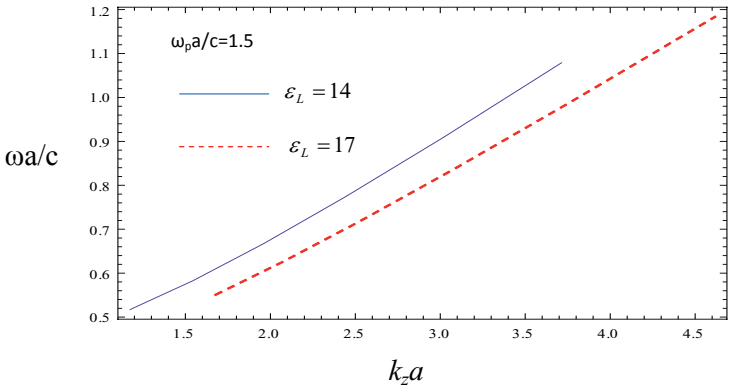

FIG 4.4 Terahertz frequency vs axial propagation constant in TM_{10} mode.

When current source is included in the wave equation the solution of wave is modified as

$$E_z = A_3(z)\psi(x)e^{-i(\omega t - k_z z)} \tag{4.25}$$

where,

$$\psi(x) = \cos k_x x \qquad -a < x < a$$
$$= \cos k_x a e^{-\beta(x-a)} \qquad |x| > a$$

Substituting Eq.(4.25) in Eq.(4.21), one obtains

$$2ik_z\psi(x)\frac{\partial A_3}{\partial z} + A_3\left[\frac{\partial^2\psi(x)}{\partial x^2} + k_x^2\psi(x)\right] = R_z \tag{4.26}$$

where

$$R_z = -\frac{4\pi i}{\omega\varepsilon_{xx}}\left(\frac{\omega^2}{c^2}\varepsilon_{xx} - k_z^2\right)J_z^{NL} \qquad -a < x < a$$
$$= 0 \qquad |x| > a$$

At phase matching the last term on LHS cancel each other, so multiplying Eq.(4.26) by $\psi^*(x)dx$ and integrating from -∞ to +∞ w.r.t. x and then integrating w.r.t z and normalizing, one obtains

$$\frac{A_3}{A_1} = \frac{1}{16}\left(\frac{n_q}{n_0}\right)\left(\frac{\omega_p^3}{\omega_1\omega_2(\omega^2-\omega_c^2)}\right)\left(\frac{\omega^2 - k_z^2/\varepsilon_{xx}}{k_z+q}\right)\left(\frac{eA_2^*}{m\omega_p c}\right)\left(\frac{2k_x}{2k_x+\sin 2k_x}\right)R \tag{4.27}$$

where all quantities are normalized w.r.t. a and c. For TM_{10} mode laser

$$R = \left(\frac{\sin(k_x-k_{1x}-k_{2x})}{k_x-k_{1x}-k_{2x}} + \frac{\sin(k_x+k_{1x}-k_{2x})}{k_x+k_{1x}-k_{2x}} + \frac{\sin(k_x-k_{1x}+k_{2x})}{k_x-k_{1x}+k_{2x}} + \frac{\sin(k_x+k_{1x}+k_{2x})}{k_x+k_{1x}+k_{2x}}\right) +$$
$$\left(\frac{k_{1z}k_{2z}}{k_{1x}k_{2x}}\right)\left(-\frac{\sin(k_x-k_{1x}-k_{2x})}{k_x-k_{1x}-k_{2x}} + \frac{\sin(k_x+k_{1x}-k_{2x})}{k_x+k_{1x}-k_{2x}} + \frac{\sin(k_x-k_{1x}+k_{2x})}{k_x-k_{1x}+k_{2x}} - \frac{\sin(k_x+k_{1x}+k_{2x})}{k_x+k_{1x}+k_{2x}}\right)$$

and for TE_{10} mode laser

$$R = \left(\frac{\sin(k_x-k_{1x}-k_{2x})}{k_x-k_{1x}-k_{2x}} + \frac{\sin(k_x+k_{1x}-k_{2x})}{k_x+k_{1x}-k_{2x}} + \frac{\sin(k_x-k_{1x}+k_{2x})}{k_x-k_{1x}+k_{2x}} + \frac{\sin(k_x+k_{1x}+k_{2x})}{k_x+k_{1x}+k_{2x}}\right)$$

The phase matching criteria is

$$q = k_{1z} - k_{2z} - k_z \tag{4.28}$$

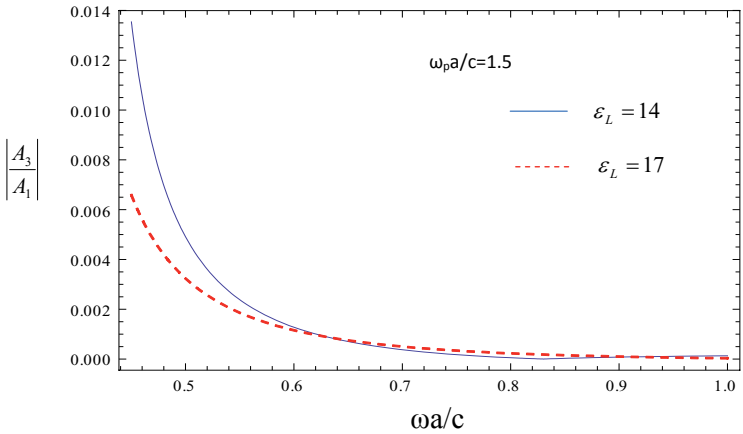

FIG 4.5 Normalized amplitude versus normalized frequency curve for TM_{10} mode laser propagation for $\omega_c a / c = 0.05$.

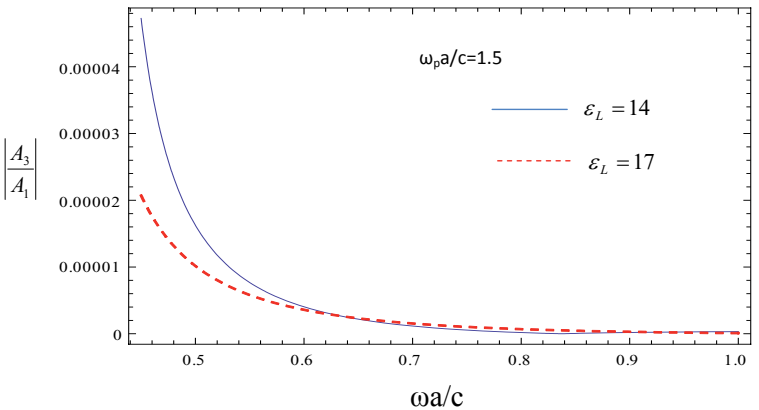

FIG 4.6 Normalized amplitude versus normalized frequency curve for TE_{10} mode laser propagation for $\omega_c a / c = 0.05$.

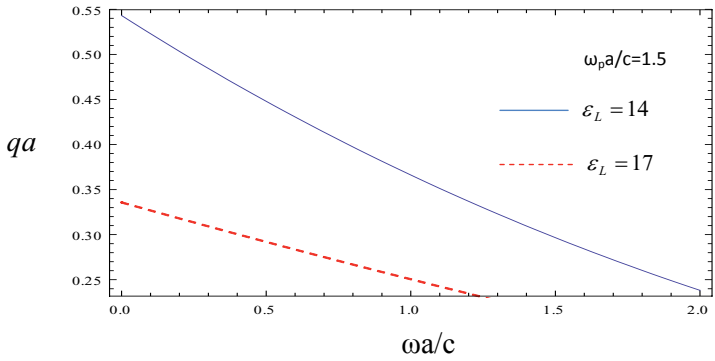

FIG 4.7 Normalized density ripple versus terahertz frequency curve for TM_{10} mode propagation.

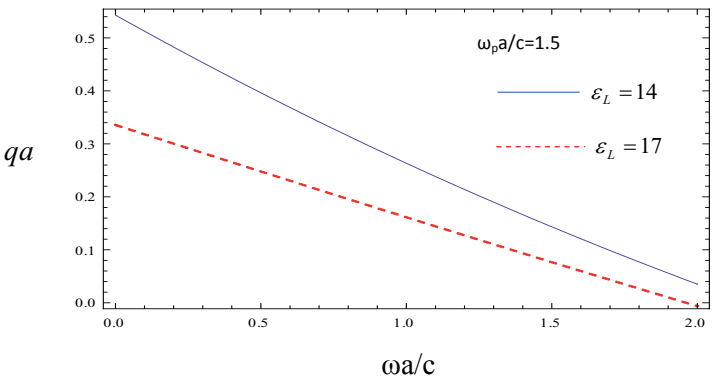

FIG 4.8 Normalized density ripple versus terahertz frequency curve for TE_{10} mode propagation.

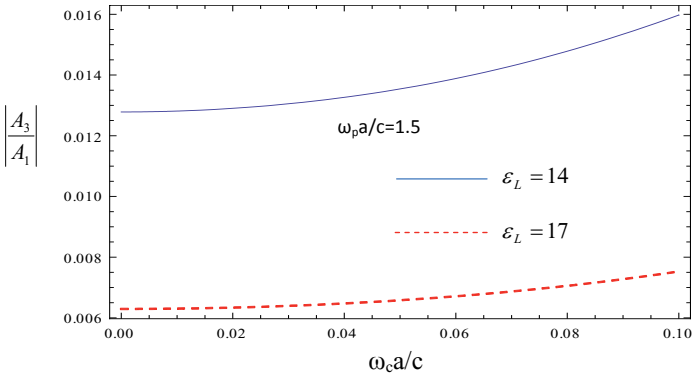

FIG 4.9 Normalized amplitude versus magnetic field for TM_{10} mode.

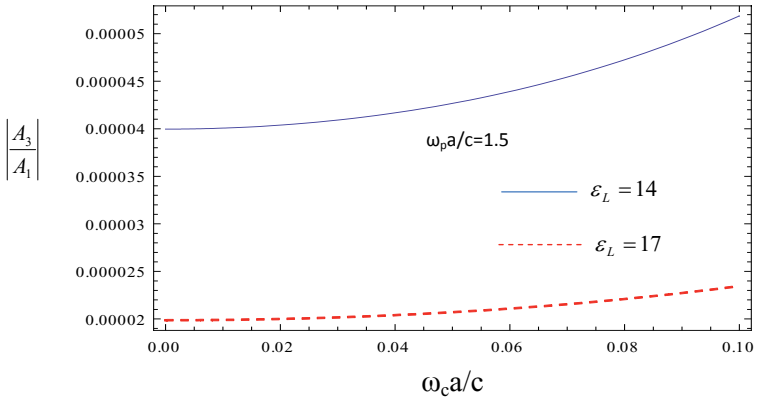

FIG 4.10 Normalized amplitude versus magnetic field for TE_{10} mode.

In figures 4.5 & 4.6, we plot normalized terahertz amplitude vs normalized terahertz frequency for TM_{10} and TE_{10} mode laser propagation respectively for the following set of parameters: $n_q / n_o = 0.1$, $eA_2 / m\omega_p c = 0.9$, $\omega_p a / c = 1.5$, $\omega_1 a / c = 20$. The terahertz yield is significantly

higher for TM mode laser propagation than TE mode propagation. Since terahertz wave has a TM polarization, a matched polarization is crucial for high output power. In figures 4.7 & 4.8 show normalized density ripple vs normalized terahertz frequency for TM and TE mode lasers. The frequency of THz radiation is decided by the difference in laser frequencies. For a given frequency difference the THz generation could be made a resonant process by a ripple of suitable wave number. This ripple wave number changes with the frequency of the THz wave.

4.5 Discussion

In this chapter we have examined terahertz generation at the beat frequency of two lasers inside a rippled semiconductor slab in the presence of transverse magnetic field. The terahertz amplitude is enhanced with magnetic field strength as observed in recent experiments [20]. Figures 4.9 & 4.10 show normalized terahertz amplitude vs normalized magnetic field strength for TM and TE mode laser propagation respectively. Also TM mode laser beating has higher yields of THz generation as compared to TE mode. The requisite phase matching is provided by the density ripple. The frequency of THz radiation is decided by the difference in laser frequencies. For a given frequency difference the THz generation could be made a resonant process by a ripple of suitable wave number. This ripple wave number changes with the frequency of the THz wave. For the parameters chosen in our calculations the normalized terahertz frequency varies in the range 0.45 – 1.0. At $\omega/2\pi$ =1 THz, the semiconductor slab could be of thickness 100 μm. The magnetic field strength required would be around 4 T.

The laser powers that we consider appropriate for THz generation in semiconductors correspond to oscillatory velocity to velocity of light in vacuum ratio $\sim e|E_1|/m\omega_1 c \approx e|E_2|/m\omega_2 c \approx .05$. For 10.6 μm CO_2 laser this requires an intensity of

$\sim 2\times10^{11} W/cm^2$. For pulse duration $\sim 1 ps$ and spot size around a THz wavelength $(\approx 3\times10^{-2} cm)$, the requisite laser pulse energy turns out to be ~ 0.6 mJ. However, any change in carrier concentration at high laser intensity is not considered. Therefore we have not included transient photocurrent and surface effects. Also we have not included the effect of any damping mechanism in our calculations. The free electron collisions with phonons and impurities limit the growth. In case of thin sample surface scattering could also be significant.

References

[1] P. Y. Han, G. C. Cho and X. –C. Zhang Opt. Lett. **25**, 242-245(2000).

[2] J. W. Waters, L. Froidevaux, R. S. Harwood, R. F. Jarnot, H. M. Pickett, W. G. Read, P. H. Siegel, R. E. Cofield, M. J. Filipiak, D. A. Flower, J. R. Holden, G. K. Lau, N. J. Livesey, G L. Manney, H. C. Pumphrey, M. L. Santee, D. L. Wu, D. T. Cuddy, R. R. Lay, M. S. Loo, V. S. Perun, M. J. Schwartz, P. C. Stek, R. P. Thurstans, M. A. Boyles, K. M. Chandra, M. C. Chavez, G.-S. Chen, B. V. Chudasama, R. Dodge, R. A. Fuller, M. A. Girard, J. H. Jiang, Y. Jiang, B. W. Knosp, R. C. LaBelle, J. C. Lam, K. A. Lee, D. Miller, J. E. Oswald, N. C. Patel, D. M. Pukala, O. Quintero, D. M. Scaff, W. V. Snyder, M. C. Tope, P. A. Wagner, and M. J. Walch, IEEE Trans. Geosci. Remot Sensing **44**, 279-290(2006).

[3] M. van Exter and D. Grischkowsky, IEEE Trans. Microwave Theory Tech. **38**, 1684(1990).

[4] Y. C. Shen, T. Lo, P. F. Taday, B. E. Cole, W. R. Tribe and M. C. Kemp, Appl. Phys. Lett. **86**, 241116(2005)

[5] M. Joffre, A. Bonvalet, A. Migus, and J.-L. Martin, Opt. Lett. **21**(13) , 964(1996).

[6] W Shi, Y J. Ding, N Fernelius, and K Vodopyanov**.** Opt. Lett., **27**(16), 1454(2002**).**

[7] K. H. Yang, P. L. Richards, and Y. R. Shen, Appl. Phys. Lett. **19,** 320(1971).

[8] G. Balestrino, S. Martellucci, P. G. Medaglia,a) A. Paoletti, G. Petrocelli, A. Tebano, A. Tucciarone, F. Gelli, E. Giorgetti, S. Sottini and L. Tapfer, Appl. Phys. Lett. **78,** 1204(2001).

[9] W. Shi and Y. J. Ding, Appl. Phys. Lett. **84,** 1635(2004).

[10] K. Kawase, M. Sato, T. Taniuchi, and H. Ito, Appl. Phys. Lett. 6**8,** 2483(1996).

[11] H. Hamster, A. Sullivan, S. Gordan, W. White and R. W. Falcone, Phys. Rev. Lett. **71**, 2725(1993).

[12] W. P. Leemans, C. G. R. Geddes, J. Faure, Cs. Tóth, J. van Tilborg, C. B. Schroeder, E. Esarey, G. Fubiani, D. Auerbach, B. Marcelis, M. A. Carnahan, R. A. Kaindl, J. Byrd, and M. C. Martin, Phys. Rev. Lett. **91**, 074802(2003).

[13] G. L. Carr, M. C. Martin, W. R. McKinney, K. Jordan, G. R. Neil and G. P. Williams, Nature **420**, 153(2002).

[14] J. Yoshii, C. H. Lai, T. Katsouleas, C. Joshi and W. B. Mori, Phys. Rev. Lett. **79**, 4194(1997).

[15] T. M. J. Antonsen, J. Palastro and H. M. Michberg, Phys. Plasmas **14**, 033107(2007).

[16] L. Bhasin and V. K. Tripathi, Phys. of Plasmas **16**, 103105(2009).

[17] M. Kumar, L. Bhasin and V. K. Tripathi, Phys. Scr. **81** 045504(2010).

[18] D. Hashimshony, A. Zigler and K. Papadopoulos, Appl. Phys. Lett. **74**(12), 1669(1999).

[19] Y. D. Glinka, D. Maryenko, and J. H. Smet, Phys. Rev. B **78**, 035328(2008).

[20] R. McLaughlin, A. Corchia, M. B. Johnstan, Q. Chen, C. M. Ciesla, D. D. Arnone, G. A. C. Jones, E. H. Linfield, A. G. Davies and M. Pepper, Appl. Phys. Lett., **76**, 2038(2000).

[21] D. D.Arnone, C. M. Ciesla, A. Corchia, S. Egusa, M. Pepper, J. M. Chanberlain, C. Bezant, R. Clothier and N. Kharmmo, presentation at the EOS/SPIE International Symposia, 14-18 June 1999.

[22] S. Izumida, S. Ono, Z. Liu, H. Ohtake and N. Sarukura, J. Nonlinear Opt. Phys. Mater. **8**, 71(1999).

[23] N. Sarukura, H. Ohtake, S. Izumuda, and Z. Liu, J. Appl. Phys. **84**, 654 (1998).

[24] S. Izumida, S. Ono, Z. Liu, H. Ohtake and N. Sarukura, Appl. Phys. Lett. **75**, 451 (1999).

[25] J. N. Heyman, P. Neocleous, D. Hebert, P. A. Crowell, T. Muller and K. Unterrainer, Phys. Rev. B **64**, 085202(2001).

[26] C.-H Pai, S.-Y. Huang, C.-C. Kuo, M.-W. Lin, J. Wang. S.-Y. Chen, C.-H. Lee and J.-Ylin, Phys. Plasmas **12**, 070707(2005).

[27] T.-Y. Chien, C.-L. Chang, C.-H. Lee, J.-Y. Lin, J.Wang and S.-Y. Chen, Phys. Rev. Lett. **94**, 115003(2005).

Chapter 5

Excitation of THz Plasmon Eigen Mode of a Parallel Plane Guiding System by an Electron Beam

5.1 Introduction

Surface plasmons have drawn vigorous attention in recent years due to their wide ranging applications [1-8]. Surface plasmons are ideally suited as sensors [9-10]. They propagate along the surface between a conductor and a dielectric or conductor and air with fields peaking at the interface and falling off exponentially away from it in either medium [11-13]. A tiny trace of a gas or DNA on the interface produces a measurable change in the propagation constant when one uses the attenuated total reflection (ATR) configuration [14-16]. In this configuration a thin film of silver (or gold) is deposited on a glass prism. Laser light is impinged on the other face of the prism so as to fall on the prism-metal interface at an angle of incidence θ (called surface Plasmon resonance angle θ_{SPW}) the laser gets mode converted into a surface plasma wave (SPW) at the metal-free space interface, and laser reflectivity sharply falls. θ_{SPW} is very sensitive to presence of gas or DNA on the free interface, hence aids their detection. Surface plasmons can increase the rate of laser ablation of materials by orders of magnitude, hence are suitable for rapid thin film deposition.

SPs are being explored for their potential in optics, magneto-optic data storage, microscopy [17] and solar cells [18-20]. Their strong localization and resonant properties find application in biosensing, optoelectronics, metamaterials [21], enhanced optical transmission through nanoapertures [22], super-resolution imaging [23], and negative refraction [24-26], and

enhanced nonlinear effects [27-28]. Welsh et.al have described the influence of surface-plasmon excitation on terahertz-pulse generation on a gold surface [29].

Significant efforts have been made on the resonant interaction of surface plasma waves with electron beams. Liu and Tripathi have studied the excitation of surface plasma wave over a planar metal surface by a sheet electron beam [30]. Surface plasma wave driven electron acceleration have been observed [31-32]. Kumar and Tripathi have developed a formalism and explained some of these results [33]. Kumar et.al has examined the possibility of stimulated emission of a surface plasma wave on a metal-vacuum interface by electron-hole recombination in a forward biased *p-n* junction located near the interface [34].

In this chapter, we study the excitation of surface plasma wave (SPW) by a relativistic sheet electron beam propagating through the space between the semiconductors (n-InSb). The parallel plane structure is chosen to have a surface wave field minimum in the middle of the planes, so that an electron beam placed over there experiences a converging force and does not diverge. In section 5.2 we derive the dispersion relation for SPW. In section 5.3 we study the beam response and obtain the growth rate. The results are discussed in section 5.4.

5.2 Surface Plasma Wave

Consider two semiconducting half spaces $x \le -a$ and $x \ge a$, separated by free space. In each semiconductor the free electron density is n_o^o (c.f. Fig. 5.1). A surface plasma wave propagates along $\hat{z}$ in this system. Taking the t, z variations of wave fields as $e^{-i(\omega t - k_z z)}$ and using $\nabla \cdot \vec{E} = 0$ in each region, one may write the electric field of the SPW [35] as

$$\vec{E} = A_I(\hat{z} - \hat{x}\frac{ik_z}{\alpha_I})e^{\alpha_I x}e^{-i(\omega t - k_z z)}, \qquad x < -a, \tag{5.1}$$

$$\vec{E} = \left[A_{II}(\hat{z} - \hat{x}\frac{ik_z}{\alpha_{II}})e^{\alpha_{II}x} + A'_{II}(\hat{z} + \hat{x}\frac{ik_z}{\alpha_{II}})e^{-\alpha_{II}x} \right] e^{-i(\omega t - k_z z)}, \qquad -a < x < a, \tag{5.2}$$

$$\vec{E} = A_{III}(\hat{z} + \hat{x}\frac{ik_z}{\alpha_I})e^{-\alpha_I x}e^{-i(\omega t - k_z z)}, \qquad x > a, \tag{5.3}$$

where $\alpha_I^2 = k_z^2 - \omega^2\varepsilon_m / c^2, \alpha_{II}^2 = k_z^2 - \omega^2 / c^2, \varepsilon_m = \varepsilon_L - (\omega_p^2 / \omega^2)(1 - i\nu/\omega)$, ε_L is the lattice permittivity $\omega_p = (4\pi n_o^o e^2 / m)^{1/2}$ is the plasma frequency, -*e* and *m* are the electron charge and effective mass and ν is the electron collision frequency.

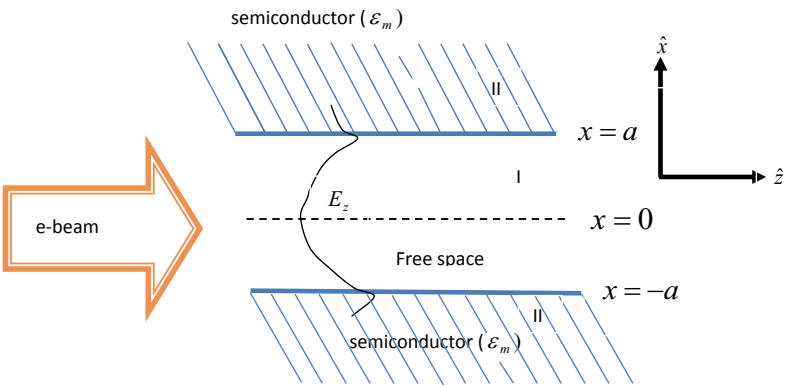

FIG 5.1 Schematic of two semiconducting parallel plane guiding system with free space in between them. A relativistic sheet electron beam, injected in the free space region, excites the surface plasma wave.

The mode structure of surface plasmon is plotted in Fig. 5.2. As seen from the plot the electric field is maximum at the inner semiconductor surfaces and reduces to minimum in the middle.

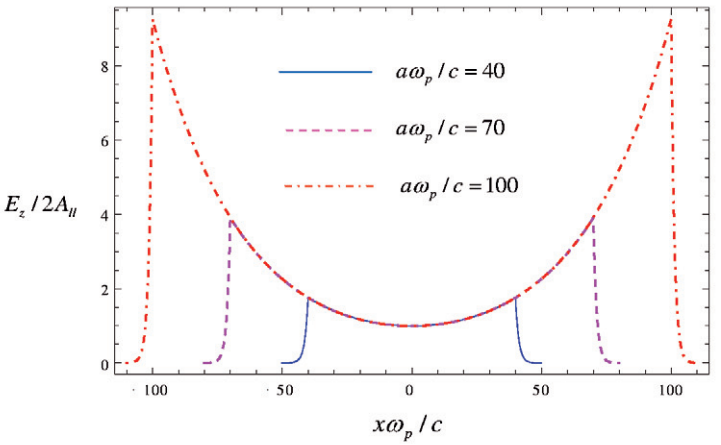

FIG 5.2 Plot of mode structure of surface plasma wave for $\omega / \omega_p = 0.15$.

The continuity of E_z and εE_x (where ε is the permittivity of the medium) at $x = -a$ yields

$$A_I e^{-\alpha_I a} = A_{II} e^{-\alpha_{II} a} + A'_{II} e^{\alpha_{II} a},$$

$$\frac{\varepsilon_m \alpha_{II}}{\alpha_I} A_I = A_{II} e^{-\alpha_{II} a} - A'_{II} e^{\alpha_{II} a}. \tag{5.4}$$

Similar conditions at x = a are

$$A_{II} e^{\alpha_{II} a} + A'_{II} e^{-\alpha_{II} a} = A_{III} e^{-\alpha_I a},$$

$$A_{II} e^{\alpha_{II} a} - A'_{II} e^{-\alpha_{II} a} = -\frac{\alpha_{II} \varepsilon_m}{\alpha_I} A_{III} e^{-\alpha_I a}. \tag{5.5}$$

For symmetric mode (E_z symmetric about x = 0),

$$A'_{II} = A_{II}, \quad A_{III} = A_I, \; A_I = A_{II} 2\cosh \alpha_{II} a e^{\alpha_I a},$$

$$\tanh \alpha_{II} a = -\frac{\alpha_{II} \varepsilon_m}{\alpha_I}, \tag{5.6}$$

$$k_z^2 = \frac{\omega^2}{c^2} \varepsilon_m \frac{\varepsilon_m - \tanh^2 \alpha_{II} a}{\varepsilon_m^2 - \tanh^2 \alpha_{II} a}. \tag{5.7}$$

For $\alpha_{II} a >> 1$, Eq. (5.7) gives the conventional SPW dispersion relation corresponding to a single semiconductor-free space interface,

$$k_z^2 = \frac{\omega^2}{c^2} \frac{\varepsilon_m}{1+\varepsilon_m}, \tag{5.8}$$

$$\alpha_{II} = \frac{\omega}{c} \frac{i}{\sqrt{1+\varepsilon_m}}. \tag{5.9}$$

For $\alpha_{II} a > 1$, the dispersion relation can be solved iteratively, by writing $\tanh^2 \alpha_{II} a \approx 1 - 4e^{-2\alpha_{II} a}$,

$$k_z^2 = \frac{\omega^2}{c^2} \frac{\varepsilon_m}{1+\varepsilon_m} \left[1 + \frac{\varepsilon_m}{\varepsilon_m^2 - 1} 4e^{-2\alpha_{II} a} \right]. \tag{5.10}$$

In Fig. 5.3 we have plotted ω / ω_p vs $k_z c / \omega_p$ for $\varepsilon_L = 17$, $a\omega_p / c = 40, 70, 100$, $n_0 = 2.4 \times 10^{16} cm^{-3}$, m is 0.015 times the free space electron mass. The frequency rises linearly with the wave number upto upper limit of frequency of surface plasmon, i.e. for higher value of wavenumber the behavior of the curve is the same as that of single semiconductor surface structure.

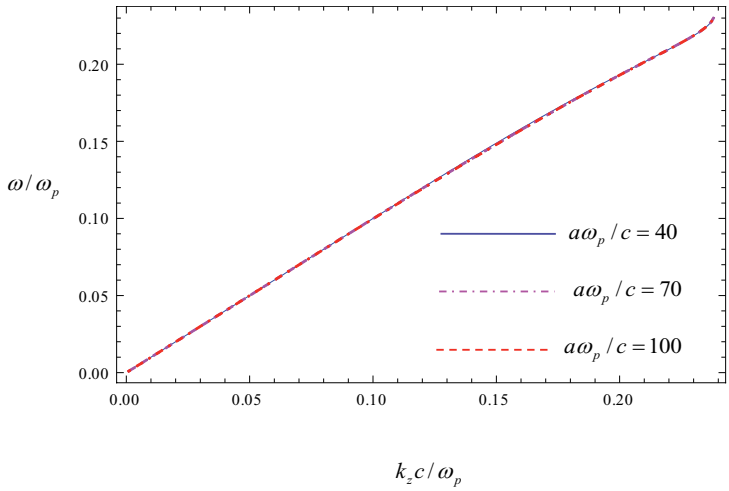

FIG 5.3 Plot of dispersion relation for surface plasma wave in double semiconductor structure for $\varepsilon_L = 17$, $\nu/\omega_p = 0.0472$.

5.3 Electron beam excitation of surface plasma wave

We launch a sheet electron beam of size r_{ob} (comparable to the spacing between planes), density n_{ob} and velocity $v_{ob}\hat{z}$ in between the semiconductor with

$$n_{ob} = N_{ob} e^{-\frac{x^2}{r_{ob}^2}}. \tag{5.11}$$

The y width of the beam is *b* and the beam current is

$$I_b = \sqrt{\pi} N_{ob} r_{ob} b e v_{ob}. \tag{5.12}$$

In the presence of the SPW, beam response is governed by the equation of motion

$$\frac{\partial}{\partial t}(\gamma\vec{v}) + \vec{v}\cdot(\nabla\gamma\vec{v}) = -\frac{e}{m}(\vec{E} + \frac{1}{c}\vec{v}\times\vec{B}), \tag{5.13}$$

where $\vec{B} = \frac{c}{i\omega}\nabla\times\vec{E}$ and $\gamma = (1 - v^2/c^2)^{-1/2}$. We express $\vec{v} = v_{ob}\hat{z} + \vec{v}_1$, $\gamma = \gamma_o + \gamma_o^3 v_{ob} v_{1z}/c^2$, $\gamma\vec{v} = \gamma_o v_{1x}\hat{x} + \gamma_o^3 v_{1z}\hat{z}$, linearize Eq. (5.13) and solve it to get

$$v_{1x} = \frac{eE_x}{mi\omega\gamma_o} - \frac{ev_{ob}}{\gamma_o m\omega(\omega - k_z v_{ob})}\frac{\partial E_z}{\partial x}, \tag{5.14}$$

$$v_{1z} = \frac{eE_z}{mi\gamma_o^3(\omega - k_z v_{ob})}, \tag{5.15}$$

where $\gamma_o = (1 - v_{ob}^2/c^2)^{-1/2}$. From the equation of continuity

$$\frac{\partial n}{\partial t} + \nabla\cdot(n\vec{v}) = 0, \tag{5.16}$$

on expressing n as $n = n_{ob} + n_1$, one obtains the perturbed beam density

$$n_1 = \frac{v_{1x}}{i(\omega - k_z v_{ob})}\frac{\partial n_{ob}}{\partial x} + \frac{n_{ob}\nabla\cdot\vec{v}_1}{i(\omega - k_z v_{ob})}. \tag{5.17}$$

The perturbed current density is

$$\vec{J}_1 = -n_{ob}e\vec{v}_1 - n_1 e v_{ob}\hat{z}. \tag{5.18}$$

For the instability, we look for terms with $(\omega - k_z v_{ob})^2$ in the denominator. The first term on RHS of Eq. (5.18) does not have such a term, hence we discard it. Thus

$$\vec{J}_1 = -\hat{z}\frac{ev_{ob}}{i(\omega - k_z v_{ob})^2}\left[-\frac{ev_{ob}}{m\gamma_o\omega}\frac{\partial n_{ob}}{\partial x}\frac{\partial E_z}{\partial x} - \frac{ev_{ob}n_{ob}}{\gamma_o m\omega}\frac{\partial^2 E_z}{\partial x^2} + \frac{n_{ob}k_z eE_z}{m\gamma_o^3}\right]. \tag{5.19}$$

As $\partial^2/\partial x^2 = \alpha_{II}^2$ & $k_z \cong \omega/v_{ob}$ for the Cerenkov resonance, the last two terms in Eq. (5.19) cancel each other. Thus

$$\vec{J}_1 = \hat{z}\frac{e^2 v_{ob}^2}{im\omega\gamma_o(\omega - k_z v_{ob})^2}\frac{\partial n_{ob}}{\partial x}\frac{\partial E_z}{\partial x}. \tag{5.20}$$

The relevant Maxwell's equations are $\nabla\times\vec{E} = -(1/c)\partial\vec{H}/\partial t$, $\nabla\times\vec{H} = 4\pi\vec{J}/c + (1/c)\partial\vec{D}/\partial t$. In the absence of the beam let the electric and magnetic fields of the SPW be $\vec{E}_s$ and $\vec{H}_s$. These fields satisfy

$$\nabla\times\vec{E}_s = i\frac{\omega}{c}\vec{H}_s, \tag{5.21}$$

$$\nabla\times\vec{H}_s = -\frac{i\omega}{c}\varepsilon'\vec{E}_s, \tag{5.22}$$

with appropriate boundary conditions at x = -a and x = a interfaces. Here $\varepsilon' = \varepsilon_m$ in medium I and III and $\varepsilon' = 1$ for –a < x < a. In the presence of beam current, let

$$\vec{E} = A(t)\vec{E}_s,\ \vec{H} = B(t)\vec{H}_s \tag{5.23}$$

$\vec{E}$ and $\vec{H}$ satisfy the Maxwell's equations

$$\nabla\times\vec{E} = -\frac{1}{c}\frac{\partial\vec{H}}{\partial t},$$

$$\nabla \times \vec{H} = \frac{4\pi}{c}(\vec{J}_{1b} + \vec{J}_{1p}) + \frac{\varepsilon_L}{c}\frac{\partial \vec{E}}{\partial t}, \tag{5.24}$$

where $\vec{J}_{1p} = \sigma_m A\vec{E}_s + i\frac{\partial \sigma_m}{\partial \omega}\frac{\partial A}{\partial t}\vec{E}_s$, $\varepsilon_m = \varepsilon_L + i\frac{4\pi\sigma_m}{\omega}$, inside the semiconductor.

Outside the semiconductor $\varepsilon_L = 1, \sigma = 0$. Using Eq. (5.23) in Eq. (5.24)

$$\frac{\partial B}{\partial t} = -i\omega(A - B), \tag{5.25}$$

$$\left[\frac{\partial A}{\partial t}\frac{\partial}{\partial \omega}(\varepsilon'\omega) - i\omega\varepsilon'(A - B)\right]\vec{E}_s = -4\pi\vec{J}_{1b}. \tag{5.26}$$

Using Eq. (5.25) in Eq. (5.26), assuming $\partial B/\partial t \cong \partial A/\partial t$, multiplying the resulting equation by $\vec{E}_s^*$ and integrating over x from $-\infty$ to $+\infty$, one obtains

$$\frac{\partial A}{\partial t} + \Gamma_c A = \frac{-2\pi\int_{-\infty}^{+\infty} J_{1z}E_{sz}^* dx}{\int_{-\infty}^{+\infty}\vec{E}_s \cdot \vec{E}_s^* dx} = \frac{4\omega_{pb}^2 v_{ob}^2 \alpha_{II} G}{\gamma_o \omega(\omega - k_z v_{ob})^2 r_{ob}^2 D} A, \tag{5.27}$$

where $G = \int_{-a}^{a} \cosh(\alpha_{II} x)\sinh(\alpha_{II} x) e^{-\frac{x^2}{r_{ob}^2}} x dx$, $\Gamma_c = k_{zi} v_g$

$$D = (1 + \cosh(2\alpha_{II} a))(\alpha_I^2 + k_z^2)/\alpha_I^3 + 2(2\alpha_{II} a(\alpha_{II}^2 - k_z^2) + (\alpha_{II}^2 + k_z^2)\sinh(2\alpha_{II} a))/\alpha_{II}^3,$$

$\omega_{pb} = \sqrt{4\pi N_{ob} e^2/m_e}$ is electron beam plasma frequency, m_e is the free space electron mass and v_g is the group velocity of the SPW. Take $\partial/\partial t = -i\delta$, $\omega = k_z v_{ob} + \delta$, one obtains

$$\delta^3 = \frac{4\omega_{pb}^2 v_{ob}^2 \alpha_{II} G}{\gamma_o \omega r_{ob}^2 D}, \tag{5.28}$$

The growth rate is

$$\Gamma = \mathrm{Im}\,\delta = \mathrm{Im}\left[\left(\frac{4\omega_{pb}^2 v_{ob}^2 \alpha_{II} G}{\gamma_o \omega r_{ob}^2 D} \right)^{1/3} \right]. \tag{5.29}$$

$$\frac{\partial \Gamma}{\partial a} = 0 \tag{5.30}$$

The partial differentiation of growth rate w.r.t spacing between the plates yields an optimum value of 0.283mm for the spacing between the plates that gives maximum growth rate of surface plasma wave. We have plotted normalized growth rate versus normalized frequency in Fig. 5.4 for the following parameters: $\omega_{pb}/\omega_p = 10^{-3}, \varepsilon_L = 17, \nu/\omega_p = 0, 0.0472, a\omega_p/c = 40$. As seen from the Fig. 5.4 that the growth rate decreases with collision frequency. The growth rate increases with increasing surface plasma wave frequency.

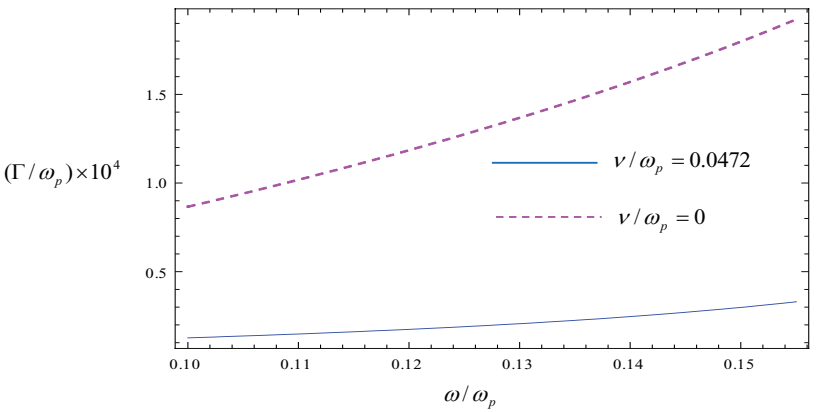

FIG 5.4 Plot of normalized growth rate vs normalized frequency for double semiconductor structure for $\omega_{pb}/\omega_p = 10^{-3}, \varepsilon_L = 17, \nu/\omega_p = 0, 0.0472, a\omega_p/c = 40$.

As shown in Fig. 5.5, we have plotted normalized growth rate vs normalized spacing between the conducting plates. The growth rate while considering the collision frequency, initially with $a\omega_p / c$ attains a peak value and then decreases to $\approx 5.93\times10^8\, rad/s$.

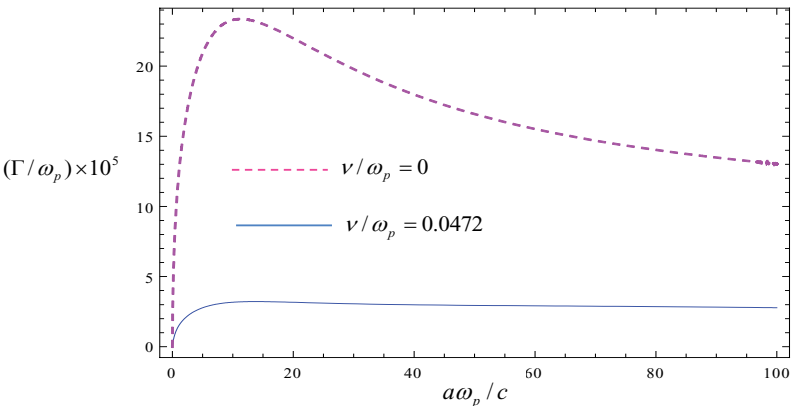

FIG 5.5 Plot of normalized growth rate vs normalized distance between the semiconductor plates for double semiconductor structure for $\omega_{pb}/\omega_p = 10^{-3}$, $\varepsilon_L = 17$, $\omega/\omega_p = 0.15, \nu/\omega_p = 0, 0.0472$, $\gamma_o = 5.94$.

5.4 Discussion

A parallel plane guiding system, with small separation between planes, supports a surface plasma wave. At low frequencies phase velocity is close to the velocity of light in vacuum. One may excite a terahertz wave using a relativistic electron beam. The double semiconductor structure helps in guiding the electron beam without diverging it as the field of surface plasma wave is minimum at the center as compared to single semiconductor structure. We have used

InSb as the material as metals put up an impractically high requirement on beam energy. The energy of the beam is 3MeV at $\omega/2\pi = 0.51THz$. The normalized growth rate increases with the normalized frequency. The growth rate decreases with the collision frequency. The growth rate of surface plasma wave attains a maximum value of $6.8\times10^{8} rad/s$ for an optimum value of 0.283mm separation between the two semiconductor plates. At the beam current $\approx 168Amp$ the growth rate of $5.93\times10^{8} rad/s$ is achieved at the frequency $\approx 0.51THz$ of SPW for the 5mm $\hat{y}$ width and spacing between the two plates of $\approx 2.83mm$. The growth rate scales as 1/3 root of the electron beam current.

References

[1] M. Moskovits, Rev. Mod. Phys. **57**, 783(1985).

[2] K. Kneipp, Y. Wang, H. Kneipp, L. T. Perelman, I. Itzkan, R. R. Dasari, and M. S. Feld, Phys. Rev. Lett. **78**, 1667 (1997).

[3] S. M. Nie and S. R. Emery, Science **275**, 1102 (1997).

[4] S. Schultz, D. R. Smith, J. J. Mock, and D. A. Schultz, Proc. Natl. Acad. Sci. U.S.A. **97**, 996 (2000).

[5] T. A. Taton, C. A. Mirkin, and R. L. Letsinger, Science **289**, 1757 (2000).

[6] K. Li, M. I. Stockman, and D. J. Bergman, Phys. Rev. Lett. **91**, 227402 (2003).

[7] T. Kalkbrenner, M. Ramstein, J. Mlynek, and V. Sandoghdar, J. Microsc. **202**, 72(2001).

[8] H. Ditlbacher, J. R. Krenn, G. Schider, A. Leitner, and F. R. Aussenegg, Appl. Phys. Lett. **81**, 1762(2002).

[9] J. Homola , S. S. Yee , G. Gauglitz, Sens. and Actuators B **54** ,3(1999).

[10] A. G. Brolo, R. Gordon, B. Leathem, and K. L. Kavanagh, Langmuir **20**, 4813(2004).

[11] R. H. Ritchie, Phys. Rev. **106**, 874 (1957).

[12] H. Raether, *Springer Tracts in Modern Physics* (Springer-Verlag, New York, 1988), p. 111.

[13] W. L. Barnes, A. Dereux, T. W. Ebbesen, Nature (London) **424**, 824 (2003).

[14] A. Otto, Z. Phys. 216, 398 (1968).

[15] E. Kretschmann and H. Raether, Z. Naturforsch. A **23A**, 2135 (1968).

[16] E. Kretschmann, Z. Phys. **241**, 313 (1971).

[17] R. Berndt, J. K. Gimzewski and P. Johansson, Phys. Rev. Lett. **67,** 3796(1991).

[18] K. R. Catchpole and A. Polman, Opt. Express **16,** 21793 (2008).

[19] S. Pillai, K. R. Catchpole, T. Trupke, and M. A. Green, J. Appl. Phys. **101**, 093105 (2007).

[20] S. Pillai, K. R. Catchpole, T. Trupke, G. Zhang, J. Zhao, and M. A. Green, Appl. Phys. Lett. **88**, 161102 (2006).

[21] N. Liu, H. Guo, F. Liwei, S. Kaiser, H. Schweizer and H. Giessen, Nature Mater. **7**, 31 (2008).

[22] T. W. Ebbesen, H. J. Lezec, H. F. Ghaemi, T. Thio, P. A. Woff, Nature (London) **391**, 667 (1998).

[23] N. Fang, H. Lee, C. Sun, and X. Zhang, Science **308**, 534 (2005).

[24] J. B. Pendry, Contemp. Phys. **45**, 191(2004).

[25] J. Parsons, E. Hendry, J. R. Sambles, and W. L. Barnes, Phys. Rev. B **80**, 245117 (2009).

[26] H. Shin and S. Fan, Phys. Rev. Lett. **96**, 073907(2006).

[27] J. A. H. van Nieuwstadt, M. Sandtke, R. H. Harmsen, F. B. Segerink, J. C. Prangsma, S. Enoch and L. Kuipers, Phys. Rev. Lett. **97**, 146102(2006).

[28] S. Kim, J. Jin, Y.-J. Kim, I.-Y. Park, Y. Kim and S.-W. Kim, Nature (London) **453**, 757 (2008).

[29] G. H. Welsh, N. T. Hunt, and K. Wynne, Phys. Rev. Lett. **98,** 026803 (2007).

[30] C. S. Liu and V. K. Tripathi, IEEE Trans. Plasma Sci. **28**, 353 (2000).

[31] S. E. Irvine and A. Y. Elezzabi, Appl. Phys. Lett. **86,** 264102 (2005).

[32] S. E. Irvine and A. Y. Elezzabi, Phys. Rev. A **73**, 013815 (2006)

[33] C. S. Liu, G. Kumar, and V. K. Tripathi, J. Appl. Phys. **100,** 013304 (2006).

[34] P. Kumar, V. K. Tripathi and C. S. Liu, J. Appl. Phys. **104**, 033306(2008).

[35] C. S. Liu and V. K. Tripathi, *Electromagnetic Theory for Telecommunications*(Cambridge University Press India Pvt. Ltd.(2007), Chapter 3.

Chapter 6

Mode Conversion of Terahertz Radiation into Surface Plasma Wave on a Rippled Magnetized n-InSb

6.1 Introduction

Surface plasmons have drawn vigorous attention in recent years due to their wide ranging applications [1-8]. They propagate along the surface between a conductor and a dielectric or conductor and air with their field amplitude peaking at the interface and falling off exponentially away from it in either medium [9-11]. A tiny trace of a gas or DNA on the interface produces a measurable change in the propagation constant when one uses the attenuated total reflection (ATR) configuration [12-14]. This makes them ideally suited as sensors. Surface plasmons (SP) can increase the rate of laser ablation of materials by orders of magnitude, hence are suitable for rapid thin film deposition. Surface waves propagating along a semiconductor/air interface can potentially be used for spectroscopy of surfaces and surface deposits such as biomolecules since their frequency can conveniently lie in the terahertz range. To excite surface terahertz waves, one can use the standard techniques of coupling bulk radiation to surface waves.

The presence of a static magnetic field significantly modifies the nature of surface plasmons, turning them into surface magnetoplasmons. Brion et al. [15] have studied surface magnetoplasmons in n-InSb when magnetic field is parallel to the surface and the direction of propagation is perpendicular to the magnetic field. The dispersion curve splits into branches, separated by a bandgap. Glass [16] has studied the coupling of electromagnetic waves with a magnetoplasmons, employing Rayleigh's method. At specific frequencies there is sharp

reduction in wave reflectivity, indicating the excitation of surface plasma wave. Flahive and Quinn [17] have studied surface plasmons, propagating along the direction of magnetic field in an electron-hole plasma and noted several interesting features.

In this chapter, we employ a density ripple model to study the excitation of terahertz surface plasma wave at rippled semiconductor- air interface by a normally incident THz radiation in the presence of a static magnetic field. The magnetic field is perpendicular to ripple wave vector and the polarization of the incident radiation field. The radiation field imparts oscillatory velocity to electrons in the ripple layer. The velocity couples with the density ripple of suitable wave number to produce a current that resonantly drives the surface plasma wave. In section 6.2, we obtain the dispersion relation and mode structure of the surface plasma wave eigenmode. In section 6.3, we study the excitation of surface plasma wave by the linear mode conversion of a normally incident terahertz wave on the rippled n-InSb surface. A discussion of results is given in section 6.4.

6.2 Surface Plasmon Eigenmode

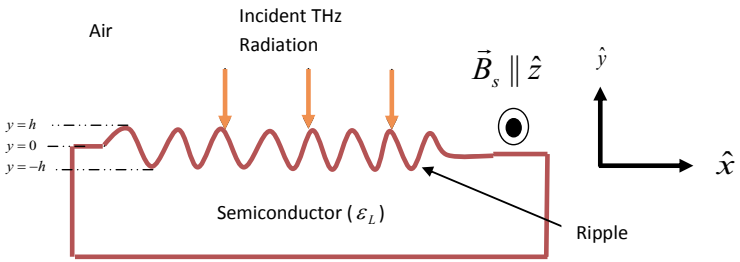

FIG 6.1 Schematic of linear mode conversion of incident THz radiation into surface plasma wave on a rippled semiconductor-air interface in the presence of transverse magnetic field.

Consider a semiconductor-free space interface y=0 with y<0 being the semiconductor and y>0 the free space. The semiconductor could be n-InSb, or for any n-type semiconductor with spherical free electron energy surfaces. A static magnetic field $B_s\hat{z}$ is applied to the semiconductor (Fig. 6.1). The effective plasma permittivity tensor $\underline{\underline{\varepsilon}}$ of the semiconductor at frequency ω has components,

$$\varepsilon_{xx} = \varepsilon_{yy} = (\varepsilon_+ + \varepsilon_-)/2,$$

$$\varepsilon_{xy} = -\varepsilon_{yx} = (\varepsilon_+ - \varepsilon_-)/2i,$$

$$\varepsilon_{zz} = 1 - (\omega_p^2)/(\omega(\omega + i\nu)),$$

$$\varepsilon_{xz} = \varepsilon_{zx} = \varepsilon_{yz} = \varepsilon_{zy} = 0,$$

$$\varepsilon_+ = \varepsilon_L - \omega_p^2/(\omega(\omega - \omega_c + i\nu)),$$

$$\varepsilon_- = \varepsilon_L - \omega_p^2/(\omega(\omega + \omega_c + i\nu)), \tag{6.1}$$

where ε_L is the lattice dielectric constant, $\omega_c = eB_s/mc$ is the electron cyclotron frequency, $\omega_p = (4\pi n_0 e^2/m)^{1/2}$ is the plasma frequency, -e, m and ν are the charge, effective mass and collision frequency of electrons. The surface supports a surface plasma wave, which we take to propagate along $\hat{x}$ with electric field [15],

$$\vec{E} = (\hat{x} + \frac{ik_x\hat{y}}{\alpha_I})A_o \exp[-i(\omega t - k_x x)]\exp(-\alpha_I y), \text{ for y>0} \tag{6.2}$$

$$\vec{E} = (\hat{x} + \beta\hat{y})A_o \exp[-i(\omega t - k_x x)]\exp(\alpha_{II} y), \text{ for y>0} \tag{6.3}$$

where $\beta = -\left(i\alpha_{II}\varepsilon_{xy} + k_x\varepsilon_{xx}\right)/\left(\varepsilon_{xy}k_x - i\alpha_{II}\varepsilon_{xx}\right), \alpha_I^2 = k_x^2 - \omega^2/c^2$,

$\alpha_{II}^2 = k_x^2 - (\omega^2/c^2)(\varepsilon_{xx}^2 + \varepsilon_{xy}^2)/\varepsilon_{xx}$ and we have employed $\nabla\cdot\vec{D} = 0$ in both the media. Continuity of $D_y = \varepsilon_{xx}E_y - \varepsilon_{xy}E_x$ across y=0, demands

$$\frac{ik_x}{\alpha_I} = \varepsilon_{xx}\beta - \varepsilon_{xy} = -\frac{k_x\varepsilon_+\varepsilon_-}{k_x\varepsilon_{xy} - i\alpha_{II}\varepsilon_{xx}} \tag{6.4}$$

giving two roots.

$$k_x^2 = k_{x\pm}^2 \equiv \frac{\omega^2}{c^2}\frac{\alpha_2 \pm \alpha_3}{\alpha_1}, \tag{6.5}$$

where $\alpha_1 = \varepsilon_+^2\varepsilon_-^2 - 2\left(\varepsilon_{xx}^2 - \varepsilon_{xy}^2\right) + 1$, $\alpha_2 = \varepsilon_+\varepsilon_-\left(\varepsilon_+\varepsilon_- - \varepsilon_{xx}\right) - \varepsilon_{xx}^2 + \varepsilon_{xy}^2 + \varepsilon_{xx}$,

$\alpha_3 = \left[\varepsilon_{xy}^2\left(\varepsilon_{xx}\varepsilon_+\varepsilon_- - 2\varepsilon_{xx}^2 + \varepsilon_{xx}\right)\right]^{1/2}$. In the absence of dc magnetic field, $\vec{B}_s = 0$, $\varepsilon_{xy} = 0, \varepsilon_+ = \varepsilon_- = \varepsilon_{xx}, \alpha_3 = 0, \alpha_1 = \left(1 - \varepsilon_{xx}^2\right)^2$, $\alpha_2 = \varepsilon_{xx}\left(1 - \varepsilon_{xx}\right)\left(1 - \varepsilon_{xx}^2\right)$ the two roots coalesce to give the conventional dispersion relation for the surface plasma wave,

$$k_x^2 = \frac{\omega^2}{c^2}\frac{\varepsilon_{xx}}{1 + \varepsilon_{xx}}. \tag{6.6}$$

With finite magnetic field, the surface wave splits into two surface plasma wave eigen modes, $k_x^2 = k_{x+}^2, k_{x-}^2$.

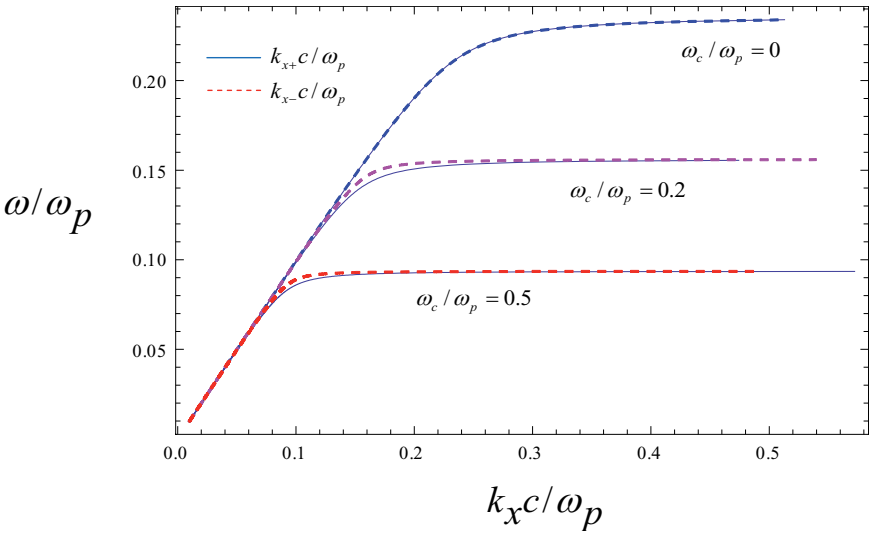

FIG 6.2 Dispersion relation of n-InSb for surface plasma wave in the collisionless regime i.e. for parameters $\omega_c/\omega_p = 0,0.2,0.5$, $\varepsilon_L = 17, \nu/\omega_p = 0$.

6.3 Mode conversion of THz radiation into surface plasmons

Now we allow surface ripple on the semiconductor $y = h\cos qx$ (c.f. Fig 6.1). As one moves along $\hat{x}$ in the ripple region, the electron density shows a periodic variation with x. One may model the surface ripple as a density ripple

$$n_0 = \frac{n_0^0}{2} + n_q, \tag{6.7}$$

$$n_q = \frac{n_0^0}{2}\cos qx, \tag{6.8}$$

where q is the wave number of the density ripple, we choose $qh < 1$. A terahertz electromagnetic wave, with electric field

$$\vec{E}_0 = \hat{x}A_0 e^{-i(\omega t + \frac{\omega}{c}y)}, \tag{6.9}$$

is normally incident on it. The transmitted field, on ignoring the effect of the ripple, can be written as

$$\vec{E}_T = (\hat{x} + \beta_1 \hat{y}) T A_0 e^{-i\omega t} e^{\alpha y}. \tag{6.10}$$

where, $\alpha = (\omega/c)((-\varepsilon_+ \varepsilon_-)/\varepsilon_{xx})^{1/2}$ and $\beta_1 = \varepsilon_{xy}/\varepsilon_{xx}$ in compliance with the Maxwell's equation $\nabla \cdot \left(\underline{\underline{\varepsilon}} \cdot \vec{E}\right) = 0$. The magnetic field of the transmitted wave using $\vec{B} = (c/i\omega)\nabla \times \vec{E}$, can be written as

$$\vec{B}_T = -\hat{z} T A_0 \frac{c\alpha}{i\omega} e^{-i\omega t} e^{\alpha y}. \tag{6.11}$$

Using boundary conditions on E_x and B_z at y=0, one obtains the amplitude transmission coefficient

$$T = \frac{2}{1 + i\alpha c/\omega}. \tag{6.12}$$

The transmitted field imparts oscillatory velocity to electrons in accordance with the equation of motion

$$m\frac{\partial \vec{v}}{\partial t} = -e\vec{E}_T - \frac{e}{c}\vec{v} \times \vec{B}_S - m\vec{v}\nu, \tag{6.13}$$

$$\vec{\mathrm{v}} = \frac{e}{m((\omega + i\nu)^2 - \omega_c^2)}\left(-i(\omega + i\nu)\vec{E}_T - \omega_c \vec{E}_T \times \hat{z}\right). \tag{6.14}$$

In the ripple region $(-h < y < h)$, $\vec{\mathrm{v}}$ couples with the density ripple n_q to produce the nonlinear current density at $(\omega, q\hat{x})$

$$\vec{J}^{NL} = -\frac{en_q^0 \vec{\mathrm{v}}}{2} = -\frac{e^2 n_0^0}{4m((\omega + i\nu)^2 - \omega_c^2)}\left(-i(\omega + i\nu)\vec{E}_T - \omega_c \vec{E}_T \times \hat{z}\right)e^{iqx}. \tag{6.15}$$

In the ripple region $e^{\alpha y} \approx 1$. The current density resonantly excites a surface plasma wave of frequency ω, when q equals the SPW wave vector given by Eq. (6.5), $q = k_{xr+}$ or $q = k_{xr-}$, where $k_{xr\pm}$ are the real parts of $k_{x\pm}$. For the moment we consider the excitation of the + mode. The wave equation governing SPW, on using Maxwell's equations $\nabla \times \vec{E} = (i\omega/c)\vec{H}$, $\nabla \times \vec{H} = -(i\omega/c)\underline{\underline{\varepsilon}} \cdot \vec{E} + (4\pi/c)\vec{J}^{NL}$, can be written as

$$\nabla^2 \vec{E} - \nabla(\nabla \cdot \vec{E}) + \frac{\omega^2}{c^2}\underline{\underline{\varepsilon}} \cdot \vec{E} = -\frac{4\pi i\omega}{c^2}\vec{J}^{NL}. \tag{6.16}$$

From the y- component of Eq. (6.16) we get

$$E_y = \frac{(\frac{\omega^2}{c^2}\varepsilon_{xy} + iq\frac{\partial}{\partial y})}{(\frac{\omega^2}{c^2}\varepsilon_{xx} - q^2)}E_x. \tag{6.17}$$

For the x-component, Eq. (6.16) gives

$$\frac{\partial^2 E_x}{\partial y^2} - k_y^2 E_x = -\frac{4\pi i}{\omega \varepsilon_{xx}} (\frac{\omega^2}{c^2} \varepsilon_{xx} - q^2) J_x^{NL}, \tag{6.18}$$

where $k_y^2 = q^2 - (\omega^2 / c^2)(\varepsilon_{xx}^2 + \varepsilon_{xy}^2) / \varepsilon_{xx}$ for $y < 0$ and $k_y^2 = q^2 - \omega^2 / c^2$ for $y > 0$ .When current source is neglected, one obtains

$$\frac{\partial^2 E_x}{\partial y^2} - k_y^2 E_x = 0. \tag{6.19}$$

The solution for Eq. (6.19) is given as

$$\vec{E} = A \vec{\psi}(y) e^{-i(\omega t - qx)}, \tag{6.20}$$

where, $\vec{\psi}(y) = (\hat{x} + i \frac{q}{\alpha_I} \hat{y}) e^{-\alpha_I y}$ for $y > 0$,

$= (\hat{x} + \beta \hat{y}) e^{\alpha_{II} y}$ for $y < 0$.

Now when the current source is retained, we presume that the mode structure of the surface wave is not modified, and write

$$\vec{E} = A(x) \vec{\psi}(y) e^{-i(\omega t - qx)}. \tag{6.21}$$

Using Eqs. (6.18) & (6.21) and letting $q -> q - i\partial / \partial x$, one obtains

$$2iq \vec{\psi}(y) \frac{\partial A(x)}{\partial x} - 2ik_{xr+} k_{xi+} A(x) \vec{\psi}(y) = -\frac{4\pi i}{\omega \varepsilon_{xx}} (\frac{\omega^2}{c^2} \varepsilon_{xx} - q^2) \vec{J}^{NL}. \tag{6.22}$$

where k_{xi+} is the imaginary part of k_{x+}. Multiplying Eq. (6.22) by $\psi^*(y)dy$ and integrating from $-\infty$ to $+\infty$, one obtains

$$\frac{\partial A}{\partial x}+k_{xi+}A=-\frac{2\pi}{q\omega\varepsilon_{xx}}\left(\frac{\omega^2}{c^2}\varepsilon_{xx}-q^2\right)\frac{\int_{-\infty}^{\infty}\vec{\psi}^*(y)\cdot\vec{J}^{NL}dy}{\int_{-\infty}^{\infty}\vec{\psi}(y)\cdot\vec{\psi}^*(y)dy}e^{i(\omega t-qx)}. \tag{6.23}$$

If one ignores the absorption of the SPW, Eq. (6.23) integrate to give over the length of illumination *d*,

$$\frac{A}{A_0}=\frac{1}{4}\left(\frac{\omega_p^2}{(\omega+i\nu)^2-\omega_c^2}\right)\left(\frac{\frac{\omega^2}{c^2}\varepsilon_{xx}-q^2}{q\omega\varepsilon_{xx}}\right)\left(i(\omega+i\nu)(2+\frac{i\beta_1 q}{\alpha_I}+\beta\beta_1)+\omega_c(2\beta_1-\beta-\frac{iq}{\alpha_I})\right)\times$$
$$\left(\frac{1}{\frac{1+(q/\alpha_I)^2}{\alpha_I}+\frac{1+\beta^2}{\alpha_{II}}}\right)dhT \tag{6.24}$$

When $d>1/k_{xi+}$, Eq. (6.24) still holds with *d* replaced by$1/k_{xi+}$. We have plotted normalized amplitude vs normalized frequency in Fig. 6.3 and in Fig. 6.4 we have plotted normalized amplitude vs normalized electron cyclotron frequency for the '+' mode for the parameters $d\omega_p/c=5$, $\varepsilon_L=17$, $\nu/\omega_p=0.014$. As seen from the figures at free electron density $n_0\approx 2.4\times10^{16}cm^{-3}$, as one increases the magnetic field the cut-off frequency of SPW decreases and at a specified magnetic field the SPW at the corresponding cut-off frequency is generated. The amplitude of the SPW increases with magnetic field. We have plotted normalized amplitude vs normalized frequency in Fig. 6.5 and in Fig. 6.6 we have plotted normalized amplitude vs normalized electron cyclotron frequency for the '-' mode for the parameters $d\omega_p/c=5$, $\varepsilon_L=17$, $\nu/\omega_p=0.014$.

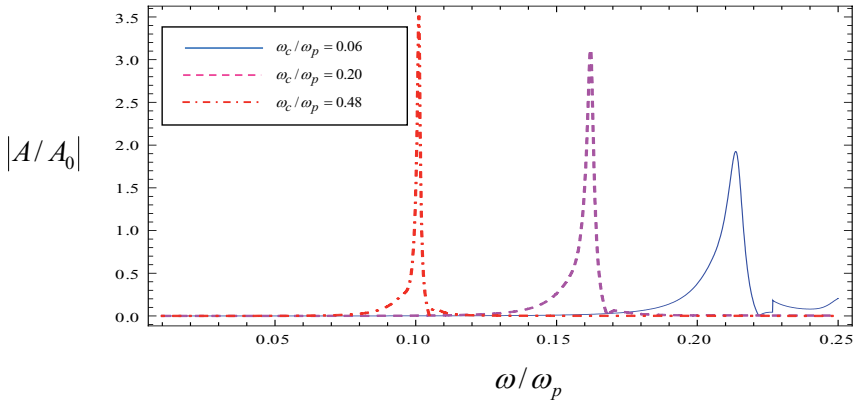

FIG 6.3 Plot of normalized amplitude vs normalized frequency for '+' mode for the parameters $\varepsilon_L = 17,\ \nu/\omega_p = 0.014, d\omega_p/c = 5.$

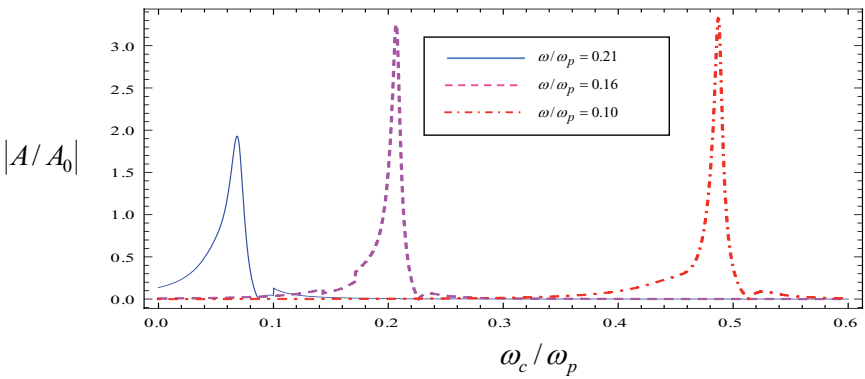

FIG 6.4 Plot of normalized amplitude vs normalized electron cyclotron frequency for '+' mode for the parameters $\varepsilon_L = 17,\ \nu/\omega_p = 0.014, d\omega_p/c = 5.$

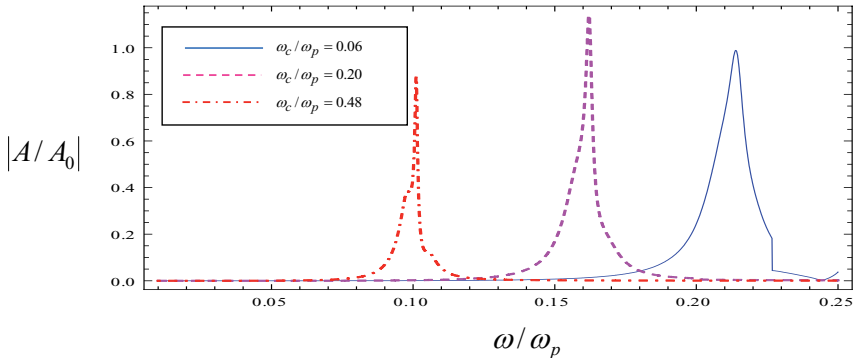

FIG 6.5 Plot of normalized amplitude vs normalized frequency for '-' mode for the parameters $\varepsilon_L = 17,\ \nu/\omega_p = 0.014, d\omega_p/c = 5.$

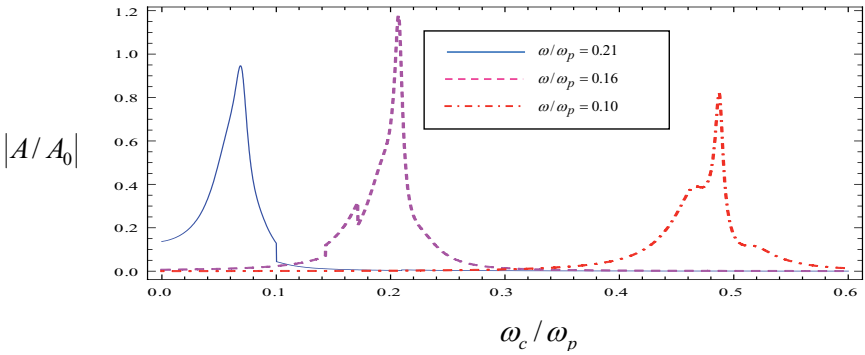

FIG 6.6 Plot of normalized amplitude vs normalized electron cyclotron frequency for '-' mode for the parameters $\varepsilon_L = 17,\ \nu/\omega_p = 0.014, d\omega_p/c = 5.$

IV Discussion

The transverse magnetic field splits the SPW into two modes '+' mode and '-' mode, with propagation constants $k_{x+}^2 \equiv (\omega^2/c^2)(\alpha_2+\alpha_3)/\alpha_1, k_{x-}^2 \equiv (\omega^2/c^2)(\alpha_2-\alpha_3)/\alpha_1$. The cut-off

frequency for both the SPW modes decreases with increasing magnetic field. At a given free electron density (say $n_0 \approx 2.4 \times 10^{16} cm^{-3}$), a specific magnetic field and ripple wave number, the SPW amplitude has a sharp maximum at a given frequency for which the phase matching condition is satisfied. As one increases the magnetic field this optimum frequency decreases for both the cases of '+' and '-'SPW modes. The amplitude of SPW for '+' mode is higher than as compared to that for the '-'mode. This is because '+' mode has lower wavenumber than the '-' mode and the amplitude is inversely proportional to the wavenumber.

References

[1] M. Moskovits, Rev. Mod. Phys. **57**, 783(1985).

[2] K. Kneipp, Y. Wang, H. Kneipp, L. T. Perelman, I. Itzkan, R. R. Dasari, and M. S. Feld, Phys. Rev. Lett. **78**, 1667 (1997).

[3] S. M. Nie and S. R. Emery, Science **275**, 1102 (1997).

[4] S. Schultz, D. R. Smith, J. J. Mock, and D. A. Schultz, Proc. Natl. Acad. Sci. U.S.A. **97**, 996 (2000).

[5] T. A. Taton, C. A. Mirkin, and R. L. Letsinger, Science **289**, 1757 (2000).

[6] K. Li, M. I. Stockman, and D. J. Bergman, Phys. Rev. Lett. **91**, 227402 (2003).

[7] T. alkbrenner, M. Ramstein, J. Mlynek, and V. Sandoghdar, J. Microsc. **202**, 72(2001).

[8] H. Ditlbacher, J. R. Krenn, G. Schider, A. Leitner, and F. R. Aussenegg, Appl. Phys. Lett. **81**, 1762 (2002).

[9] R. H. Ritchie, Phys. Rev. **106**, 874 (1957).

[10] H. Raether, Springer Tracts in Modern Physics (Springer-Verlag, New York, 1988), p. 111.

[11] W. L. Barnes, A. Dereux, T. W. Ebbesen, Nature **424**, 824 (2003).

[12] A. Otto, Z. Phys. **216**, 398 (1968).

[13] E. Kretschmann and H. Raether, Z. Naturforsch. A **23**A, 2135 (1968).

[14] E. Kretschmann, Z. Phys. **241**, 313 (1971).

[15] J. J. Brion, R. F. Wallis, A. Hartstein and E. Burstein, Phys. Rev. Lett., **28**(22), 1455(1972).

[16] N. E. Glass, Phys. Rev. B, **41**(11), 7615(1990).

[17] P. G. Flahive and J. J. Quinn, Phys. Rev. Lett., 31(9), 586(1973).

Chapter 7

Conclusions and Future Prospects

The plasma appears to have significant influence on the mode structure, phase velocity and power handling capability of a travelling wave tube. It allows larger beam current hence can produce higher powers. The beam excites an azimuthally symmetric slow wave via Cerenkov resonance. In the case of a strongly magnetized plasma when $\omega_p > \omega$ (where ω_p is the plasma frequency), the amplitude of the axial electric field peaks on the axis and phase velocity is suppressed, whereas for $\omega_p < \omega$ the field amplitude peaks at the helix surface and phase velocity is enhanced. As a consequence, when beam is placed close to the helix, the growth rate increases with ω_p as long as $\omega_p < \omega$ and decreases with ω_p when $\omega_p > \omega$. In the case of unmagnetised plasma, the mode is more strongly localized near the helix and growth rate increases with ω_p.

The beat ponderomotive force due to two Gaussian laser beams in a magnetized plasma channel resonantly excites difference frequency terahertz radiation when the plasma has a density ripple. The density ripple provides phase synchronism while the axial magnetic field enhances the nonlinear coupling through cyclotron resonance. The terahertz power scales as the square of density ripple amplitude and inversely with the square of laser frequencies.

Thin semiconductor slabs offer a fascinating nonlinear medium for the generation of terahertz radiation via the nonlinear mixing of two infrared lasers. Both the lasers must propagate either in TM mode or TE when ripple wave number is suitably chosen to satisfy the phase matching. To offset the phase mismatch between the laser ponderomotive force and terahertz radiation the semiconductor must have a density ripple. A surface ripple may also be effective.

We find that the presence of a transverse static magnetic field enhances the amplitude of the terahertz wave. The terahertz yield is significantly higher in the TM mode laser propagation than in the TE mode. n-InSb appears to be giving higher yields.

Two parallel semiconductor plates, separated by a short distance, appear suitable for surface plasmon excitation by an electron beam. The SPW eigen mode has amplitude maxima at the inner surfaces of the plates and minimum at the center. A relativistic sheet electron beam propagating through the space between the planes resonantly excites the surface plasma wave (SPW). The frequency of the driven SPW decreases with the energy of the beam while the growth rate increases. At the beam current $\approx 168 Amp$ the growth rate of $5.93\times10^{8} rad/s$ is achieved at the frequency $\approx 0.51 THz$ of SPW for the 5mm $\hat{y}$ width and spacing between the two plates of $\approx 2.83 mm$. The growth rate scales as 1/3 root of the electron beam current.

The linear mode conversion of terahertz radiation into a surface plasma wave on a rippled surface of magnetized n-InSb offers a via medium for surface plasmon devices. The radiation, polarized in the direction of ripple wave vector, imparts oscillatory velocity to electrons in the ripple layer. The velocity beats with the ripple density to produce a current that resonantly drives the surface plasma wave. The magnetic field splits the SPW mode into '+' & '-'modes and reduces the cut-off frequency. The amplitude of SPW for '+' mode is higher than as compared to '-'mode.

Scope for Future Work

The introduction of plasma into the interaction region of other microwave and millimeter wave devices may be a very worthwhile study to carry out. Semiconductors having energy band other than spherical may be tried for coherent radiation generation.

In some instances, THz wireless communication links offer some advantage over microwave links as well as free-space infrared IR based systems. THz communications have the potential for increased bandwidth capacity compared to microwave systems. THz communications are inherently more directional than microwave or millimeter _MMW_ links due to less free-space diffraction of the waves. THz communications can be implemented as a "secure" communications link. THz can support ultrahigh bandwidth spread spectrum systems, which can enable secure communication, large capacity networks, and protection against channel jamming attacks. There is lower attenuation of THz radiation compared to IR under certain atmospheric conditions e.g., fog. Under certain weather conditions and for specific link length requirements THz can enable reliable communication where IR based systems would fail.

Surface-plasmon based circuits are known to merge the fields of photonics and electronics at the nanoscale, thereby enabling to overcome the existing difficulties related to the large size mismatch between the micrometer-scale bulky components of photonics and the nanometer scale electronic chips. Indeed, the surface-plasmon polariton can serve as a base for constructing nano-circuits that will be able to carry optical signals and electric currents. These optoelectronic circuits would consist of various components such as couples, waveguides, switches, and modulators.

Appendix A

Consider a n-type semiconductor with free electron density n_0 immersed in a dc magnetic field $B_s \hat{y}$. It is subjected to an ac electric field, $\vec{E} = \vec{A}e^{-i(\omega t)}$. The electron response to this field is governed by the linearized equation of motion

$$m\frac{\partial \vec{v}}{\partial t} = -e\vec{E} - \frac{e}{c}\vec{v} \times \vec{B}_s \tag{1}$$

Replacing $\partial / \partial t$ by $-i\omega$ one obtains the drift velocity components

$$v_x = -\frac{e}{m(\omega^2 - \omega_c^2)}\left[i\omega E_x + \omega_c E_z\right] \tag{2}$$

$$v_y = -\frac{ie}{m\omega}E_y \tag{3}$$

$$v_z = \frac{e}{m(\omega^2 - \omega_c^2)}\left[-i\omega E_z + \omega_c E_x\right] \tag{4}$$

The current density $\vec{J} = -n_0 e\vec{v}$ thus has the following components:

$$J_x = \frac{n_0 e^2}{m(\omega^2 - \omega_c^2)}\left[i\omega E_x + \omega_c E_z\right] \tag{5}$$

$$J_y = \frac{in_0 e^2}{m\omega}E_y \tag{6}$$

$$J_z = -\frac{n_0 e^2}{m(\omega^2 - \omega_c^2)}\left[-i\omega E_z + \omega_c E_x\right] \tag{7}$$

One may write $\vec{J} = \underline{\underline{\sigma}}.\vec{E}$ with the effective permittivity tensor is defined as

$$\underline{\underline{\varepsilon}} = \varepsilon_L \underline{\underline{I}} + \frac{i4\pi\underline{\underline{\sigma}}}{\omega} \tag{9}$$

where $\underline{\underline{I}} = \begin{vmatrix} 1 & 0 & 0 \\ 0 & 1 & 0 \\ 0 & 0 & 1 \end{vmatrix}$ is unit dyadic,

$$\varepsilon_{xx} = \varepsilon_{zz} = \varepsilon_L - \frac{\omega_p^2}{\omega^2 - \omega_c^2},$$

$$\varepsilon_{yy} = \varepsilon_L - \frac{\omega_p^2}{\omega^2}, \varepsilon_{xz} = -\varepsilon_{zx} = -i\frac{\omega_c}{\omega}\frac{\omega_p^2}{\omega^2 - \omega_c^2},$$

Manish Kumar

Department of Electrical Engineering

Institute of Technology, Banaras Hindu University,

Varanasi-221005, India

Academics

Ph.D. Plasma Physics, Physics Department, IIT Delhi, India, January 2008 -December 2010. CGPA (Pre Ph.D. Courses): 8/10

Thesis Title: Coherent radiation generation by particle beams and nonlinear mixing of lasers.

M. Tech. M. Tech. (Energy Studies) in year 2000 from IIT Delhi, India, with 8.5 CGPA.

B. E. B. E. (Electrical Engineering) in year 1997 from MNNIT Allahabad, India, with 69.22% Marks.

List of Publications

Published:

1. "Plasma effects in a travelling wave tube ", **Manish Kumar**, Lalita Bhasin and V. K. Tripathi, **Phys. Scr. 81 025502 (2010).**
2. "Resonant beat wave excitation of terahertz radiation in a magnetized plasma channel", **Manish Kumar**, Lalita Bhasin and V. K. Tripathi, **Phys. Scr. 81 045504 (2010).**
3. "Excitation of THz plasmons eigen mode of a parallel plane guiding system by an electron beam", Pawan Kumar, **Manish Kumar** and V. K. Tripathi, **J. Appl. Phys. 108, 123303(2010)**.

Communicated:

4. "Beat excitation of Terahertz radiation in a semiconductor slab in a magnetic field ", **Manish Kumar**, Lalita Bhasin and V. K. Tripathi.

5. "Mode conversion of terahertz radiation into surface plasma wave on a rippled magnetized n-InSb", **Manish Kumar**, Pawan Kumar and V. K. Tripathi.

Conferences

1. " Resonant beat wave excitation of terahertz radiation in a magnetized plasma channel ", **Manish Kumar,** Lalita Bhasin and V. K. Tripathi, **International Workshop on the Terahertz Technology 2009,** Osaka, Japan 30 Nov – 03 Dec, 2009.
2. Participated in **International Conference on Multifunctional Material-2010 (ICMM-2010)** held on 6-9 December 2010, at the Department of Physics, Banaras Hindu University, Varanasi, India.

Computation skills

Programming Language: FORTRAN, C++

Scientific Software's: MATLAB, Mathematica

Operating Systems: Windows

Personal Details

The author was born on June 21, 1974 in Azamgarh (Uttar Pradesh), India. He got his basic education in Varanasi. His father is a Professor of Physics in BHU and mother is a housewife. Currently he is a Ph.D. student in Physics Department, IIT Delhi on study leave from Department of Electrical Engg., IT,BHU, Varanasi.

When not working, he spends time in social work related to Denotified Tribes.